HEAT UTILIZATION IN SUBMERGED ARC WELDING

by

Michel Delsol

B.Sc., Metallurgy, Massachusetts Institute of Technology, 1964.

Submitted in Partial Fulfillment of the Requirements
for the Degree of

DOCTOR OF SCIENCE

at the

Massachusetts Institute of Technology

1968

Signature of Author
Department of Metallurgy
and Materials Science

Signature Redacted

Signature of Professor
in Charge of Research

Signature Redacted

Signature of Chairman of
Departmental Committee on
Graduate Students

Signature Redacted

HEAT UTILIZATION IN SUBMERGED ARC WELDING

by

Michel Delsol

Submitted to the Department of Metallurgy on January 5, 1968

in Partial Fulfillment of the Requirements for the

DOCTOR OF SCIENCE

ABSTRACT

Empirical equations for bead-on-plate submerged arc weld dimensions and for the cross-sectional area of the heat affected zone in HY-80 steel have been obtained. The welding variables considered are: wire feed rate, travel speed, voltage, wire size, and nozzle height. Empirical equations relate the amperage to the welding variables.

A new mathematical model for the heat source is introduced. The model is based on the formation of parabolic isotherms caused by the contimuous release of heat from a line source of finite length traveling in the direction of its length. Results based on heat transfer efficiencies indicate that the peak temperature distribution derived from the finite line source model is more realistic than the peak temperature distribution derived from the point source model.

The model for a line source of finite length traveling in the direction of its length is characterized by an intensity and by a length approximately equal to that of the weld pool. The model leads directly to the formulation of a shape factor which, when taken together with the travel speed, defines a moving paraboloid corresponding to the melting point isotherm.

Thesis Supervisor: Clyde M. Adams Jr.

Title: Professor of Metallurgy

TABLE OF CONTENTS

LIST OF ILLUSTRATIONS

LIST OF TABLES

ACKNOWLEDGMENT

The author wishes to express his sincere gratitude to Professor Clyde M. Adams for his supervision and guidance and to Mr. H. J. Nichols, from the United States Steel Corporation, for his helpful suggestions throughout the course of this work. A small note of thanks is due to Mr. Anthony J. Zona who proved invaluable in overcoming many of the day to day problems that occured and to the other members of the Welding Laboratory at M.I.T. who provided a pleasant research environment. The author appreciates the continued sponsorship of the United States Steel Corporation throughout this and previous programs on heat flow study in welding.

I. INTRODUCTION

Fusion welding is characterized by a heat source intense enough to melt part of the materials which are to be joined. Of the variety of welding processes available in the industry, a whole family stands out in that the heat source is an arc associated with a substantial addition of material to the area where fusion is to be effected -- this family of processes, called consumable electrode welding, is to be differentiated from welding processes in which the addition of filler material is external to the heat source.

Different types of consumable electrode welding techniques exist; the more common are metal-inert-gas (MIG), submerged-arc, and the hand held stick electrode. The hand held stick electrode welding process is a useful tool but is not of such a nature as to allow long continuous automated welding. MIG and submerged arc welding, on the other hand, are processes in which a machine can do an endless weld of consistent quality. Of the two processes, MIG and submerged-arc, the latter is cheaper, easier to use, and produces a more intense heat source; however, it is of limited application. MIG welding is considerably more versatile.

Due to its very nature, consumable electrode welding is characterized not only by the presence of an intense heat source but also, by the dynamic effect of mass flow impinging upon the base plate, through a heat source, at a rate anywhere from 60 to 1000 inches per minute depending upon conditions. In the case of submerged-arc welding, this dynamic effect can lead to high penetration welds.

Welding processes have long suffered from operative difficulties in that no practical means of predicting thermal events were available. Research on heat transfer during welding has gone far towards overcoming these difficulties; however, a great deal of work needs to be done before all thermal events in welding can be accurately predicted given any set of conditions. Due to this, welding is still considered by many to be an art rather than a science.

The objectives of this work were the following:

(1) To determine the effect of each of the several variables used in submerged-arc welding. These are: arc voltage, amperage, travel speed, wire size, nozzle height, and to a minor extent, angle of incidence of the filler wire.

(2) To relate experimental results to heat transfer theory.

II. REVIEW OF THE LITERATURE

The mathematical interpretation of heat transfer in arc welding derives from a single concept - a point source releases an amount of heat (Q) at time (t) equal to zero. The principle of superposition makes the point source a versatile tool in that continuous moving point or line sources can be obtained by appropriate integration.[1]

In 1941 Rosenthal[2] published an equation which relates the centerline cooling rate behind a point source moving in a straight line in a semi-infinite solid to that temperature at which the cooling rate is to be determined (equation II-1).

$$\frac{dT}{d\theta} = 2\pi K \frac{V}{q} (T - T_o)^2 \quad \text{. . . . . II-1}$$

T = temperature, °F
θ = time, seconds
V = travel speed, inches per minute
q = arc power, joules/minute
T_o = preheat, °F
K = thermal conductivity, joules/Sec in °F

Since 1941, Adams[3] has developed a similar equation for the cooling rate in thin plates (i.e., under conditions such that heat flow is essentially parallel to the plate surfaces). For a thin plate, the cooling rate behind a line source is given by equation II-2.

$$\frac{dT}{d\theta} = 2\pi K \rho C_p \left(\frac{Vt}{q}\right)^2 (T - T_o)^3 \quad \text{. . . . . II-2}$$

ρC_p = volumetric heat capacity, joules/in^3 °F
t = plate thickness, inches

Adams has also developed peak temperature distribution equations in which time is not a variable. For a thick plate, the peak temperature experienced

at a location r inches away from the weld centerline is given by equation II-3.

$$\frac{1}{T_r - T_o} = \frac{2.72\rho C_p \pi r^2}{q/V} \quad \text{II-3}$$

r = distance from weld centerline
T_r = peak temperature experienced at r for single pass weld

For a thin plate, the peak temperature is given by equation II-4.

$$\frac{1}{T_y - T_o} = \frac{4.13\rho C_p t y}{q/V} \quad \text{II-4}$$

y = distance from plane created by moving line source, inches
T_y = peak temperature experienced at y for single pass weld

By using areas rather than linear dimensions the peak temperature distribution equations can be related to the cross sectional area of the heat affected zone if characterized by etching boundaries corresponding to known peak temperatures. Equation II-5 applies to the thick plate and equation II-6, to the thin plate.

$$\frac{1}{T_c - T_o} - \frac{1}{T_m - T_o} = \frac{2.72\rho C_p A_z}{q/V} \quad \text{II-5}$$

$$\frac{1}{T_c - T_o} - \frac{1}{T_m - T_o} = \frac{2.06\rho C_p A_z}{q/V} \quad \text{II-6}$$

T_c = etching boundary defined by lowest critical peak temperature for solid state phase transformation, °F
T_m = etching boundary defined by fusion zone, °F
A_z = area included between two etching boundaries associated with known peak temperatures, in^2

In 1963 Adams found that characteristic etching boundaries in several steels were associated with specific peak temperatures independent of heating and cooling rates, at least over the range of conditions encountered in submerged-arc welding. The significance of this finding is that, given a heat affected zone of area A_Z existing between the fusion boundary and a known critical peak temperature, the effective amount of heat which has entered the plate could, in principle, be calculated. This effective amount of heat could, in turn, be used to calculate the peak temperature at any location outside the fusion zone.

Up to 1963 the experiments conducted by Adams and coworkers[4,5,6] were chiefly performed with the objective of testing the equations since serious simplifications were involved, mainly: (1) thermal properties were assumed constant, and (2) the heat source was assumed infinitesimally small. They found the equations to be reliable when carefully used.

In 1966 Parker [7] completed a series of experiments in which he applied the peak temperature distribution equation for a thick plate to results obtained from a variety of welding processes and configurations. Among his findings were calculated values of the effective energy input for bead on plate submerged-arc welds considerably lower than those obtained by Adams.[4,5,6] Parker based his calculations on measurements of the heat affected zone and derived ratios of calculated energy inputs to actual energy inputs in the order of 0.3 to 0.6. By measuring peak temperatures experienced at edge locations and bottom centerlines, Adams found this same ratio to be in the order 0.8. Both sets of experiments were bead on plate submerged-arc welds consequently, the peak temperature distribution equation should have led to similar values of the

calculated to actual energy input ratio. The fact that these ratios differ lead to the presumption that the peak temperature distribution equation for thick plates (equation II-5) is considerably less accurate when applied to the heat affected zone than when applied further away as was done by Adams.

Upon completion of Parker's work the situation could be summarized as follows:

(1) Cooling rate equations can be considered accurate when applied to locations close to the fusion boundary for temperatures below the melting point of the metal.

(2) The peak temperature distribution equation for two dimensional heat flow is accurate when applied to locations far from the weld centerline.

(3) For thick plates, the peak temperature distribution equation is in considerable error when applied within the heat affected zone.

III. EXPERIMENTAL PROCEDURE

A. Apparatus

The apparatus used for welding can be broken down into three independent components; these are: the power supply, the wire drive, and the travel speed control.

1. Power supply -- The power supply is a direct current constant amperage unit with an output of approximately 700 amperes at 38 volts; its open circuit voltage setting can be varied continuously from approximately 15 to 42 volts.

2. Wire drive -- Amperage is controlled through control of the wire feed rate. For a given wire feed rate and given open circuit voltage setting on the power supply, the amperage-voltage combination to occur upon welding will depend upon the slope characteristics of the power supply and upon the overall resistance of the circuit.

3. Travel speed control -- Travel speed is controlled independently of the wire drive and power supply. The welding head and wire drive are supported by a carriage which moves on a rail.

The significance of a three component approach in running a weld is that two points of view can be considered. A weld can either be considered from the standpoint of metal deposition and characteristics of the reinforcement or from the standpoint of energy input and consequent thermal events. A step by step outline of materials used and of the experimental procedure follows.

B. Materials and Materials Preparation

1. Steel plates -- HY-80 steel plates from the United States Steel Corporation were flame cut into pieces 4 inches by 10 inches. These

plates (1 inch thickness) had mill scale which was believed not to affect results. A few test runs have indicated that mill scale has no noticeable effect upon thermal events. Table I lists the nominal composition of HY-80 steel.

2. Filler wire -- Three wire sizes were used (1/16, 3/32, and 1/8 inch diameter) from two manufacturers - A675 (from AIRCO) and Oxweld 40 (from LINDE). The wires were essentially the same, low carbon copper flashed steel. Table I lists the nominal composition of the wires.

TABLE I -- Nominal composition of the base metal and filler wires used (w/o)

Material	C	Mn	Ni	Cr	Mo	V	Si	Ti	S	P
HY-80	0.14	0.26	2.54	1.25	0.40	0.001	-	0.002	-	-
A675	0.10	1.10	-	-	-	-	0.50	-	0.035	0.025
Oxweld40	0.15	2.00	-	-	0.50	-	0.03	-	0.024	0.017

3. Flux -- Unionmelt 50 was used as fluxing material. This flux can be considered of medium viscosity in the range of viscosities commercially available for submerged arc welding.

C. Welding Procedure

Due to the importance of preheat, samples were allowed to cool for one day after flame cutting. Welding consisted in centering the plate on two rails, adjusting the nozzle to plate distance, clamping the ground on to the plate, covering the plate with flux, and turning on the weld control. Once the bead ran the length of the plate, power was turned off.

C. Instrumentation

Amperage and voltage were measured with a D. C. Millivoltmeter and D. C. Voltmeter to an accuracy of $\pm$ 1 Mv and 1/2 volt respectively

(± 25 amps and 1/2 volt respectively). The wire feed rate was determined from R.P.M. readings of the drive shaft. Tachometer readings were calibrated directly to the wire feed rate.

E. Data

1. Preparation of samples for area measurements -- Two transverse sections (four different cross sections) were cut from each plate by means of a cutting wheel and macro etched with Nital of 3 to 10 percent concentration. Etching revealed the presence of two phase boundaries: (1) a fusion boundary corresponding to a peak temperature of 2750 °F and a boundary separating metal which has undergone a solid state phase change from metal which has been untransformed corresponding to a peak temperature, found by Adams, of 1300 °F.[5]

2. Bead measurements -- Areas and linear dimensions were obtained from photographs of the welds. Areas were measured by means of a conventional planimeter accurate to within ± 5 percent.

F. Summary of Welding Conditions

Table II lists the welding conditions applicable to results presented in chapter IV. All results presented deal with welds satisfying the requirements for thick plate conditions. Thin plates are a different problem and do not present heat transfer difficulties encountered with thick plates.

TABLE II - Summary of welding conditions

Base Material - HY-80 steel from U.S.Steel, 1" x 4" x 10"

Filler Wire - Oxweld 40 (LINDE) and A675 (AIRCO) - copper flashed

Wire Sizes - 1/16, 3/32, and 1/8 inch diameter

Flux - Uniomelt 50

Reverse Polarity (electrode Positive)

Preheat - 70 °F $\pm$ 5 °F

Configuration - bead-on-plate, thick plate conditions.

Voltage Range - 20 to 41 Volts

Amperage Range - 250 to 1000 amperes

Travel Speed Range - 6 to 80 inches per minute

Nozle Heights - 0.375, 0.50, and 0.75 inches

Angle of Incidence of Wire - trailing, 25° from vertical

IV. RESULTS

A. Theoretical

The equation for the temperature distribution when a point source releases an amount of energy $\rho C_p Q$ at time t equal to zero in an infinite solid [1] is given by equation IV-1.

$$T - T_o = \frac{Q\, e^{-[(x-x')^2+(y-y')^2+(z-z')^2]/4\alpha t}}{4(\pi\alpha t)^{3/2}} \quad \text{IV-1}$$

x', y', z'	--	coordinates of the point source
x, y, z	--	coordinates at which the temperature T is to be determined
α	--	thermal diffusivity
t	--	time
Q	--	strength in °F or °C per unit volume
ρC_p	--	volumetric heat capacity

An instantaneous line source, and a plane source, can be obtained by integrating along one or two coordinates respectively.

For an instantaneous line source , the equation becomes

$$T - T_o = \frac{Q\, e^{-[(x-x')^2+(y-y')^2]/4\alpha t}}{4\pi\alpha t} \quad \text{IV-2}$$

Q -- strength in °F or °C per unit area

Equations for both a moving continuous point source and a moving continuous line source can be obtained by using the variables $[x-V(t-t'), y, z]$ (V is the travel speed) and integrating in time.

Adams [3] has developed two equations for the peak temperature distribution around a point or line source moving in a straight line

at constant velocity V in a solid of uniform properties constant with temperature. These equations, presented in chapter II, are:

thick plate $$\frac{1}{T_c - T_o} - \frac{1}{T_m - T_o} = \frac{2.72\ \rho C_p A_z}{q/V} \quad \text{II-5}$$

thin plate $$\frac{1}{T_c - T_o} - \frac{1}{T_m - T_o} = \frac{2.06 \rho C_p A_z}{q/V} \quad \text{II-6}$$

The theoretical energy requirement to produce a given size heat affected zone in HY-80 steel based on etching boundaries corresponding to peak temperatures of 1300 °F and 2750 °F can be calculated from equations II-5 and II-6. The introduction of these two peak temperatures leads to the following two equations:

thick plate $$\frac{q}{V} = 6180\ \rho C_p A_z \quad \text{IV-3}$$

thin plate $$\frac{q}{V} = 4695\ \rho C_p A_z \quad \text{IV-4}$$

q/V -- energy input, joules/in
ρC_p -- volumetric heat capacity, joules/in^3°F
A_z -- heat affected zone, in^2

These equations predict that for a given energy input, the heat affected zone will be approximately 30 percent larger in a thin plate than in a thick plate.

In equations IV-3 and IV-4 numerical values for ρC_p have been purposely left out because C_p undergoes a strong variation with temperature. Adams has developed a means of overcoming this difficulty by calculating an average specific heat ($\overline{C_p}$) for a given peak temperature.[5] For the two temperatures of interest $\overline{C_p}$ equals 0.135 BTU/lb °F when the peak temperature is 1300 °F and, 0.160 BTU/lb °F when the peak temperature

is 2750 °F. By taking into account these two values for the heat capacity and for the density, equations IV-3 and IV-4 become:

thick plate $\frac{q}{V} = 293{,}000\ A_z$ IV-5

thin plate $\frac{q}{V} = 222{,}500\ A_z$ IV-6

Parker,[7] by using the room temperature density (0.284 lb/in^3) and a heat capacity of 0.167 BTU/lb °F, came to the following equation for the heat affected zone under thick plate conditions:

$$\frac{q}{V} = 310{,}000\ A_z \quad \text{. . . . . IV-7}$$

The significance of equation IV-7 is that, given two etching boundaries, the peak temperature at any location inside the two boundaries, and possibly outside, can be determined. This information can be of valuable metallurgical interest when investigating such phenomena as hot cracking or constitutional liquation.

It should be clearly understood that the coefficient 310,000 is based on a peak temperature distribution derived from the point source model and as such, its validity is warranted only to the extent that the point source model is reasonable when considering thermal events in the heat affected zone.

In order to determine whether thick plate conditions apply, Adams [6] devised the following criterion: at a location 2t (t is the plate thickness) away from the weld centerline, the peak temperature experienced on the top surface of the plate is substantially the same as that experienced directly below on the bottom surface. For a one inch thick plate, the

criterion for thin plate conditions would simply be two inches away from the weld centerline independent of the energy input. Measurements of weld dimensions presented in section B of this chapter fall well within the two inch criterion.

The point source and line source approach presented so far is not the only means of bridging the gap between experimental results and heat transfer theory. Chapter V presents a new model. A continuous line source of finite length travels in the direction of its own length on the surface of a semi-infinite solid.

B. Experimental

Six directly measurable quantities can be readily identified on the cross-section of a bead-on-plate submerged-arc weld (Figure 1); these are:

1) A_z = Portion of base metal adjacent to the weld which has undergone a phase transformation due to heating above a critical temperature.
2) A_m = Cross-sectional area of molten and resolidified base metal.
3) D_w = Bead width
4) D_p = Penetration
5) A_r = Cross-sectional area of reinforcement

This part of Chapter IV covers empirical correlations between the following experimental variables and weld dimensions itemized above:

I	= Amperage	H_n	= Nozzle Height
E	= Voltage	W_d	= Wire Diameter
V	= Travel Speed	A	= Angle of incidence of the filler wire upon the base plate.

Although of important character, the following experimental variables were not investigated:

1) Preheat
2) Joining configuration
3) Properties of the materials used.
4) Types of consumable electrode welding processes other than submerged-arc.
5) Multipass welding.

Empirical equations have been obtained. These fully characterize the extent and approximate shape of a weld and the size of its heat affected zone. The results are presented in summary form in Table III.. The derivation of the equations of Table III and the data supporting these derivations constitute the remainder of this chapter. The significance of the results is discussed in Chapter V.

TABLE III -- Empirical equations of weld dimensions

(1) $A_z = 1.22\times10^{-7}\left[\frac{q}{V} - 6{,}000\right]\left(\frac{I}{W_c}\right)^{1/3}$

(2) $A_m = 0.565 D_p D_w e^{12.0A_w}$

(3-1) $D_p = 1.77\times10^{-3}[I - 255]\, e^{-0.0292V} + 0.11$ 1/16"

(3-2) $D_p = 1.21\times10^{-3}[I - 280]\, e^{-0.0206V} + 0.11$ 3/32"

(3-3) $D_p = 1.72\times10^{-3}[I - 460]\, e^{-0.043V} + 0.20$ 1/8"

(4) $D_w = 2.44\times10^{-3} E \left(\frac{I}{V}\right)^{0.555}$

(5-1) $A_m = 2.51\times10^{-6} E \left(\frac{I}{V}\right)^{0.555}\left\{[I - 255]\, e^{-0.0292V} + 62\right\}$ 1/16"

(5-2) $A_m = 1.84\times10^{-6} E \left(\frac{I}{V}\right)^{0.555}\left\{[I - 280]\, e^{-0.0206V} + 91\right\}$ 3/32"

(5-3) $A_m = 2.69\times10^{-6} E \left(\frac{I}{V}\right)^{0.555}\left\{[I - 460]\, e^{-0.043V} + 128\right\}$ 1/8"

(6) $A_r = A_w/V[AI/E + BI^2/E]$ See Table IV for values of A and B.

A_z = Heat affected zone, in^2

A_m = Base plate melting, in^2

$\frac{q}{V} = \frac{60xIE}{V}$, energy input, joules/in

D_p = Penetration, inches

I = Amperes

D_w = Bead width, inches

E = Volts

V = Travel speed, in/min

W_c = Wire circumference, inches

A_w = Cross section of wire, in^2

A_r = Reinforcement, in^2

Heat Affected Zone -- A_z

1. Effect of voltage and of travel speed -- Figures 2 and 3 show the effect which voltage and travel speed respectively have upon the heat affected zone (3/32 inch wire). The following observations can be made:

   a. A_z is linear with q/V; the intercept seems to be 6,000 joules/in on both Figure 2 and figure 3.

   b. The slopes seem to be the same.

   c. Increasing amperage increases the slope.

   d. The exact effect of amperage is not determinable.

2. Effect of nozzle height -- Figure 4 shows that the nozzle height is not a significant variable on runs where amperage is varied. Its effect on runs in which travel speed or voltage are varied remains undetermined.

3. Effect of amperage -- Figure 4 (variable amperage runs) reveals two things:

   a. The slope is radically different than on runs in which travel speed or voltage are varied; compare to figures 2 and 3.

   b. If A_z vs. q/V in Figure 4 is linear, the intercept is considerably greater than the 6,000 joules/in of Figures 2 and 3.

The data for Figure 4 is somewhat misleading in that due to the slope characteristics of the power supply, as amperage increases, voltage decreases (form 40 volts at 400 amperes to 33 volts at 750 amperes). Figure 5 presents the same data, corrected to 38 volts, on log-log coordinates. The correction was made by using Figure 2 and neglecting the amperage effect on the slope (equation IV-8).

$$\Delta A_z = 1.7 \times 10^{-6} [60I/V][38 - E] \quad \text{IV-8}$$

The corrected data (Figure 5) indicates that at 38 volts and 21.2 inches

the heat affected zone is reasonably well represented by an equation of the following form.

$$A_z = C\, I^{4/3} \quad \ldots\ldots\ldots\ldots\ldots\ldots \text{IV-9}$$

By combining this result with the results from Figures 2 and 3, a final equation for the heat affected zone, valid for the 3/32 inch wire, is obtained (equation IV-10).

$$A_z = 1.87\times10^{-7}[q/V - 6{,}000]\, I^{1/3} \quad \ldots\ldots\ldots\ldots \text{IV-10}$$

4. Effect of angle of incidence -- Four runs at constant amperage (Figure 6) do not resolve this issue. If anything, Figure 6 indicates that a trailing angle (nozzle inclined away from the direction of motion of the head) causes a higher heat affected zone than in welds where the nozzle is perpendicular to the base plate. If this issue is to be settled, more data is required.

5. Effect of wire diameter -- Proceeding in the same manner as with the 3/32 inch wire, runs on 1/8 and 1/16 inch wire yield the results as presented by equations IV-11 and IV-12 respectively. In order to simplify the derivation of equations IV-11 and IV-12, certain assumptions

1/16" $$A_z = 1.66\times10^{-7}[q/V - 6{,}000]\, I^{1/3} \quad \ldots\ldots\ldots\ldots \text{IV-11}$$

1/8" $$A_z = 2.01\times10^{-7}[q/V - 6{,}000]\, I^{1/3} \quad \ldots\ldots\ldots\ldots \text{IV-12}$$

were made, as follows:

a. The effect of voltage is equivalent to the effect of the reciprocal of travel speed.

b. The intercept of 6,000 joules/in is independent of wire size.

c. The 1/3 exponent is independent of wire size.

6. Final equation for the heat affected zone -- The validity of the results can best be checked by plotting $A_z/I^{1/3}$ against [q/V - 6,000]. This has been done in Figures 11, 12, and 13 for the three wire sizes. Linearity and slopes close to values obtained before obtain. Results derived from Figures 11, 12, and 13 may be summarized as follows:

Wire Size	Slope	Slope x (Circumference)$^{1/3}$
1/16	2.06×10^{-7}	1.20×10^{-7}
3/32	1.81×10^{-7}	1.21×10^{-7}
1/8	1.72×10^{-7}	1.26×10^{-7}

The figures in the last column agree to within half of one percent. In view of the scatter inherent in the data, it is justifiable to take the average of the last column and assign one equation to the heat affected zone valid for the three wire sizes. By doing this, the empirical equation for the heat affected zone is:

$$A_z = 1.22 \times 10^{-7} [q/V - 6,000] [I/W_c]^{1/3} \quad \ldots\ldots \text{IV-13}$$

q/V - energy input, joules/in
I - amperes
W_c - wire circumference, inches

Plate melted area -- A_m

One of the surprising results obtained is that, regardless of the welding conditions, the plate melted area is directly proportional to the product between bead width and penetration, the constant of proportionality depending uniquely on wire diameter (Figures 14, 15, and 16). The constant of proportionality, tabulated below, was evaluated by least squares on a computer. Equation IV-14 combines the three constants into

one equation.

Wire Size	1/16	3/32	1/8
Constant of Proportionality	0.581	0.625	0.643

$$A_m = 0.565\ D_p D_w\ e^{12.0\ A_w} \quad \text{IV-14}$$

A_m = Plate melted area, in^2
D_p = Penetration, inches
D_w = Bead width, inches
A_w = Cross sectional area of wire, in^2

The relationship between penetration, bead width, and the plate melted area shows that A_m can be derived from equations for penetration and bead width. The derived equation can then be checked against the data to asses its validity.

Penetration -- D_p

1. Effect of amperage -- Penetration was found to be linear with amperage (Figures 17, 18, and 19) with an intercept estimated at 140 amperes.

2. Effect of voltage -- Figure 20 shows the effect of voltage upon penetration. It is apparent that, as presented in Figure 20, voltage does affect penetration. This observation is not quite correct since, for the two runs of Figure 20, it was the wire feed rate which was kept constant and not the amperage. In fact amperage underwent a variation of approximately 50 amperes and 100 amperes in the two runs at 450 amperes and 600 amperes respectively. The effect of this variation upon penetration can be accounted for by using figure 18. The corrected data, plotted in Figure 21, indicates that voltage does have an effect upon penetration, but somewhere below 25 volts; above 25 volts

penetration tends to remain constant. Figure 18 shows that at 450 amperes (38 volts) penetration is 0.24 inches and that at 600 amperes (38 volts) penetration is 0.36 inches. These values compare favorably with those of Figure 21 (0.225 and 0.345 inches respectively).

3. Effect of travel speed -- Data on penetration in runs in which travel speed was varied is not altogether satisfactory. The most successful attempt at obtaining the functional effect of travel travel speed was to plot penetration against travel speed on semi-log coordinates (Figures 22, 23, and 24). The data seems to indicate that penetration approaches an asymptotic minimum as travel speed increases; such a minimum is estimated at 0.11, 0.11, and 0.20 inches for the 1/16, 3/32, and 1/8 inch wire respectively. In Figures 25, 26, and 27 the quantity $[D_p - D_p(\text{min.})]$ is plotted against travel speed on semi-log coordinates. The results are straight lines whose slope depends only on wire size. A look at Figures 22, 23, and 24 shows that the data is not very good, consequently only the best runs have been plotted in Figures 25, 26, and 27. The slopes of these lines are 0.0126, 0.0089, and 0.0186 (min/in) for the three wire sizes (1/16, 3/32, and 1/8 inch respectively).

4. Summary of data on penetration -- The information derived from figures showing the effect of the different variables upon penetration can be combined into three equations, one for each of the wire sizes. The following equations for penetration (valid between 25 and 42 volts to an accuracy of approximately 15 percent) have been obtained:

1/16" $\quad D_p = 1.77\times10^{-3}[I - 255]e^{-0.0292V} + 0.11 \quad \ldots \quad$ IV-15

3/32" $\quad D_p = 1.21\times10^{-3}[I - 280]e^{-0.0206V} + 0.11 \quad \ldots \quad$ IV-16

1/8" $\quad D_p = 1.72\times10^{-3}[I - 460]e^{-0.043V} + 0.20 \quad \ldots \quad$ IV-17

Bead width -- D_w

1. Effect of voltage -- Bead width is plotted against voltage in Figure 28. Although there is scatter in the data, two things stand out:

   a. There is no noticeable resolution between a 450 ampere run and a 600 ampere run.

   b. Bead width is linear with voltage with an intercept estimated at zero.

2. Effect of amperage -- With the help of Figure 28, runs in which amperage was varied were corrected to a constant value of voltage (38 volts). The corrected data is plotted in Figures 29, 30, and 31. These graphs indicate that a single equation is sufficient for the three wire sizes. At constant travel speed (21.2 inches per minute), the equation for bead width, valid for the three wire sizes, is:

$$D_w = 4.11 \times 10^{-4} E(I)^{0.555} \quad \text{IV-18}$$

3. Effect of travel speed -- Bead width is plotted against travel speed in Figures 32, 33, and 34. The data is fairly well represented by an equation of the form:

$$D_w \simeq \frac{C}{V^{0.555}} \quad \text{IV-19}$$

The constant C in equation IV-19 depends upon both amperage and voltage. The exponent in equation IV-19 has the same value as in equation IV-18; this is no accident, it was chosen at 0.555 to make the overall equation for penetration that much simpler. The justification for such a choice is that the value 0.555 falls well within the limit of resolution of the slope.

4. Summary on bead width -- The three sets of graphs presented above can be combined into one equation for bead width, independent of wire size:

$$D_w = 2.44 \times 10^{-3} E \left|\frac{I}{V}\right|^{0.555} \quad \ldots\ldots\ldots\ldots\ldots \text{IV-20}$$

When checked against Figures 32, 33, and 34, equation IV-20 is good to within plus or minus 10 percent of the experimental value.

Plate melted area -- derived equation -- A_m

As mentioned before, an equation for the plate melted area can be derived because of its relationship with bead width and penetration. The following are the derived equations:

1/16" $$A_m = 2.51 \times 10^{-6} E \left|\frac{I}{V}\right|^{0.555} [(I - 255)e^{-0.0292V} + 62] \ldots \text{IV-21}$$

3/32" $$A_m = 1.84 \times 10^{-6} E \left|\frac{I}{V}\right|^{0.555} [(I - 280)e^{-0.0206V} + 91] \ldots \text{IV-22}$$

1/8" $$A_m = 2.69 \times 10^{-6} E \left|\frac{I}{V}\right|^{0.555} [(I - 460)e^{-0.043V} + 128] \ldots \text{IV-23}$$

The experimental data for the plate melted area can serve as an independent test of the accuracy in arriving at empirical equations for penetration and for bead width. Values of A_m calculated from the equations above are plotted against experimental values of A_m in Figures 35 to 40. Figures 35, 36, and 37 deal with runs at constant travel speed (21.2 inches per minute) and Figures 38, 39, and 40, with runs in which travel speed was varied. The six graphs show that the equations predict a fit good to within ten percent of the experimental value.

Figures 35 to 40 do show a consistent pattern: the larger the weld, the larger the calculated value of A_m relative to the experimental value. The cause for this deviation may arise, in part, from an inadequacy in the empirical equation however, it should be noted that the larger the weld, the greater the distortion of the plate upon welding. This distortion is clearly visible in Figure 41. The plate bends such that the top surface is concave resulting in a squeezing out of molten metal which tends to undervalue measurements of A_m and correspondingly overvalue measurements of the reinforcement (A_r). This effect is particularly noticeable in electron-beam welding where a definite reinforcement appears although no filler wire was used.

Wire feed rate (S) and prediction of reinforcement (A_r)

The wire feed rate measured on variable amperage runs (three wire sizes and three nozzle heights) was found, by least squares, to fit an equation of the following form:

$$S = AI/E + BI^2/E \quad \text{IV-24}$$

I = amperage, 300 to 800 amperes
E = voltage, 35 to 42 volts
S = wire feed rate, inches per minute
A = constant which depends on nozzle height and wire size
B = constant which depends on nozzle height and wire size

Equation IV-24 can be used to predict the size of the reinforcement (A_r) by assuming the following:

a. The filler wire and the base plate have the same density.
b. There is no metal loss.
c. There is no distortion of the base plate.
d. There is no slag entrapment nor the formation of any pores.

Based on the above assumptions, an equation which predicts the size of the reinforcement falls out readily (Equation IV-25).

$$A_r = [A_w/V][AI/E + BI^2/E] \quad \text{IV-25}$$

A_r = Reinforcement, in^2
A_w = Wire Size, in^2
V = Travel Speed, inches per minute.

In welding amperage is a dependent variable of welding conditions set by the experimenter. The welder sets the open circuit voltage of the power supply, the nozzle height, the travel speed, and the wire feed rate; amperage is a consequence of these. Due to this dependence, it makes more sense to write equation IV-24 with amperage as dependent variable. This has been done and is presented as equation IV-26. Table IV lists values of A and of B for the three wire sizes at different nozzle heights.

$$I = \frac{\sqrt{4SEB + A^2} - A}{2B} \quad \text{IV-26}$$

Constant wire feed rate runs show that a decrease in voltage is accompanied by a decrease in amperage (Figure 42). Although the nature of the relationship between amperage and voltage is not quite that of equation IV-24, the equation may nevertheless be considered valid between 35 and 42 volts to an accuracy of plus or minus 5 percent.

TABLE IV — Values of the constants A and B in the empirical equation for the wire feed rate.

$$S = \frac{AI}{E} + \frac{BI^2}{E}$$

Wire Size	Nozzle Height	A	B
1/16 inch	0.375"	4.890	0.0360
	0.50"	4.808	0.0412
	0.75"	3.783	0.0564
3/32 inch	0.375"	7.585	0.00126
	0.50"	7.253	0.00218
	0.75"	5.809	0.00644
1/8 inch	0.375"	4.037	0.000762
	0.50"	4.143	0.000759
	0.75"	3.44	0.00223

S — Wire Feed Rate, in/min
I — Amperes, 300 to 800
E — Volts, 35 to 42

Effect of Arc Power upon Reinforcement Configuration

The shape of the reinforcement was found to depend upon the relationship between arc energy input and filler metal deposition. If the arc energy input is less than 1.1 million joules/in^3 times the volume of filler wire deposition per inch of weld then the weld will overlap, i.e. it will have the same shape as the weld shown in Figure 41. Mathematically the criterion for no overlap is:

$$q > 1.1x10^6 A_w S \quad \ldots\ldots\ldots\ldots\ldots \text{IV-27}$$

Since, given the assumptions presented at the bottom of page 24, the product of wire feed rate times the cross-sectional area of the wire equals the product of reinforcement (A_r) times the travel speed equation IV-27 can be transformed to relate energy input to reinforcement (equation IV-28).

$$q/V > 1.1x10^6 A_r \quad \ldots\ldots\ldots\ldots\ldots \text{IV-28}$$

q -- Arc Power, joules/minute
V -- Travel Speed, inches/minute
S -- Wire Feed Rate, inches/minute

It is interesting that the heat requirement for boiling pure iron at one atmosphere pressure should happen to be 1.1x10^6 joules/in^3. The amount of energy involved in welding reflects the possibility of considerable superheat of the weld metal.

V. DISCUSSION OF RESULTS

The ultimate goal in the study of heat flow in welding is to describe the heat source in useful mathematical terms such that it be possible to predict thermal events. It may be necessary to give it shape, intensity and direction. The first attempt at giving the heat source a mathematical interpretation dealt with the continuous point or line source. Under certain conditions peak temperature distributions obtained from these were found reliable, under other conditions, considerably less reliable.

An interesting result obtained from this work is the range of heat transfer efficiencies which the point source equation provided. By measuring peak temperatures at edges and bottom centerlines, Adams (5) found heat transfer efficiencies in the order of 80 percent. Efficiencies calculated with the same equation, based on the heat affected zone (equation IV-7), are in the order of 30 to 60 percent. The discrepancy relates to the fact that close to the fusion zone the heat source cannot be realistically represented by a point source, but must be given a definite shape and possibly, a finite intensity.

By taking the solution to the time dependent differential equation for heat conduction in cylindrical coordinates it is possible to derive a new model applicable to welding. The method consists in determining the temperature distribution produced by a finite line source traveling in the direction of its own length. The empirical equation for the heat

affected zone can then be used to evaluate the kind of results which this model offers; however, before doing this, the model is to be formally presented below.

A solution to the time dependent differential equation for the conduction of heat in a solid of uniform thermal properties is:

$$T - T_o = C_1 I\left(\frac{r}{2\sqrt{\alpha\theta}}\right) \quad \text{V-1}$$

where:

$$I(\eta) \quad \int_{\eta}^{\infty} \frac{e^{-x^2}}{x}\, dx \quad \text{V-2}$$

α = Thermal diffusivity
θ = Time
r = Distance from heat source
T = Temperature at position r and time θ.
T_o = Initial temperature

The properties of the integral are that for η equal to zero, $I(\eta)$ equals infinity, and for η equal to infinity, $I(\eta)$ equals zero.

The model may be interpreted in two ways:

(1) A continuous line source of heat is turned on and allowed to liberate heat at constant rate until the temperature at a certain value of r (defined ξ) reaches the melting point of the metal, at which time the source is turned off.

(2) A line source of finite length travels down its axis liberating heat continuously. As an approximation heat flow parallel to the direction of travel is neglected. The consequence of this assumption is that the nose of the isotherm becomes a parabola.

The two models presented above are equivalent since the length of the heat source in model (1) and the time the heat source is turned on in model (2) are related to each other (equation V-2).

$$\theta = \frac{L}{V} \quad \ldots\ldots\ldots\ldots\ldots\ldots \text{V-2}$$

L - Length of the heat souce, model (1)
θ - Length of time that the heat source is turned on, model (2)
V - Travel speed

The quantity of heat conducted away per unit length into the solid at time θ from a location at which the temperature equals that of the melting point of the metal is:

$$\frac{Q_c}{L} = \int_{\xi}^{\infty} (T - T_o)\rho C_p 2\pi r dr \quad \ldots\ldots\ldots\ldots \text{V-3}$$

Equations V-1 and V-3 can be combined, then:

$$\frac{Q_c}{L} = 2\pi\rho C_p C_1 \int_{\xi}^{\infty} r\, I\left(\frac{r}{2\sqrt{\alpha\theta}}\right) dr \quad \ldots\ldots\ldots\ldots \text{V-4}$$

C_1 can be obtained by fitting the condition that at r equal to ξ, the temperature must equal that of the melting point of the metal, then:

$$T_m - T_o = C_1\, I\left(\frac{\xi}{2\sqrt{\alpha\theta}}\right) = C_1\, I(\beta) \quad \ldots\ldots\ldots \text{V-5}$$

then:

$$\frac{Q_c}{L} = 2\pi\rho C_p \frac{(T_m - T_o)}{I(\beta)} \int_{\xi}^{\infty} r\, I\left(\frac{r}{2\sqrt{\alpha\theta}}\right) dr \quad \ldots\ldots\ldots \text{V-6}$$

The integral in equation V-6 can be readily solved by parts; after re-aranging the result is:

$$\frac{Q_c}{L} = 4\pi K\theta (T_m - T_o)\beta^2 \left[\frac{1}{2\beta^2 e^{\beta^2} I(\beta)} - 1\right] \quad \ldots\ldots \text{V-7}$$

K - Thermal conductivity
$\beta = (\xi/2\sqrt{\alpha\theta})$

Since the quantity in brackets is to appear on several occasions, it is now defined such that:

$$U(\beta) = \left[\frac{1}{2\beta^2 e^{\beta^2} I(\beta)} - 1 \right] \quad \text{V-8}$$

The energy input required for melting is defined as follows:

$$\frac{Q_m}{L} = \pi \xi^2 H_m = 4\pi\beta^2 \alpha\theta H_m \quad \text{V-9}$$

H_m - Energy required to melt a unit volume of metal initially at room temperature.

Equation V-7 can be divided by equation V-9 and the result simplified, (equation V-10).

$$\frac{Q_c}{Q_m} = \frac{\rho C_p (T_m - T_o)}{H_m} U(\beta) = \frac{H_c}{H_m} U(\beta) \quad \text{V-10}$$

H_c - Energy requirement per unit volume to raise the temperature of the solid from room temperature to its melting point without melting.

A new parameter will now be defined and β recalled:

$$\gamma = \frac{r_1}{2\sqrt{\alpha\theta}} \qquad \beta = \frac{\xi}{2\sqrt{\alpha\theta}}$$

r_1 - Location at which the temperature equals the critical temperature.

ξ - Location at which the temperature is at the melting point of the metal (2750 °F).

γ and β are related to each other by the temperature distribution equation (equation V-1) such that:

$$\frac{T_1 - T_o}{T_m - T_o} = \frac{I(\gamma)}{I(\beta)} \quad \text{or} \quad I(\gamma) = 0.459\, I(\beta) \quad \text{V-11}$$

$T_1 = 1300$ °F; $T_m = 2750$ °F; $T_o = 70$ °F

γ and β are also related in the following way:

$$\frac{A_z}{A_m} = \frac{\gamma^2-\beta^2}{\beta^2} = \frac{\gamma^2}{\beta^2} - 1$$

or

$$\frac{\gamma}{\beta} = \left| \frac{A_z}{A_m} + 1 \right|^{1/2} \quad \text{V-12}$$

Due to the requirement that the ratio of $I(\gamma)$ to $I(\beta)$ must equal 0.459, a value of the ratio γ/β leads to a unique value of γ and a unique value of β (Figure 43).

Up to this point the mathematics have only served to present the model. The energy requirement for welding is derived from equation V-10 as follows:

$$\frac{Q_t}{L} = \frac{Q_c+Q_m}{L} = \left| \frac{Q_c}{Q_m} + 1 \right| \frac{Q_m}{L} \quad \text{V-13}$$

Q_t/L = energy input per unit length of weld.

$$\frac{Q_t}{L} = \left| \frac{H_c}{H_m} U(\beta) + 1 \right| \frac{Q_m}{L}$$

then:

$$\frac{Q_t}{L} = \left| \frac{H_c}{H_m} U(\beta) + 1 \right| A_m H_m \quad \text{V-14}$$

If β is known from equation V-12 and Figure 43, and A_m is known, the length of the heat source can be calculated from the defining equa-

tion for β. Then,

$$L = \frac{A_m V}{2\pi\alpha\beta^2} \quad \text{V-15}$$

Once the length of the heat source has been obtained from equation V-15, the intensity can be calculated by dividing the real arc power by the length of the heat source.

The mathematics have now been presented. The finite line source model makes use of experimental data to get at information about the effective characteristics of the heat source. Two things are of interest: the intensity of the heat source and β, which is now called the shape factor. If these two parameters are known as a function of welding conditions, the physical characteristics of the weld fall right out.

The intensity of the heat source, the shape factor (β), the length of the heat source, and the heat transfer efficiency (ratio of calculated to actual energy input in percent) are all calculable from values of the area of the heat affected zone and of the fusion zone. The calculation can be done as follows (shown in outline form):

1. The ratio A_z/A_m defines a unique value of β by use of equation V-12 and Figure 43.
2. Given A_m and β, Q_t/L can be calculated form equation V-14 and Figure 44.
3. L is calculated from equation V-15.
4. The intensity of the heat source is calculated by dividing real arc power by the length of the heat source. The intensity has units of watts/inch.
5. The heat transfer efficiency can be calculated in a variety of ways. This is left for latter discussion.

The different definitions of efficiencies are summarized below. Before proceeding into a discussion of their significance, it is necessary to point out that the quantity H_m defined under equation V-9 takes into account superheat of the liquid metal. Based on information obtained by Adams and Paley,[6] the heat content of the liquid metal in the weld zone, refered to room temperature, averages 180,000 joules per cubic inch rather than 160,000. The superheat corresponds to a temperature approximately 400 °F above the melting point of iron. During the course of the same work, Adams and Paley found the heat transfer efficiency in bead on plate submerged arc welding, based on peak temperatures at edges and bottom centerlines, to be in the order of 75 percent. This value of the heat transfer efficiency can be used as point of reference in evaluating the finite line source model. Table V lists efficiencies defined in different ways and Tables VI, VII, and VIII present quantitative values of these efficiencies and of other derived quantities.

The heat transfer efficiency does not necessarily have to be 100 percent in order that a given model be considered fully representative of heat transfer in welding. On the contrary, thermal events in welding are associated with high temperature heat consequently, only this heat should be considered in the heat transfer efficiency. The heat associated with melting of the slag and possibly, the heat content of the reinforcement, may have to be discounted since these may affect thermal events only some time after the establishment of a peak temperature distribution in the heat affected zone. Tables VI, VII, and VIII show that in all cases the heat transfer efficiency based on the finite line source model is considerably larger than the heat transfer efficiency based on the point source model. This

Table V -- Definitions of efficiencies

f_1 -- Plate melting efficiency

$$f_1 = 100\frac{180{,}000A_m}{(q/V)_o}$$

$f_{2,P}$ -- Heat transfer efficiency based on the point source model

$$f_{2,P} = 100\frac{310{,}000A_z}{(q/V)_o}$$

$f_{2,L}$ -- Heat transfer efficiency based on the finite line source model, discounts melting and superheat of the filler wire.

$$f_{2,L} = 100\frac{(Q_c + Q_m)/L}{(q/V)_o - 180{,}000A_r}$$

$(q/V)_o$ - Actual arc energy input, joules/in

$(Q_c + Q_m)$ - Energy input from equation V-14

Values of the physical constant inherent in the above definitions --

T_o - 70°F T_c - 1300°F T_m - 2750°F

H_c - 126,000 joules/in^3 H_m - 180,000 joules/in^3

ρC_p - 50 joules/in^3 α - 0.01 in^2/Sec

I amps	V in/min	A_z in^2	A_m in^2	A_r in^2	β ---	q/L watts/in	L in	f_1 %	$f_{2,P}$ %	$f_{2,L}$ %	$\frac{Q_c+Q_m}{L}$ joules/in	q/V joules/in
800	5	0.644	0.787	0.529	0.710	13,600	2.06	41.9	59.4	107.1	254,000	336,000
	20	0.152	0.248	0.132	0.875	16,250	1.72	53.2	51.1	117.3	70,700	84,000
	60	0.043	0.058	0.044	0.775	18,200	1.54	37.3	47.5	85.5	17,800	28,000
650	5	0.486	0.530	0.359	0.660	14,100	1.61	34.9	55.8	86.4	181,500	273,000
	20	0.114	0.170	0.090	0.830	17,400	1.31	44.9	51.8	95.9	50,000	68,250
	60	0.030	0.043	0.030	0.800	21,200	1.07	34.1	41.6	74.8	13,000	22,750
500	5	0.344	0.311	0.216	0.575	14,000	1.25	26.3	50.1	67.8	117,800	212,500
	20	0.077	0.104	0.054	0.770	18,800	0.93	35.8	45.7	74.6	31,900	52,500
	60	0.019	0.030	0.018	0.855	26,800	0.65	30.8	33.8	61.7	8,660	17,500

Table VI -- Calculations based on the finite line source model, 1/16 inch wire.

I	V	A_z	A_m	A_r	β	q/L	L	f_1	$f_{2,P}$	$f_{2,L}$	$\frac{\theta_c + \theta_m}{L}$	q/V
amps	in/min	in^2	in^2	in^2	---	watts/in	in	%	%	%	joules/in	joules/in
	5	0.564	0.606	0.187	0.650	14,750	1.90	32.4	52.6	69.6	210,500	336,000
800	20	0.133	0.215	0.047	0.870	18,550	1.51	46.1	49.1	80.9	61,400	84,000
	60	0.038	0.066	0.016	0.925	22,800	1.22	42.3	41.6	72.4	18,200	28,000
	5	0.427	0.422	0.148	0.630	15,950	1.42	27.8	48.5	60.8	150,000	273,000
650	20	0.100	0.150	0.037	0.830	19,600	1.16	39.6	45.4	71.6	44,200	68,250
	60	0.027	0.048	0.012	0.925	25,400	0.90	38.2	36.5	65.0	13,350	22,750
	5	0.301	0.241	0.109	0.525	14,900	1.17	20.4	43.9	51.7	99,500	212,500
500	20	0.679	0.091	0.027	0.770	21,400	0.82	31.4	40.1	59.0	28,100	52,500
	60	0.017	0.032	0.009	0.960	30,200	0.56	33.5	29.7	55.5	8,800	17,500

Table VII -- Calculations based on the finite line source model, 3/32 inch wire.

I amps	V in/min	A_z in^2	A_m in^2	A_r in^2	β ---	q/L watts/in	L in	f_1 %	$f_{2,P}$ %	$f_{2,L}$ %	$\frac{Q_c+Q_m}{L}$ joules/in	q/V joules/in
800	5	0.515	0.634	0.290	0.715	17,000	1.64	33.9	47.5	72.2	204,500	336,000
	20	0.121	0.199	0.072	0.875	20,300	1.38	42.6	45.0	80.0	56,700	84,000
	60	0.034	0.061	0.024	0.915	24,100	1.16	39.2	38.0	71.7	16,950	28,000
650	5	0.384	0.397	0.210	0.630	17,100	1.33	26.2	43.6	60.0	141,000	273,000
	20	0.090	0.135	0.053	0.830	21,900	1.04	35.6	40.9	67.6	39,700	68,250
	60	0.024	0.050	0.018	0.990	27,600	0.82	39.9	32.8	68.9	13,500	22,750
500	5	0.273	0.196	0.158	0.480	15,450	1.13	16.6	39.8	48.1	88,600	212,500
	20	0.061	0.081	0.039	0.760	23,400	0.75	28.0	36.3	55.8	25,300	52,500
	60	0.015	0.040	0.013	1.100	30,300	0.58	43.3	26.9	66.9	10,130	17,500

Table VIII — Calculations based on the finite line source model, 1/8 inch wire.

finding alone substantiates the conclusion that the finite line source model offers a more accurate prediction of thermal events within the heat affected zone. At low travel speeds the improvement is not much greater however, at high travel speeds (60 inches per minute) the improvement is very significant. Of the two heat transfer efficiencies listed, the more significant is the heat transfer efficiency based on the finite line source model [$f_2(L)$]. $f_2(L)$ covers a range which is considerably closer to the 75 percent reported by Adams [6] than the heat transfer efficiency based on the point source model [$f_2(P)$]. Moreover, at times the heat transfer efficiency based on the point source model yields results which are inconsistent - it is not possible that the plate melting efficiency be higher than the heat transfer efficiency because the total ammount of high temperature heat should be higher than the amount required to melt a given ammount of the base plate. Due to these two considerations: 1) that the heat transfer efficiency based on the finite line source is generally in closer agreement to Adams previous work and 2) that this same heat transfer efficiency is never smaller than the plate melting efficiency, it is possible to conclude that the finite line source model is a more realistic model of thermal events close to the fusion zone than the point source model.

The calculations on $f_2(L)$ reveal the existence of two trends, listed below:

1. An increase in amperage increases $f_2(L)$.
2. Welds with abnormally large reinforcements have abnormally high efficiencies.

A possible cause for these two trends may be attributed to the effect

of convection. The reasoning underlying the form of the denominator in $f_2(L)$ is that the heat content of the reinforcement should not be considered as high temperature heat. In welds with abnormally large reinforcements (welds made with a 1/16 inch wire), the wire is fed in at a rate close to 1000 inches per minute. This causes the weld pool to be violently stirred and the weld to have the configuration of Figure 41 - (d). The violent stirring probably causes heat contained in the reinforcement and in the slag to be released as high temperature heat. Violent stirring may also cause a decrease in the resistance to heat flow in the liquid region of the solid-liquid interface, thereby contributing to a larger amount of base plate melting and a larger heat affected zone. These two factors taken together may explain the abnormally high values of $f_2(L)$ in Table VI.

Tables VI, VII, and VIII also show that an increase in amperage increases the heat transfer efficiency $[f_2(L)]$. It is possible to deduce from the reasoning of the previous paragraph that convection is again the cause behind the increase in $f_2(L)$ with an increase in amperage. Amperage can only be increase by increasing the wire feed rate or drastically increasing the voltage, which is not done. An increase in the wire feed rate means a greater extent of convection. Thus, the combined effect of decreased resistance to heat transfer and the increased importance of the heat content of the reinforcement and of the slag, lead to larger values of the heat transfer efficiency, and sometimes, to unreasonably high values.

Figure 41 shows different weld characteristics. A high heat transfer

efficiency would correspond to Figure 41-(d) and a low heat transfer efficiency, to Figure 41-(a). Figures 41-(b) and 41-(c) correspond to normal heat transfer efficiencies (70 to 80 percent). In going from (b) to (c) it is possible to decrease base plate melting by trading off high temperature for low temperature heat. Nevertheless, the heat transfer efficiency is approximately the same because the denominator in the defining equation for $f_2(L)$ compensates for the trade off through a comparatively larger reinforcement.

It is possible to conclude from the above discussion that, within the range of welding conditions of practical interest, the heat transfer efficiency based on the finite line source model lies between 60 and 80 percent.

The significance of the figures on the shape factor (β), intensity (q/L), and the length of the heat source (L) is not completely clear. The model is only an approximate representation of the actual heat source. It does happen that L is approximately equal to the length of the weld pool within 50 percent consequently, L does have some physical significance.

The shape factor (β), when taken together with velocity, has some physical significance. It has the effect of characterizing the heat source as a moving paraboloid whose shape corresponds to that of the moving isotherms. The location at which the metal is at its melting point (ξ) can be determined by modifying the defining equation for β. Equation V-16 relates ξ to the perpendicular distance from the leading edge of the heat

source (x); see Figure 47. Equation V-16 is valid for values of x from zero to L (the length of the heat source).

$$\xi^2 = \frac{4\beta^2 \alpha x}{V} \quad \text{. . . . . V-16}$$

The intensity (q/L) is a defined quantity introduced for convenience. It is an abstract mathematical term which appears to have some physical significance. Its usefulness derives from the fact that it is related to the ratio A_z/A_m - An increase in q/L will generally cause a decrease in A_z/A_m.

The figures in Tables VI, VII, and VIII reveal the existence of two general trends:

1. The intensity of the heat source, in watts/inch, increases logarithmically with travel speed (Figure 45).
2. The shape parameter β increases linearly with intensity (Figure 46).

These trends present all that is required in predicting the extent of melting and the size of the heat affected zone. Unfortunately the data for Figures 45 and 46 define a rather wide band instead of a line, therefore, if predictions based on β or q/L are derived, they should be taken as approximations. The equations for β and for q/L are:

$$\beta = 0.289 \times 10^{-4}(q/L) + 0.142 \quad \text{. . . . . V-17}$$

$$\frac{q}{L} = 1.05 \times 10^{4}(V)^{0.215} \quad \text{. . . . . V-18}$$

then

$$\beta = 0.314(V)^{0.215} + 0.142 \quad \text{. . . . . V-19}$$

As presented the model offers the possibility of defining a heat source in unambiguous terms - it has definite length and intensity. The model is useful because both the intensity and the shape factor are experimentally linked to the travel speed.

Before closing this discussion it is necessary to point out one important approximation made. The discussion deals with peak temperature distributions whereas the model refers to an instantaneous temperature distribution (equation V-20) at a time equal to L/V.

$$\frac{T_\eta - T_o}{T_m - T_o} = \frac{I(\eta)}{I(\beta)} \qquad \text{V-20}$$

$$\beta^2 = \frac{\xi^2 V}{4\alpha L} \qquad \eta^2 = \frac{r^2 V}{4\alpha L}$$

The problem consists in determining the peak temperature distribution in a solid whose initial temperature distribution is given by equation V-20. Such a problem has been solved. Several calculations show that the instantaneous temperature distribution of equation V-20 and the peak temperature distribution which would obtain a short time latter in the heat affected zone are in good agreement. The mathematics of the calculations are outlined in the appendix.

Conclusions concerning heat conduction in the solid may be summarized as follows:

1. The peak temperature distribution equations based on the moving point source or the instantaneous line source should be considered inaccurate in the heat affected zone due to the low values of heat transfer efficiencies obtained.

2. The mathematical formulation of a new model for the heat source has been presented. One way of representing the heat source is as a continuous line source of finite length traveling in the direction of its length. The length varies from 0.5 to 1.75 inches and the intensity, from 14,000 to 30,000 watts per inch.

3. Based on calculations of the heat transfer efficiency, the finite line source model offers a more realistic peak temperature distribution than that obtained from the point source model.

4. The range of heat transfer efficiencies obtained appears mainly related to the degree of convection in the weld pool.

5. The heat source itself can be represented by a traveling paraboloid whose convexity depends only on the shape factor β and the travel speed.

6. Two general trends based on the finite line source model have been found. Both intensity and the shape factor β are experimentally related to the travel speed, enabling the extent of base plate melting and the size of the heat affected zone to be roughly determined.

VI. SUMMARY AND CONCLUSIONS

1. Empirical equations for bead-on-plate submerged arc weld dimensions and for the cross-sectional area of the heat affected zone have been obtained. The variables investigated are: 1) amperage, 2) voltage, 3) travel speed, and 4) wire size.

2. The cross sectional area of molten base metal is found to be related to the product of penetration times bead width by a constant of proportionality which depends uniquely on wire diameter.

3. Empirical equations for amperage as a function of wire feed rate, wire size, voltage, and nozzle height, have been obtained.

4. Within the range of welding conditions studied, the reinforcement can be made not to overlap the weld by supplying to the arc 1,100,000 joules per cubic inch of filler metal.

5. Heat transfer efficiencies based on the continuous point source peak temperature distribution equation are in the order of 30 to 60 percent. Such low values suggest that the point source peak temperature equation is not reliable in the heat affected zone.

6. The finite line source traveling in the direction of its length offers a definite improvement over the continuous point source model. Two general trends indicate the potential usefulness of the finite line source model.

7. Based on the finite line source model, it is possible to describe the heat source in terms of a shape factor and the travel speed which together define a moving paraboloid. The heat source can be visualized as being a bullet shaped isotherm advancing at velocity V.

VII. SUGGESTIONS FOR FURTHER WORK

1. The form of the empirical equations for penetration should be revised through variable amperage - constant travel speed runs at different levels of travel speed. The purpose of such revision is to reduce the empirical equations for the three wire sizes to one equation.

2. The equations relating amperage to the wire feed rate need to be revised if their range of validity is to extend beyond the 35 to 42 volt limit. It would be helpful to have one equation covering the effect of wire size.

3. Once a strong set of empirical equations for weld dimensions in submerged arc welding has been obtained, their form should be checked against experimental results from other welding configurations, preheats, and processes.

VIII. BIBLIOGRAPHY

1. Carslaw, H.S. and Jaeger, J.C., "Conduction of Heat in Solids," Clarendon Press, Oxford (1959).

2. Rosenthal, D., "Mathematical Theory of Heat Distribution During Welding and Cutting," The Welding Journal, 20(5), Research Supplement, 220-s to 225-s (1941).

3. Adams, C.M., Jr., "Cooling Rates and Peak Temperatures in Fusion Welding," The Welding Journal, 37(5), Research Supplement, 210-s to 215-s (1958).

4. Adams, C.M., Jr., Moffatt, W.G., and Jhaveri, P., "The Effect of Plate Thickness and Radiation on Heat Flow in Welding and Cutting," The Welding Journal, 41(1), Research Supplement, 12-s to 16-s (1962).

5. Barry, J.M., Paley, Z., and Adams, C.M., Jr., "Heat Conduction from Moving Arcs in Welding," The Welding Journal, 42(3), Research Supplement, 97-s to 104-s, (1963).

6. Paley, Z., Lynch, J.M., and Adams, C.M., Jr., "Heat Flow in Welding Heavy Steel Plate" The Welding Journal, 43(2), Research Supplement, 71-s to 79-s (1964).

7. Parker, D.P., "Heat flow in Arc Welding Heavy Steel Plate," Sc.D. Thesis, 1966, Massachusetts Institute of Technology.

APPENDIX

The temperature distribution at time t and position r in cylindrical coordinates in an infinite solid whose initial temperature is given by f(r) is (1)

$$T - T_o = \frac{1}{2\alpha t}\int_o^\infty e^{-(r^2+r'^2)/4\alpha t}\, I_o\left(\frac{rr'}{2\alpha t}\right) f(r')r'dr' \quad \text{. . . . . A-1}$$

I_o - Modified Bessel function of zero order.

The continuous line source of finite length predicts an instantaneous temperature distribution at time θ equal to L/V to be:

$$\frac{T_\eta - T_o}{T_m - T_o} = \frac{I(\eta)}{I(\beta)} \quad \text{. . . . . A-2}$$

$$\eta^2 = \frac{r^2}{4\alpha\theta} \qquad \beta^2 = \frac{\xi^2}{4\alpha\theta}$$

$I(x)$ - Exponential integral on x.

ξ - Location at which the temperature is at T_m at θ equal to L/V.

Equation A-2 can be introduced into equation A-1 in two ways. The integration in equation A-1 can be carried out with equation A-2 from zero to infinity [equation A-3], or with f(r') equal to the quantity $(T_m - T_o)$ for r' between zero and ξ and f(r') equal to $(T_\eta - T_o)$ for r' between ξ and infinity [equation A-4].

$$\frac{T - T_o}{T_m - T_o} = \frac{e^{-r^2/4\alpha t}}{2\alpha t}\int_o^\infty e^{-r'^2/4\alpha t}\, I_o\left(\frac{rr'}{2\alpha t}\right) \frac{I\left(\frac{r'}{2\sqrt{\alpha\theta}}\right)}{I\left(\frac{\xi}{2\sqrt{\alpha\theta}}\right)} r'dr' \quad \text{. . A-3}$$

$$\frac{T - T_o}{T_m - T_o} = \frac{e^{-r^2/4\alpha t}}{2\alpha t}\int_o^{\xi} e^{-r'^2/4\alpha t}\, I_o\left(\frac{rr'}{2\alpha t}\right)\, r'dr'$$

$$+ \frac{e^{-r^2/4\alpha t}}{2\alpha t}\int_{\xi}^{\infty} e^{-r'^2/4\alpha t}\, I_o\left(\frac{rr'}{2\ t}\right)\, \frac{I\left(\frac{r'}{2\sqrt{\alpha\theta}}\right)}{I\left(\frac{\xi}{2\sqrt{\alpha\theta}}\right)}\ r'dr' \quad \ldots \text{A-4}$$

The peak temperature distribution can be obtained by differentiating equation A-3 or A-4 with respect to time at constant r, setting the result equal to zero, and finding the time at which that particular location experiences its peak temperature; the two, introduced into equation A-3 or A-4, will give the peak temperature experienced at the particular location of interest. This exercise has been carried out. The instantaneous temperature distribution given by equation A-2 is, in the heat affected zone, in good agreement with the peak temperature distribution derived from equation A-3 or A-4 within 20 to 30 degrees Fahrenheit.

BIOGRAPHICAL NOTE

The author was born in Paris, France, in 1943. After graduating from the St.Leo College Preparatory School in Florida he entered the Massachusetts Institute of Technology from which he received the degree of Bachelor of Science in June of 1964. In September of 1964 he entered the Cornell Law School from which he withdrew after several months. In February of 1965 he entered the Sloan School of Industrial Management at the Massachusetts Institute of Technology as Special Graduate Student and in September of 1965 became a Regular Graduate Student in the Department of Metallurgy.

The author is a member the American Institute of Metallurgical Engineers, of the American Society of Metals, and of the American Welding Society.

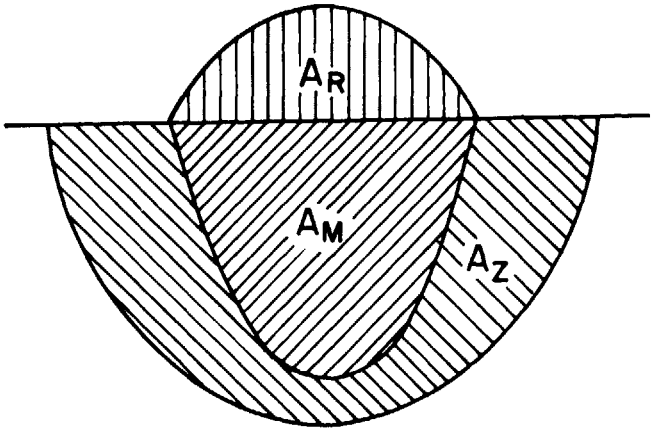

Area measurements

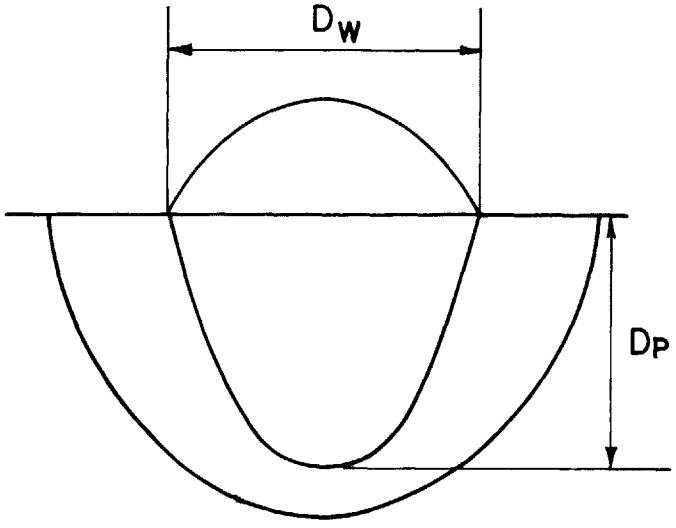

Linear measurements

Figure 1. Weld dimensions

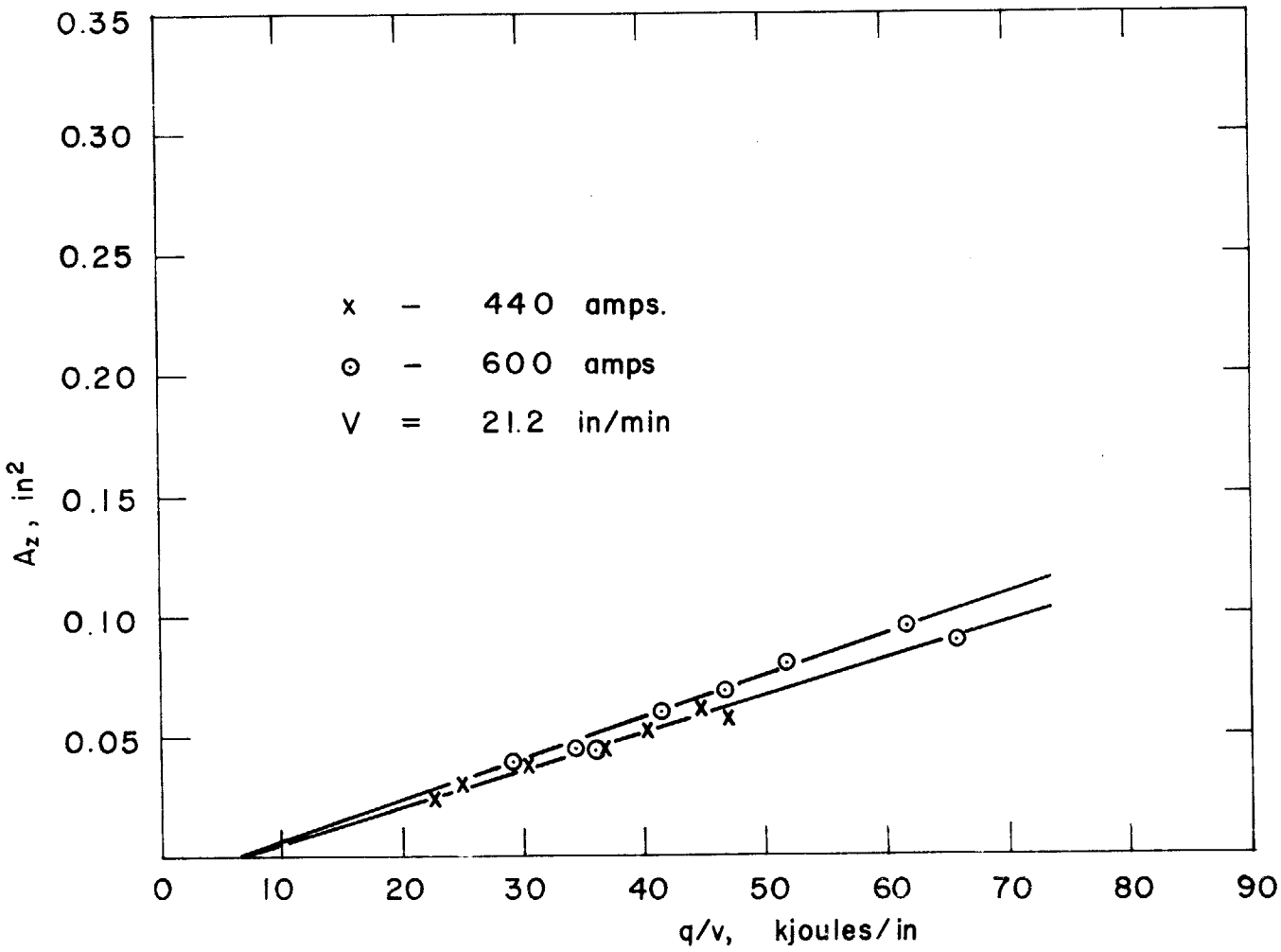

Figure 2. Heat affected zone vs. energy input, 3/32 inch wire variable voltage runs.

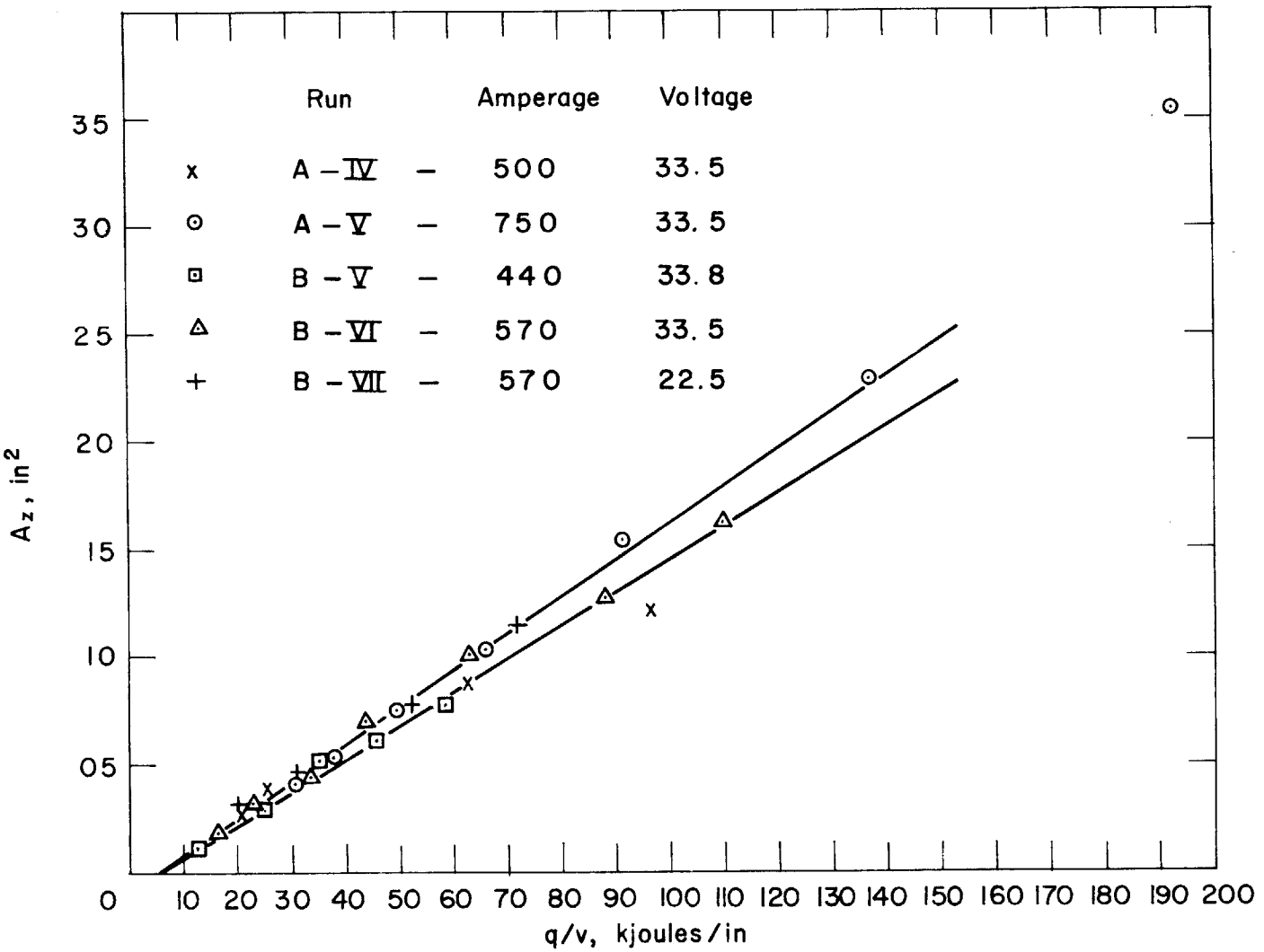

Figure 3. Heat affected zone vs. energy input, 3/32 inch wire, variable travel speed runs.

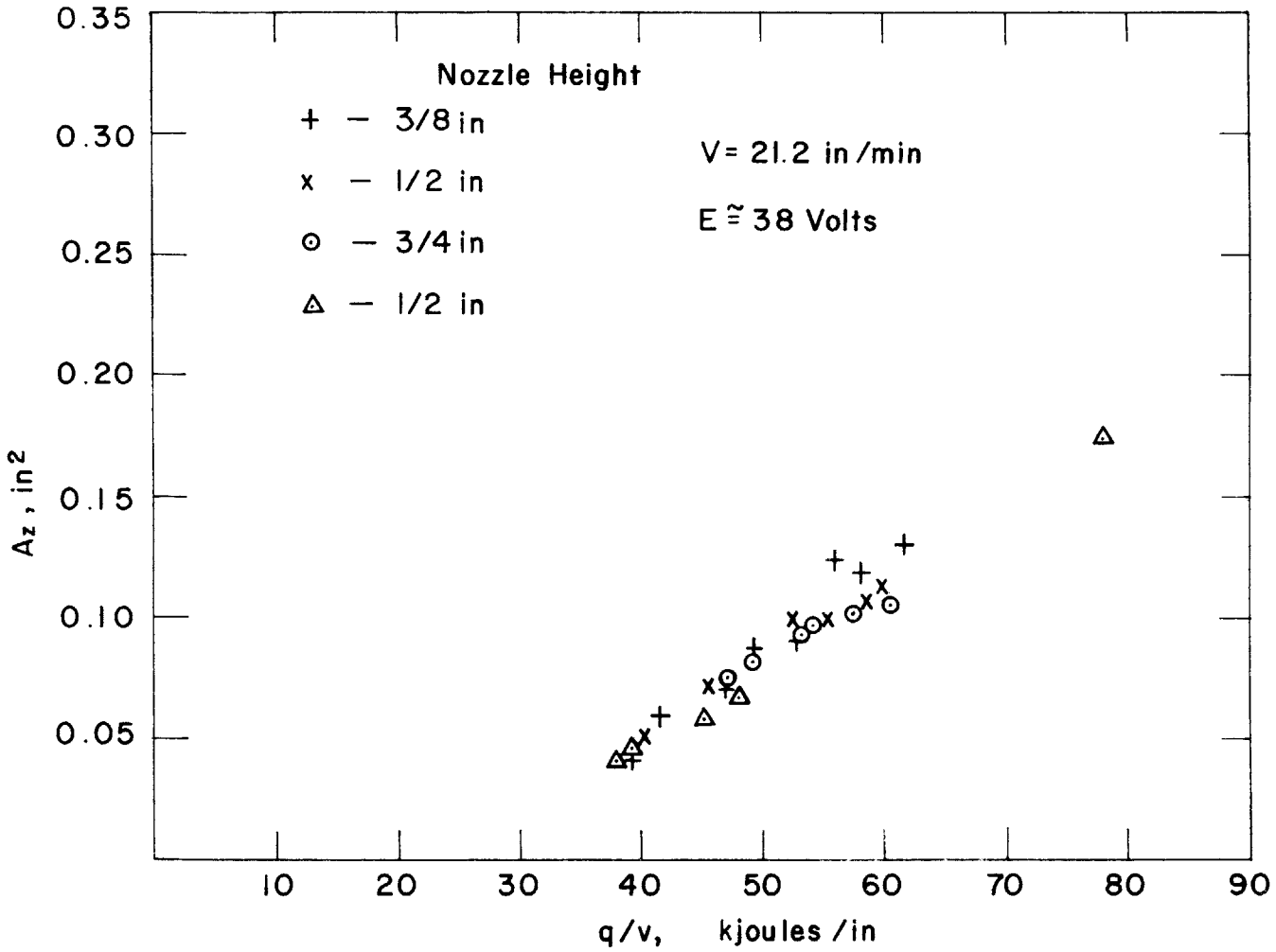

Figure 4. Heat affected zone vs. energy input, 3/32 inch wire.
Effect of amperage at different nozzle heights.

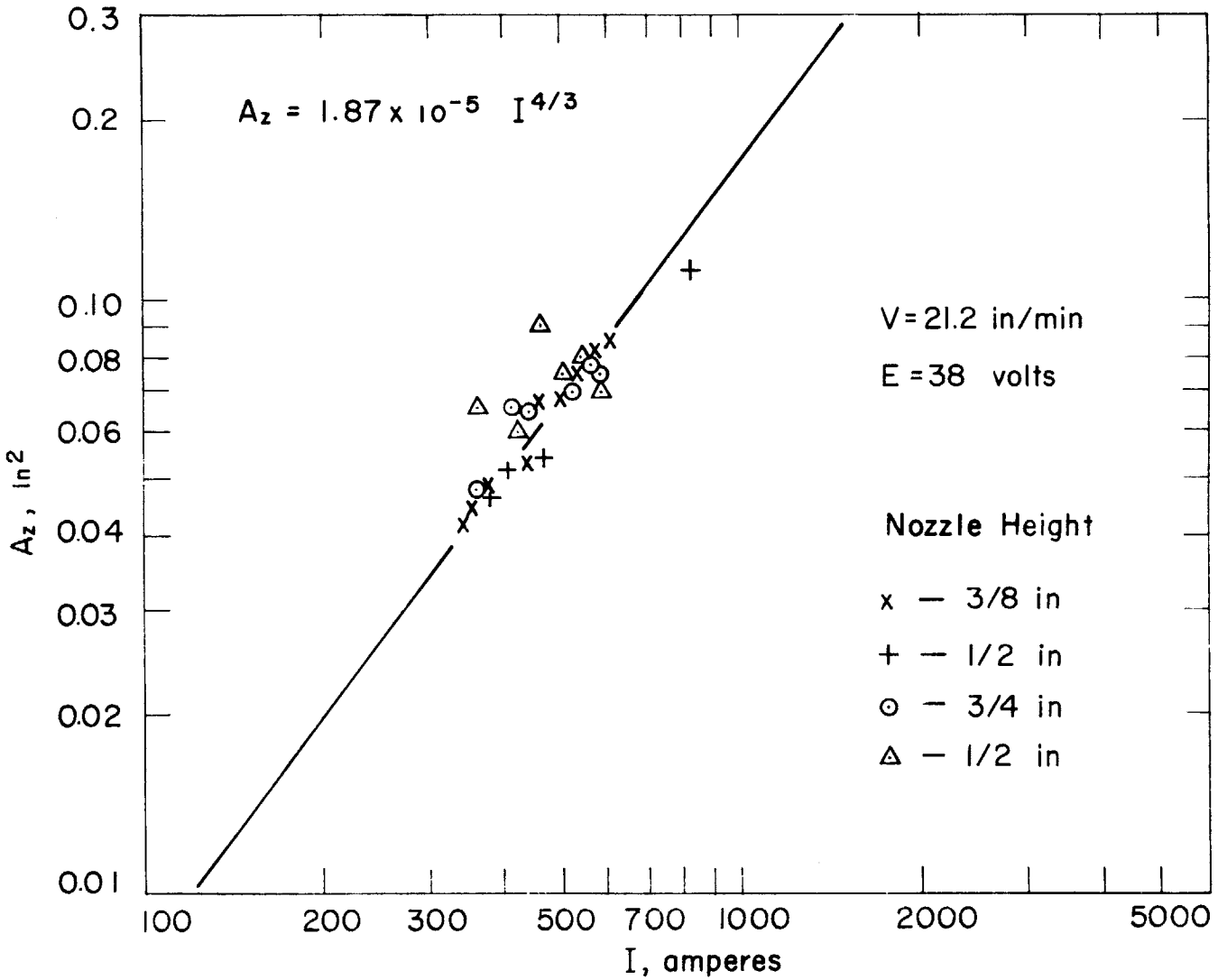

Figure 5. Heat affected zone vs. amperage - 3/32 inch wire. Az adjusted to constant value of voltage.

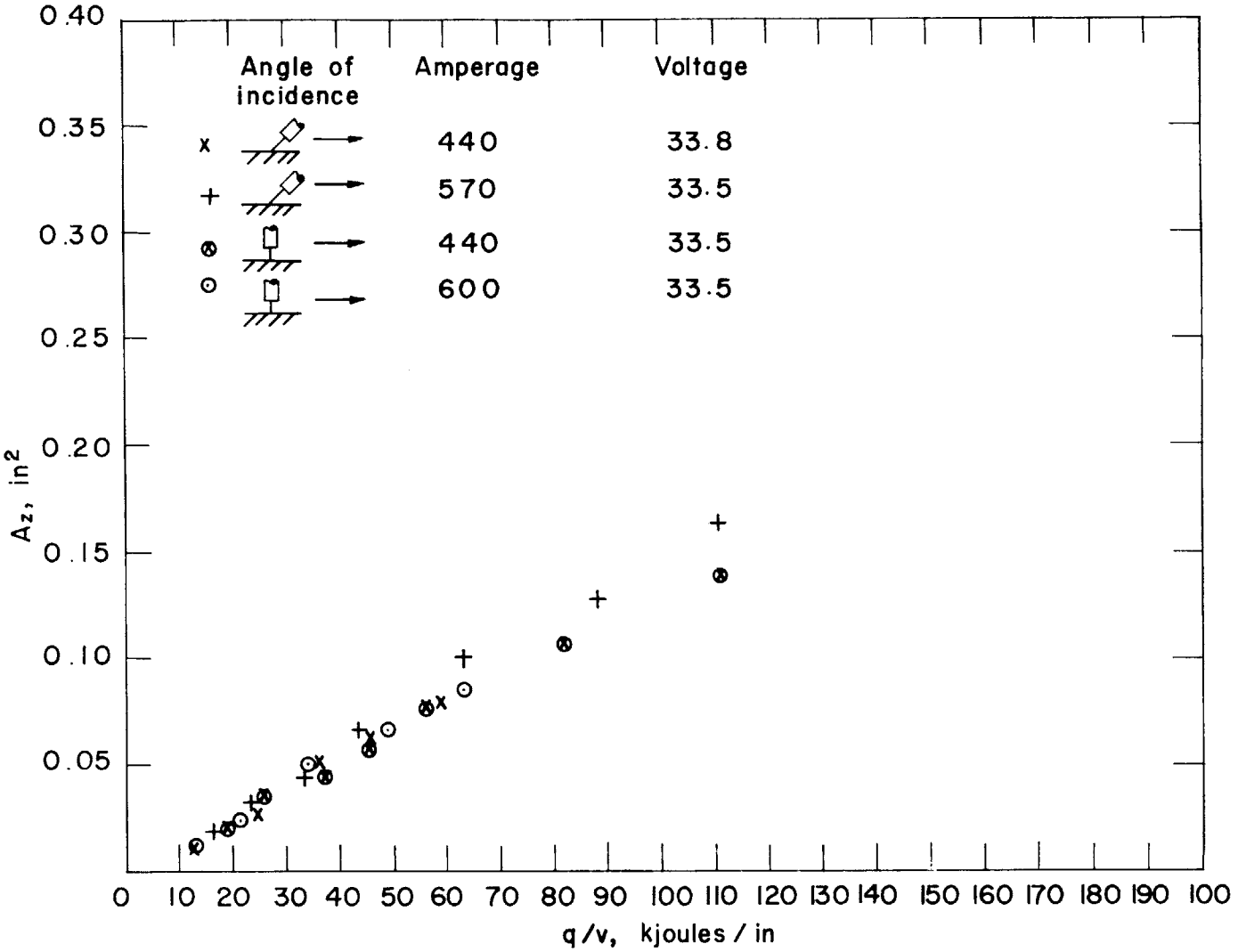

Figure 6. Effect of angle of incidence upon the heat affected zone, 3/32 inch wire, travel speed varied.

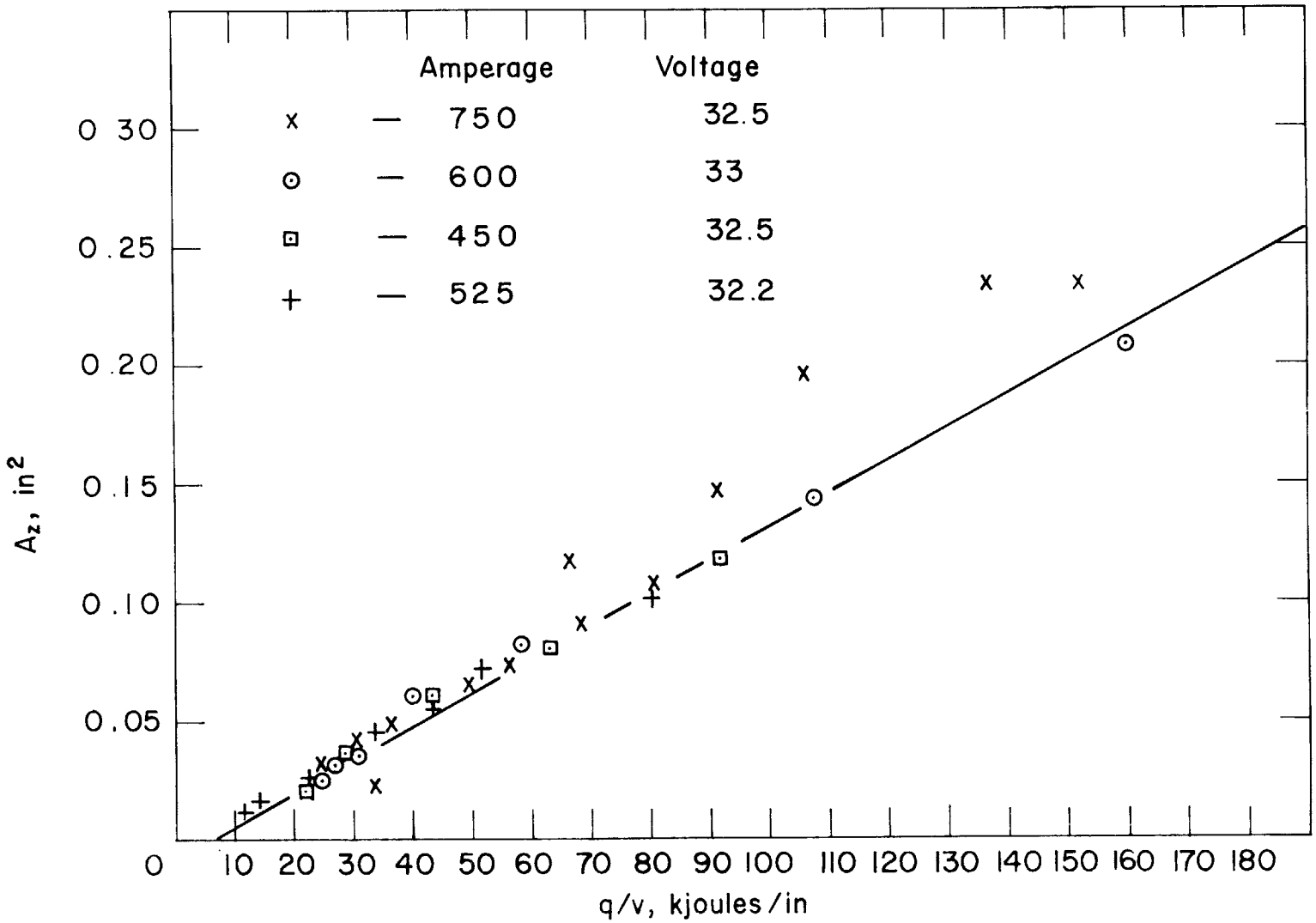

Figure 7. Heat affected zone vs. energy input — 1/8 inch wire. Effect of travel speed.

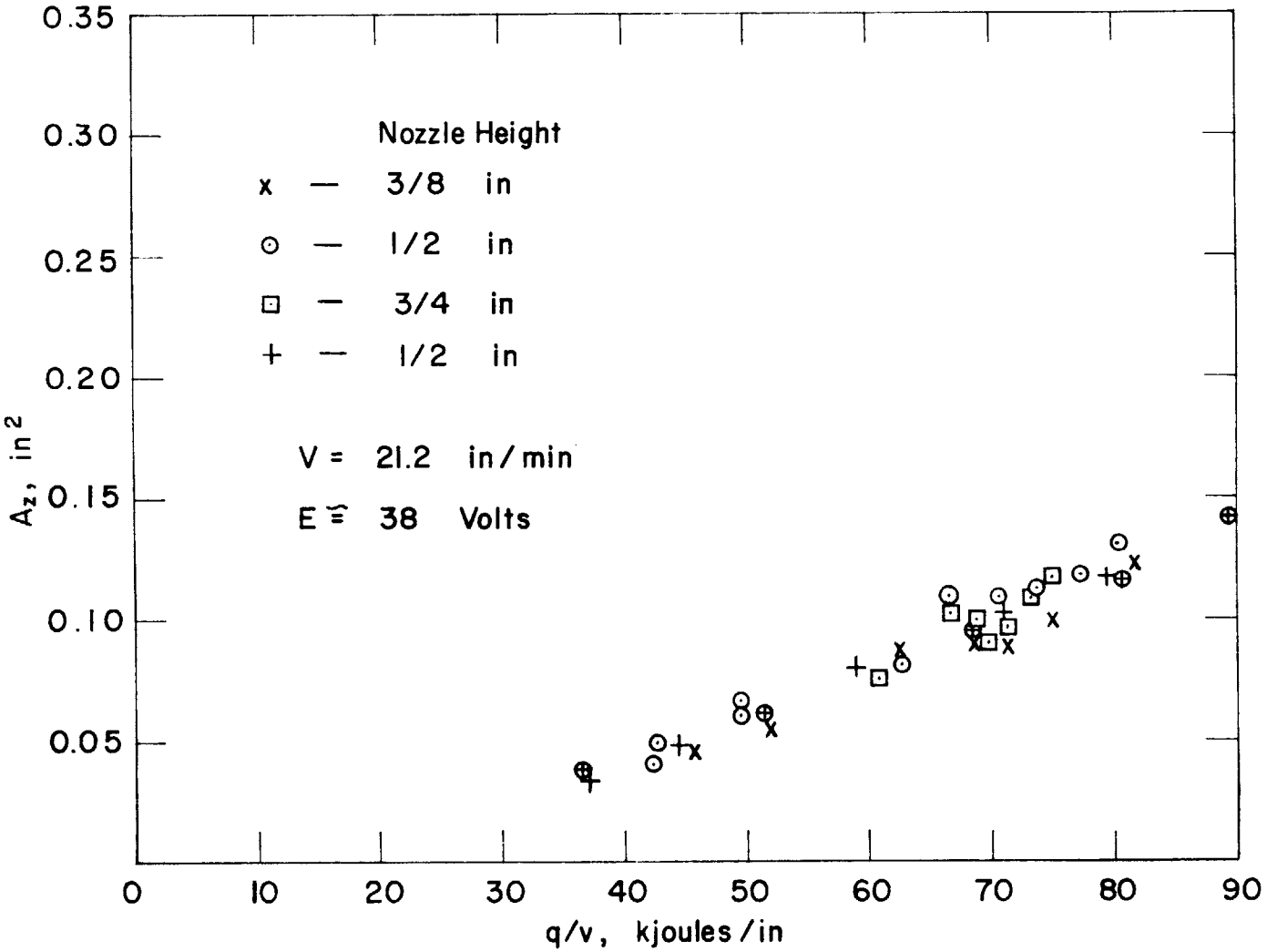

Figure 8. Heat affected zone vs. energy input, 1/8 inch wire. Effect of amperage at different nozzle heights.

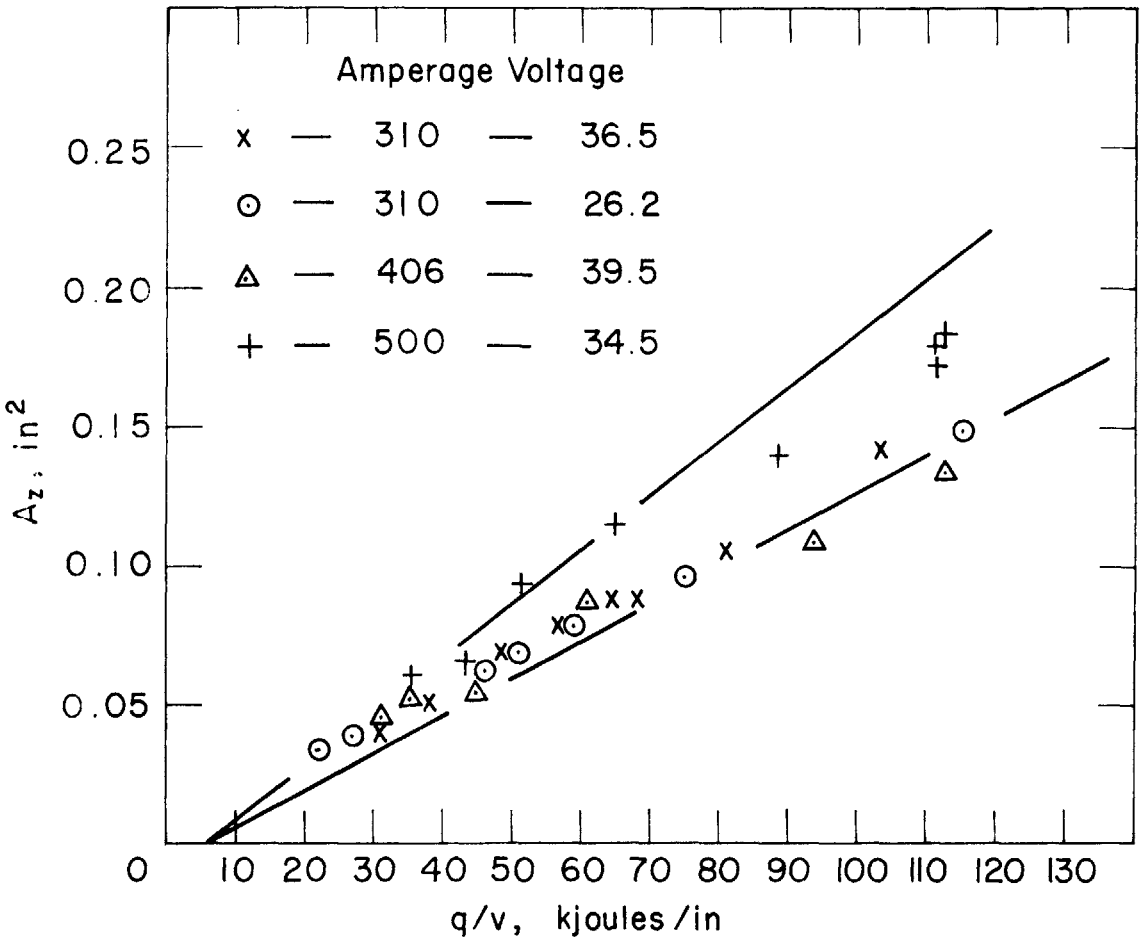

Figure 9. Heat affected zone vs. energy input, 1/16 inch wire, effect of travel speed

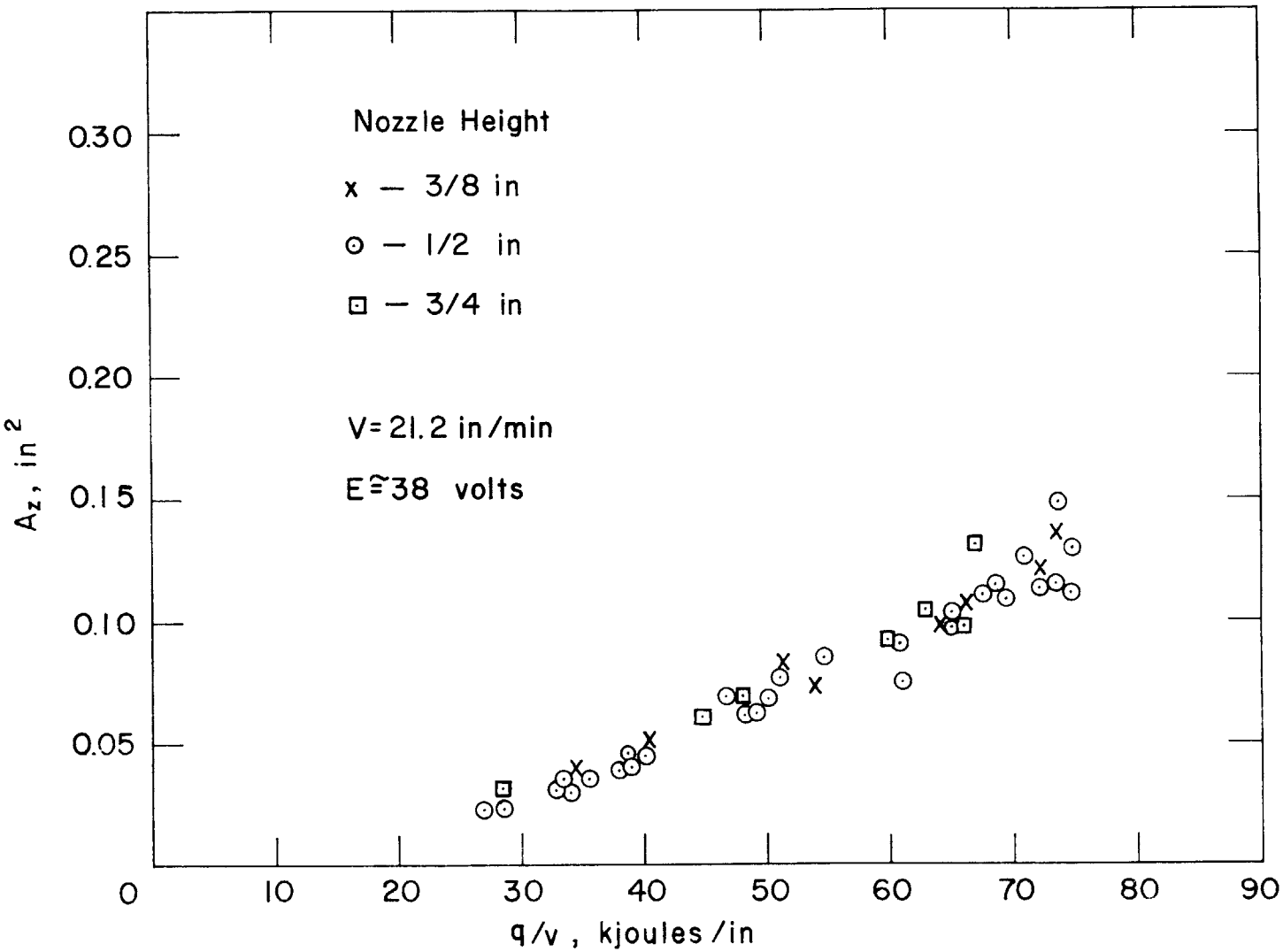

Figure 10. Heat affected zone vs. energy input, 1/16 inch wire. Effect of amperage at different nozzle heights.

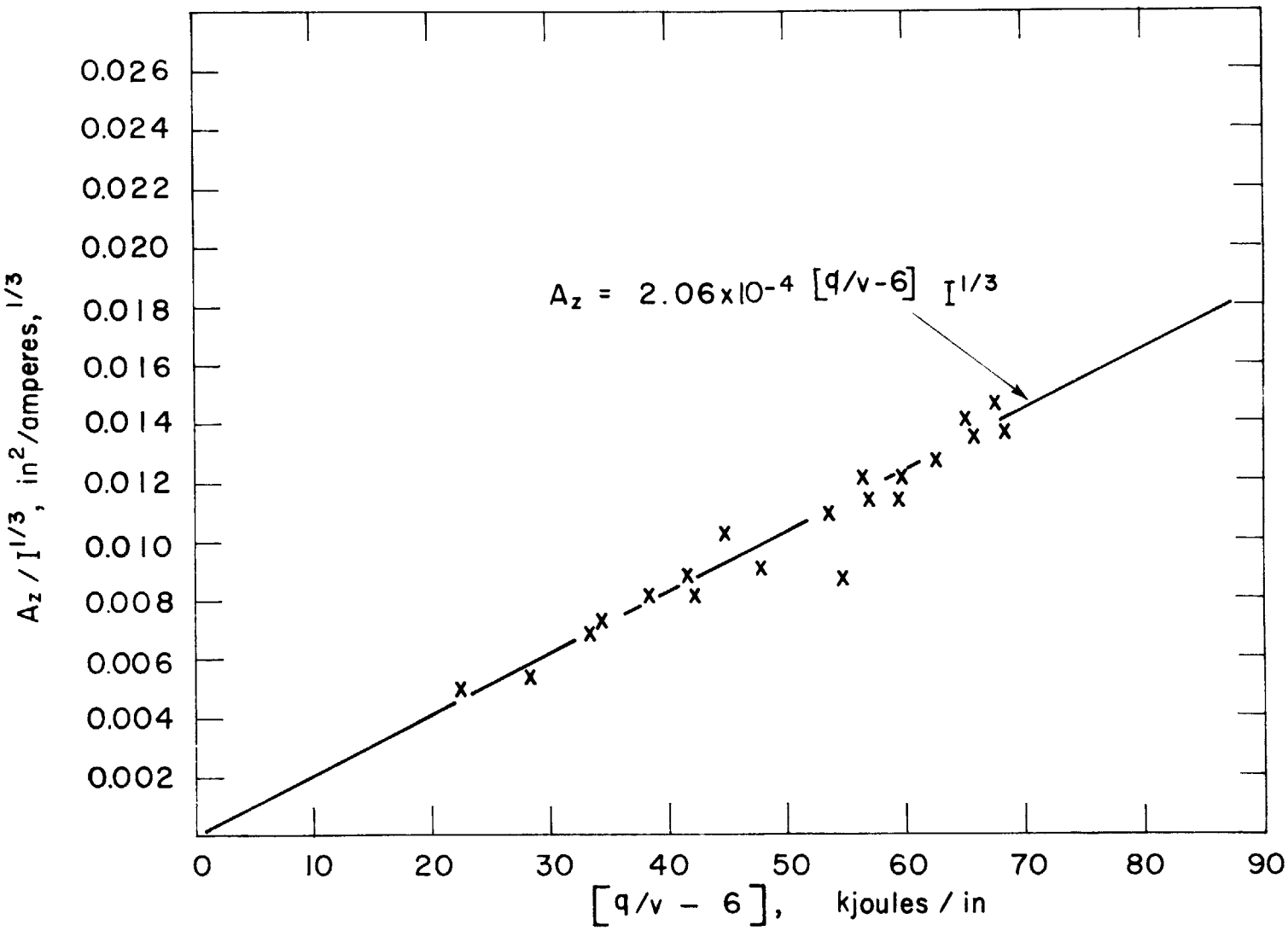

Figure II. Empirical check of the derived equation for the heat affected zone, 1/16 inch wire

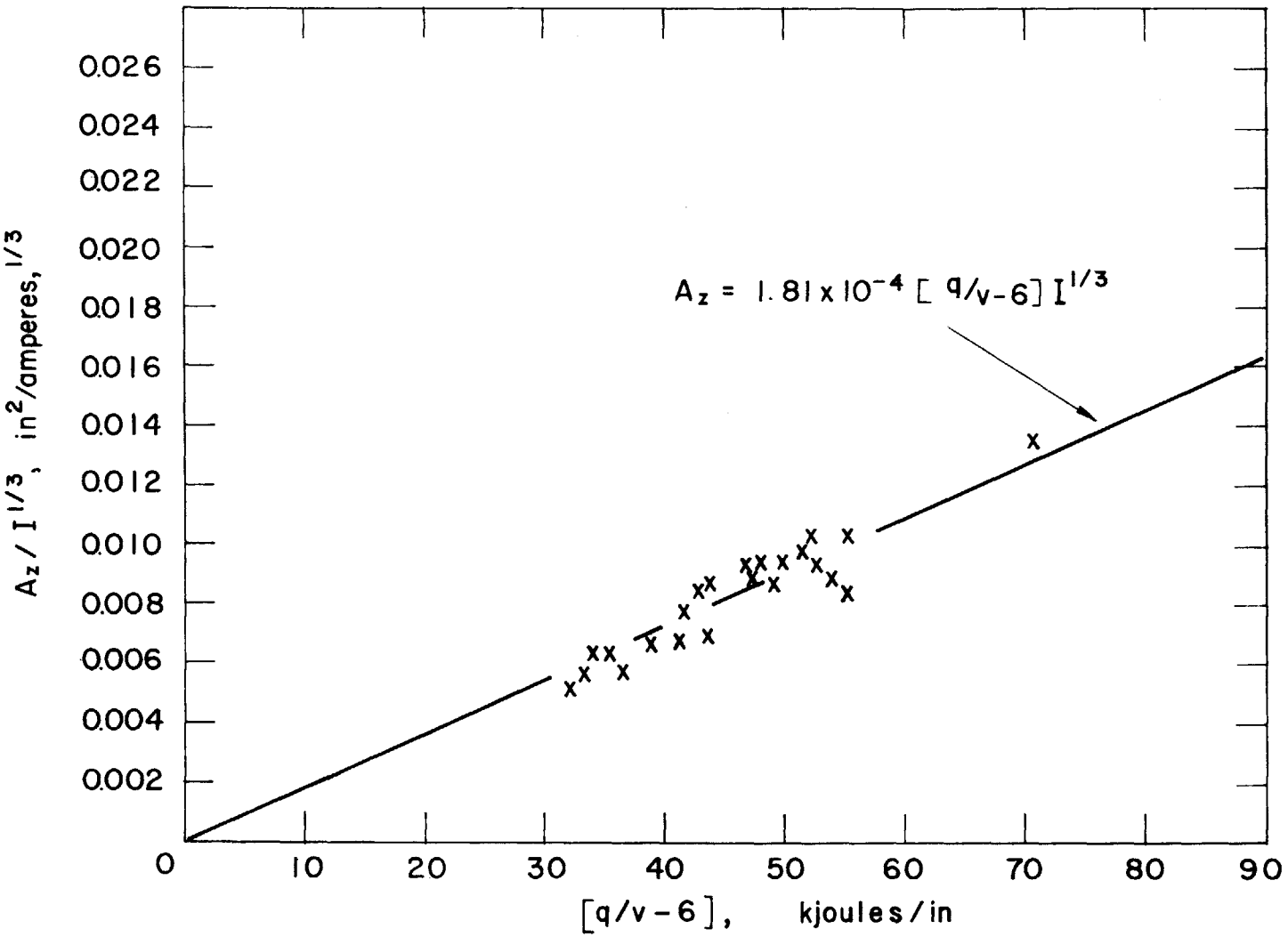

Figure 12. Empirical check of the derived equation for the heat affected zone, 3/32 inch wire

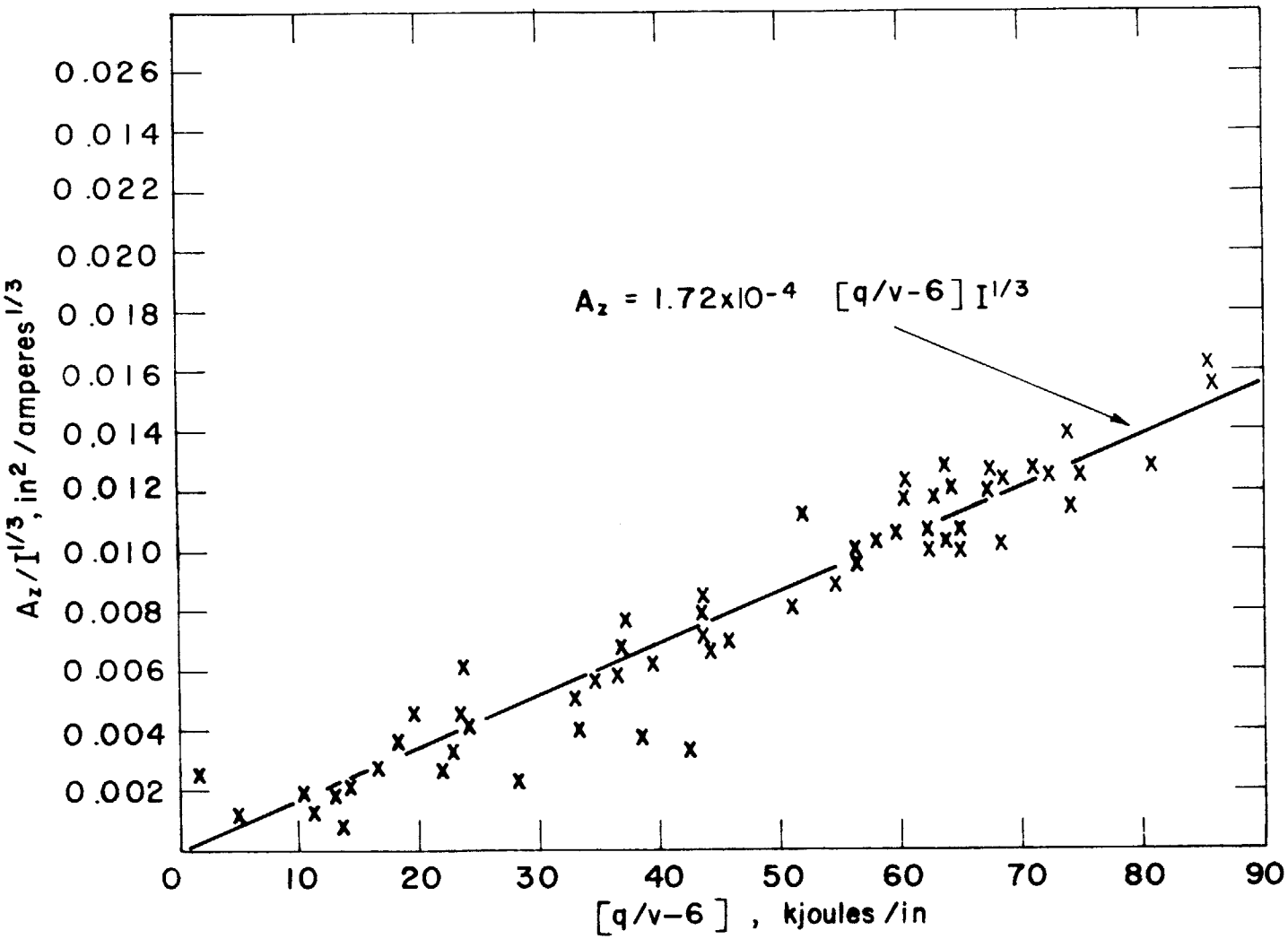

Figure 13. Empirical check of the derived equation for the heat affected zone, 1/8 inch wire.

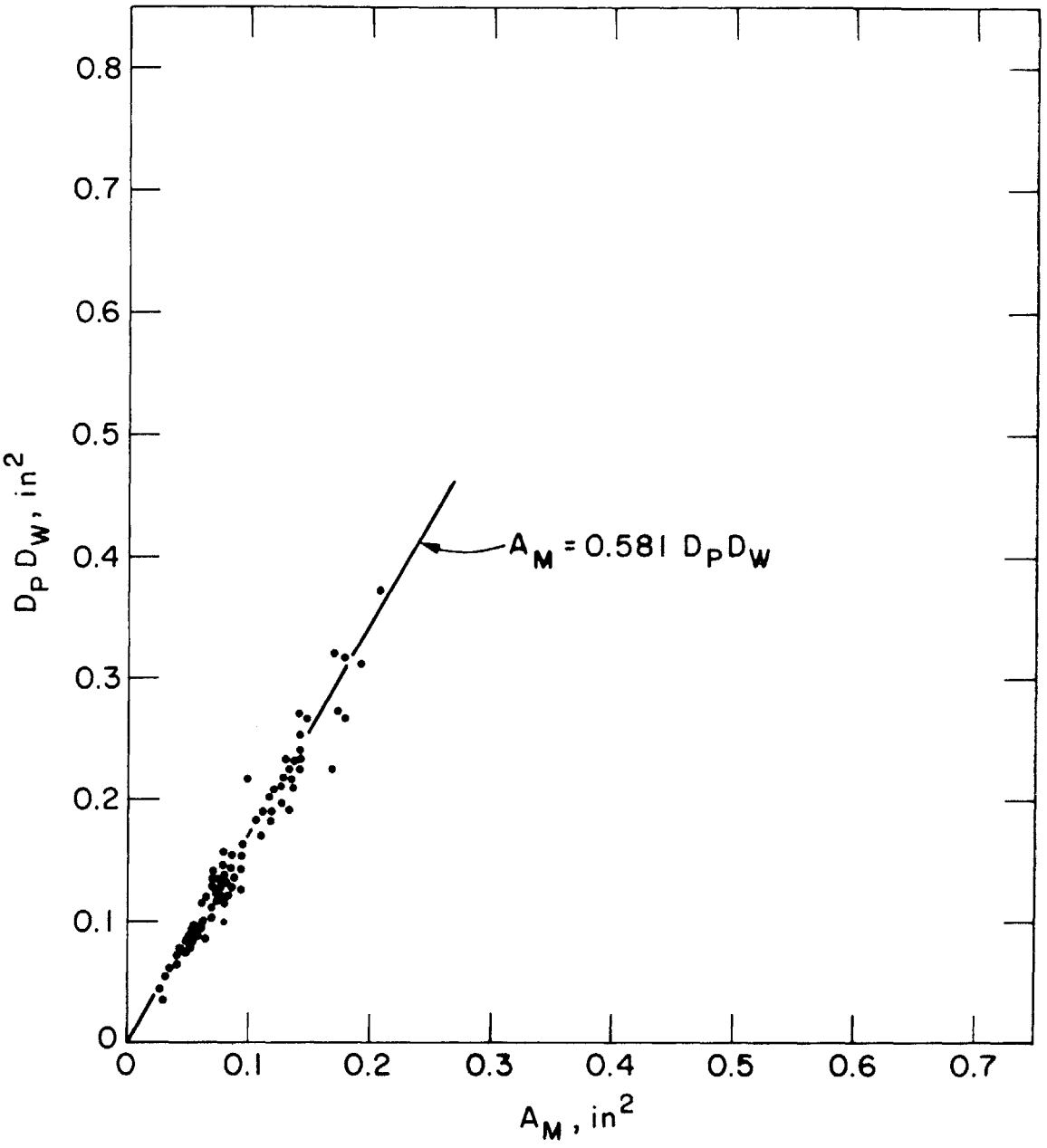

Figure 14. Relationship between the plate melted area and the penetration to bead width product, 1/16 inch wire.

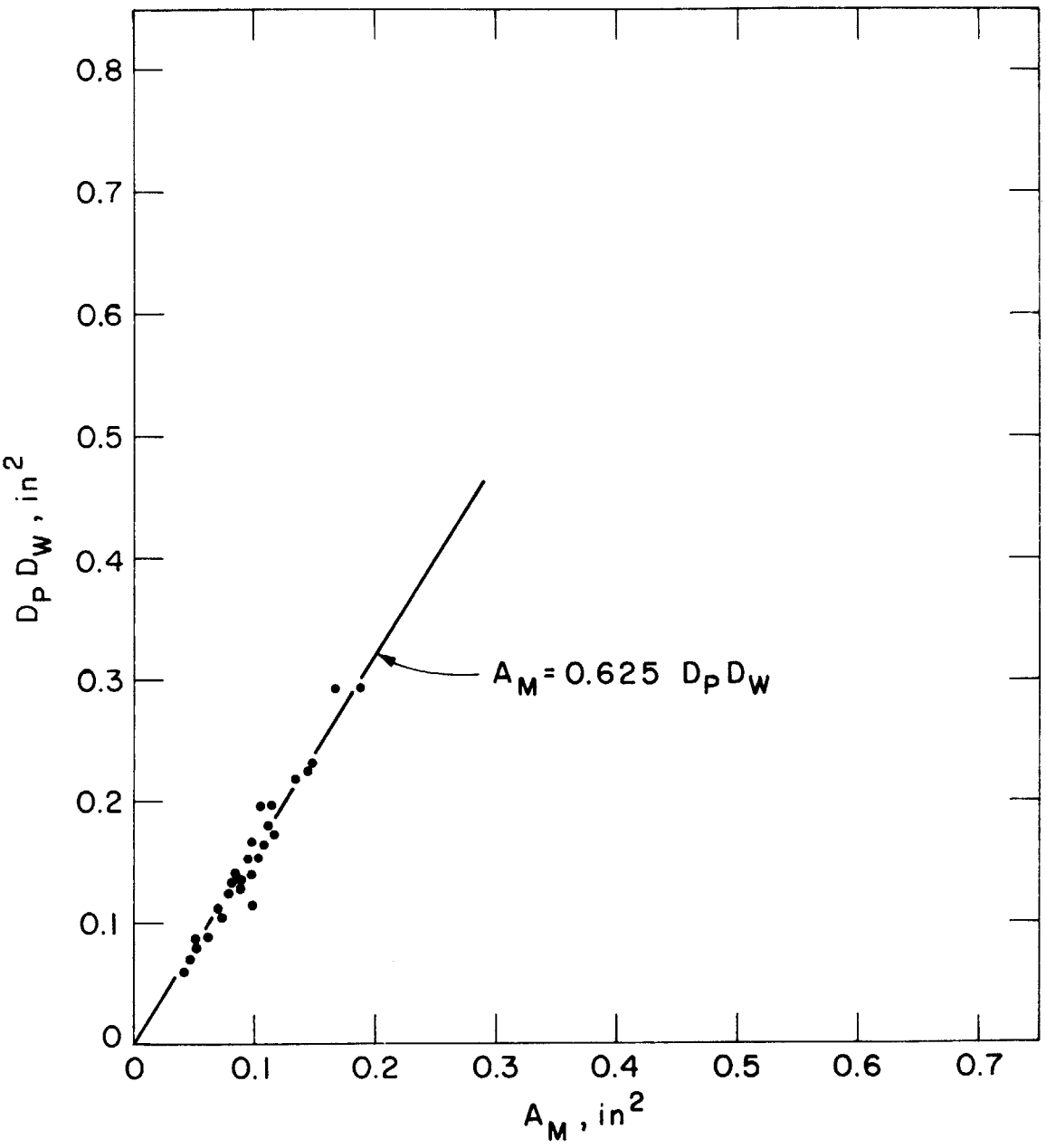

Figure 15. Relationship between the plate melted area and the penetration to bead width product, 3/32 inch wire.

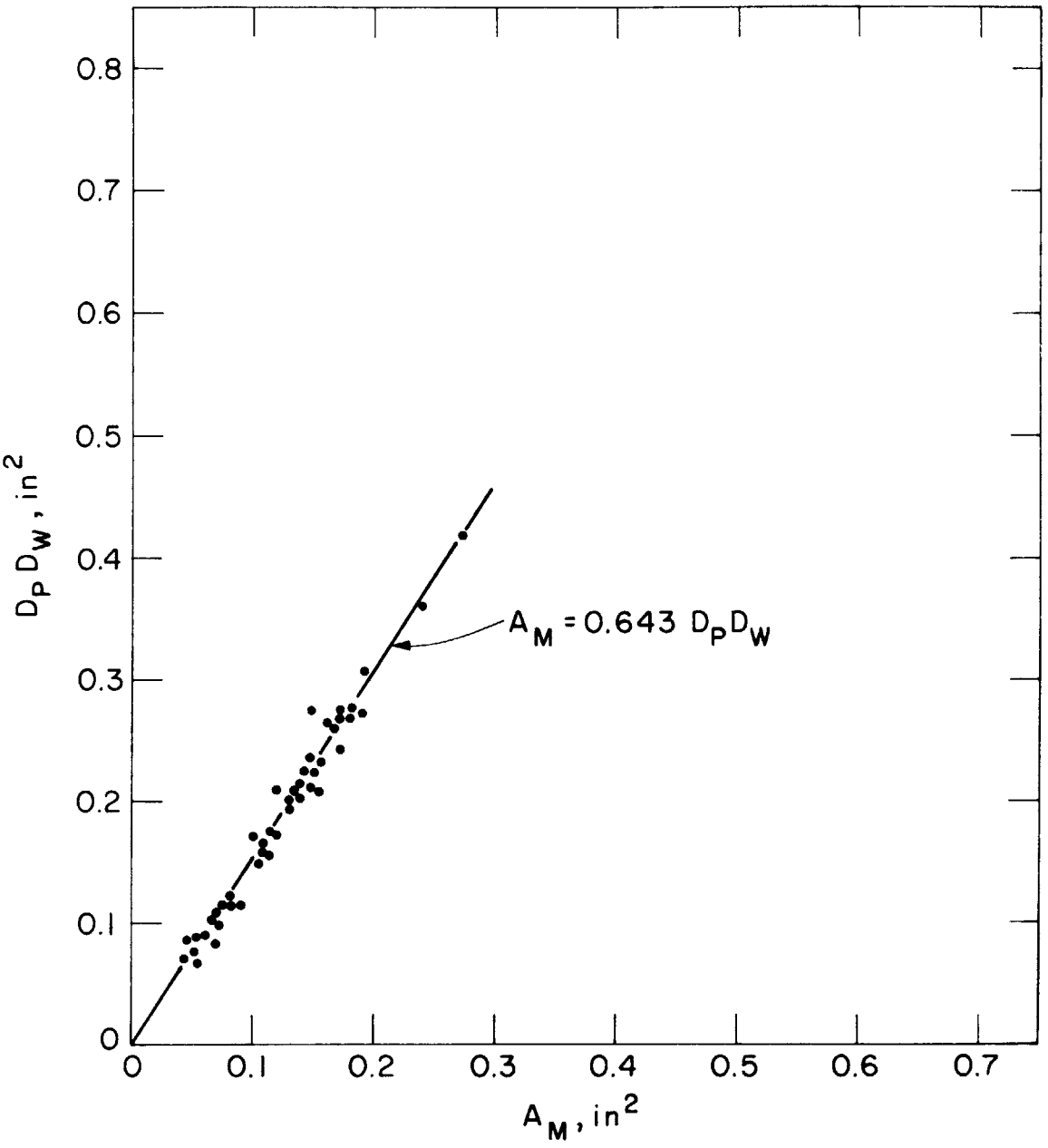

Figure 16. Relationship between the plate melted area and the penetration to bead width product, 1/8 inch wire.

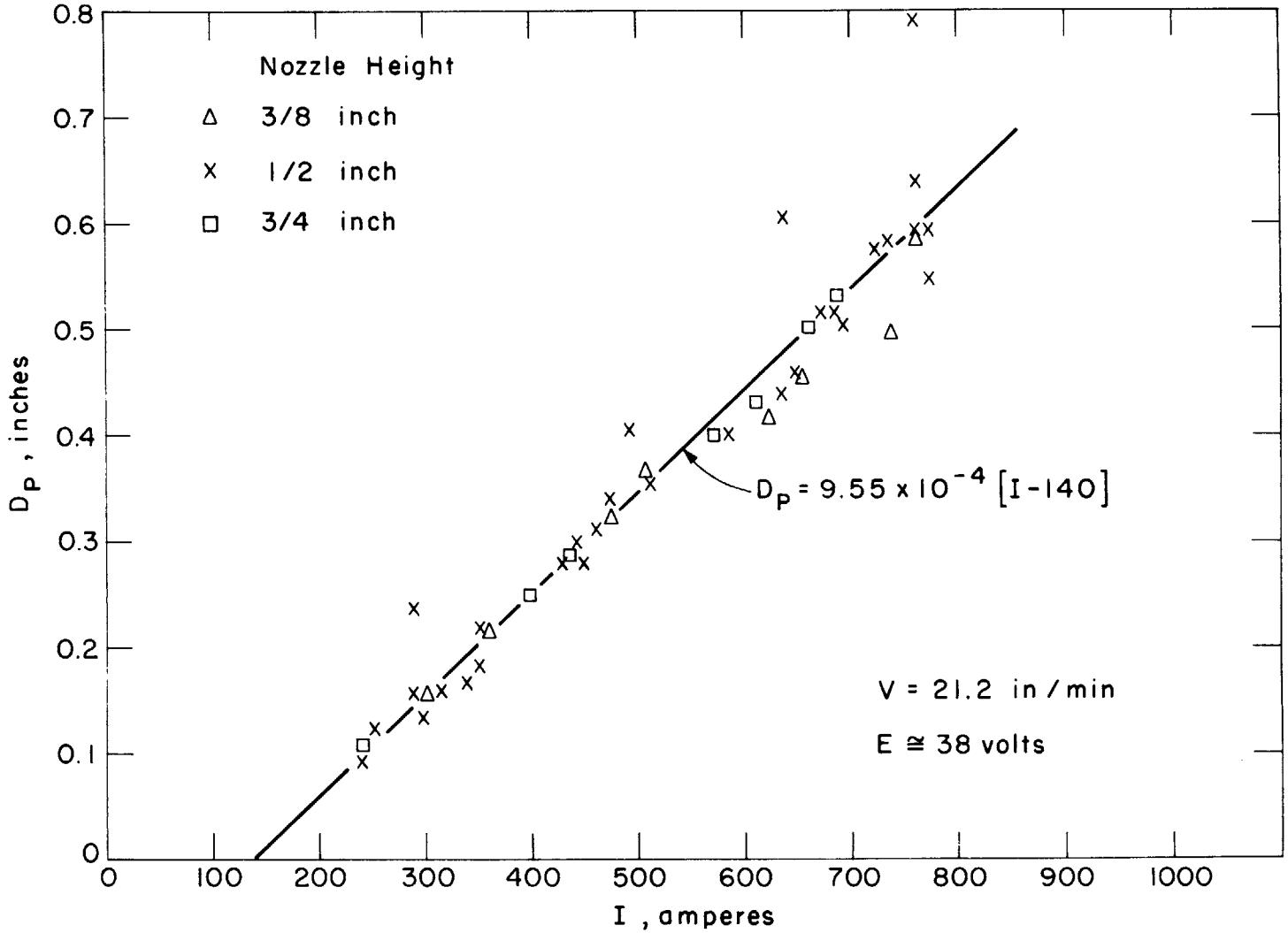

Figure 17. Penetration vs. amperage at different nozzle heights, 1/16 inch wire.

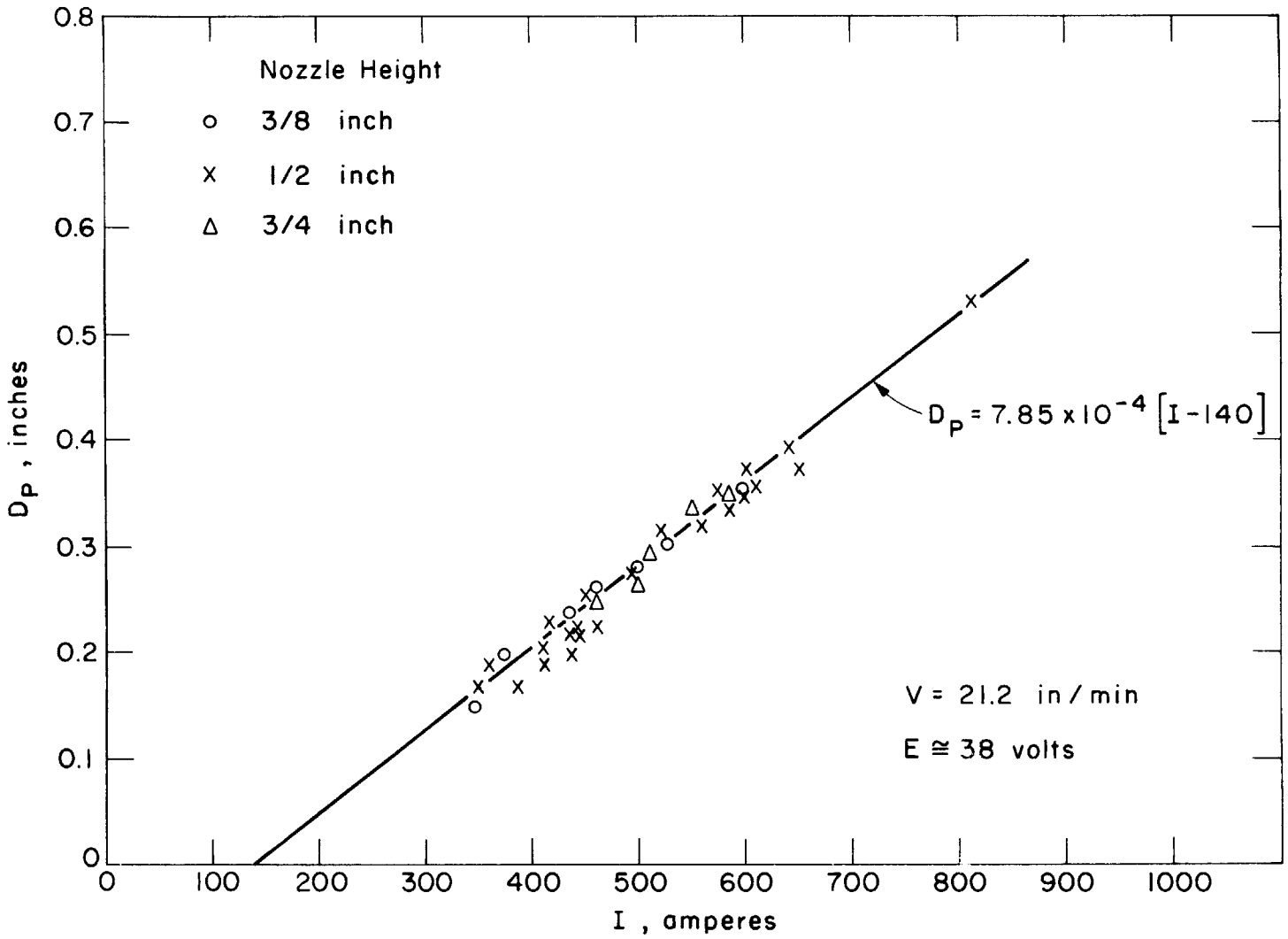

Figure 18. Penetration vs. amperage at different nozzle heights, 3/32 inch wire.

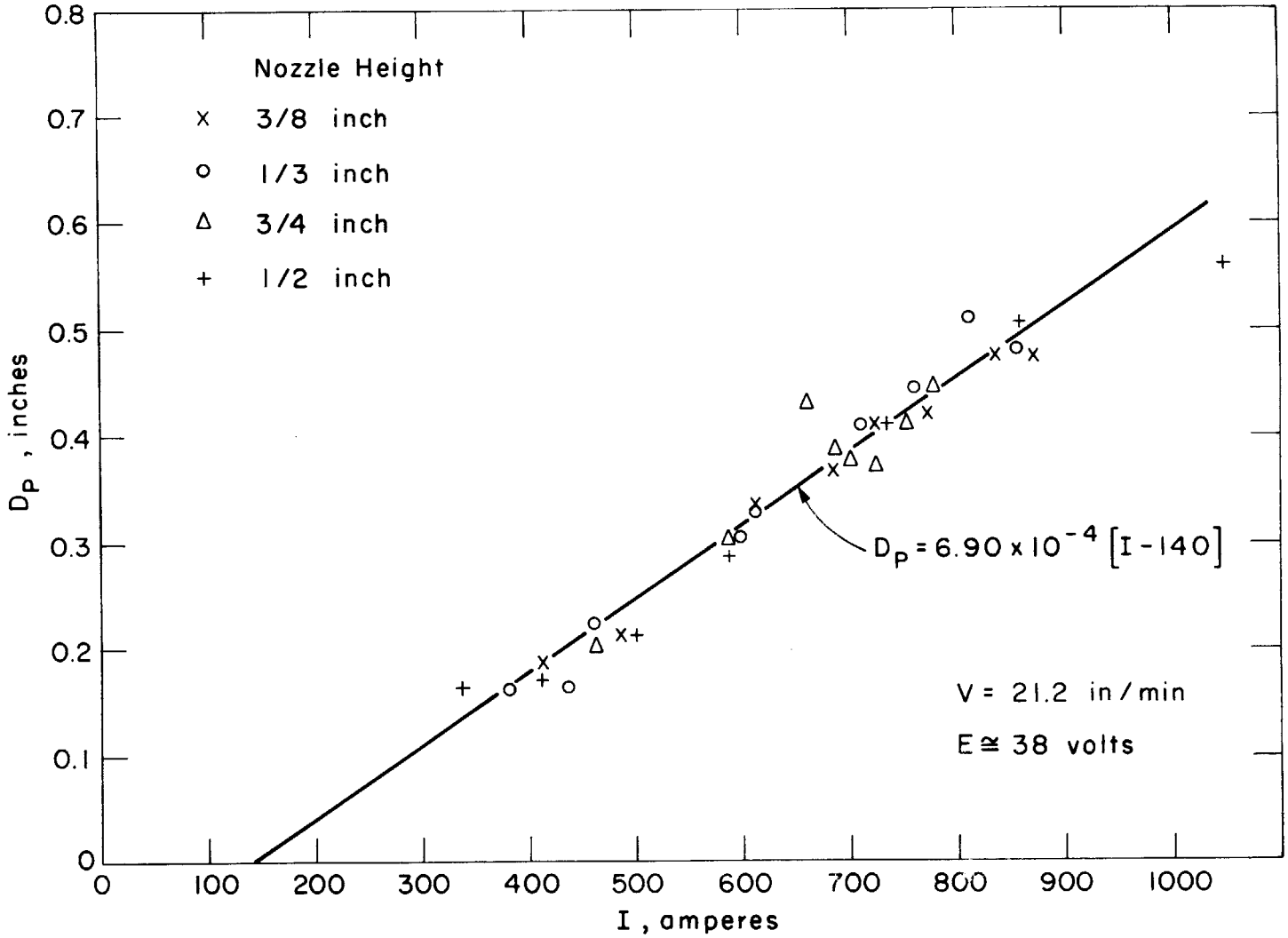

Figure 19. Penetration vs. amperage at different nozzle heights, 1/8 inch wire.

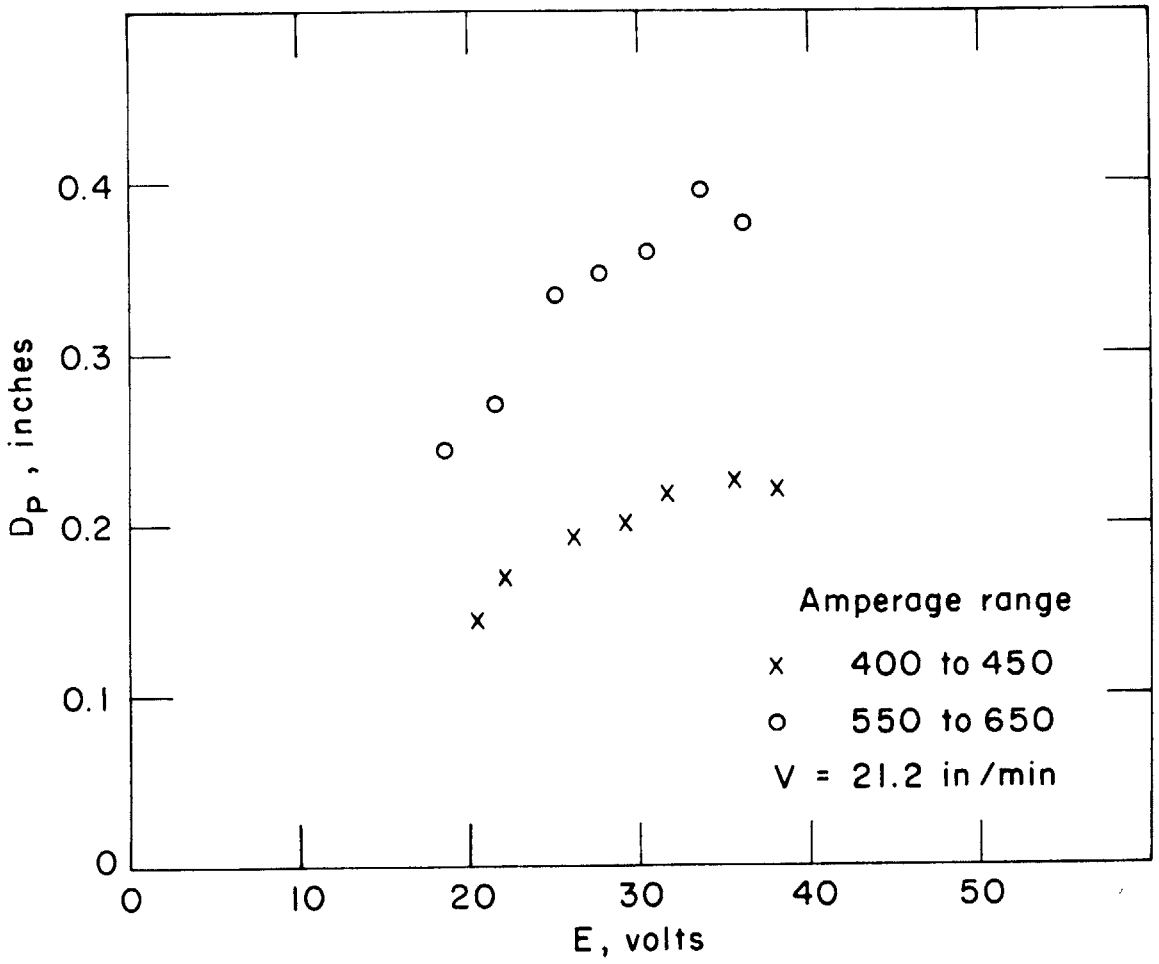

Figure 20. Penetration vs. voltage, with same variation in amperage, 3/32 inch wire.

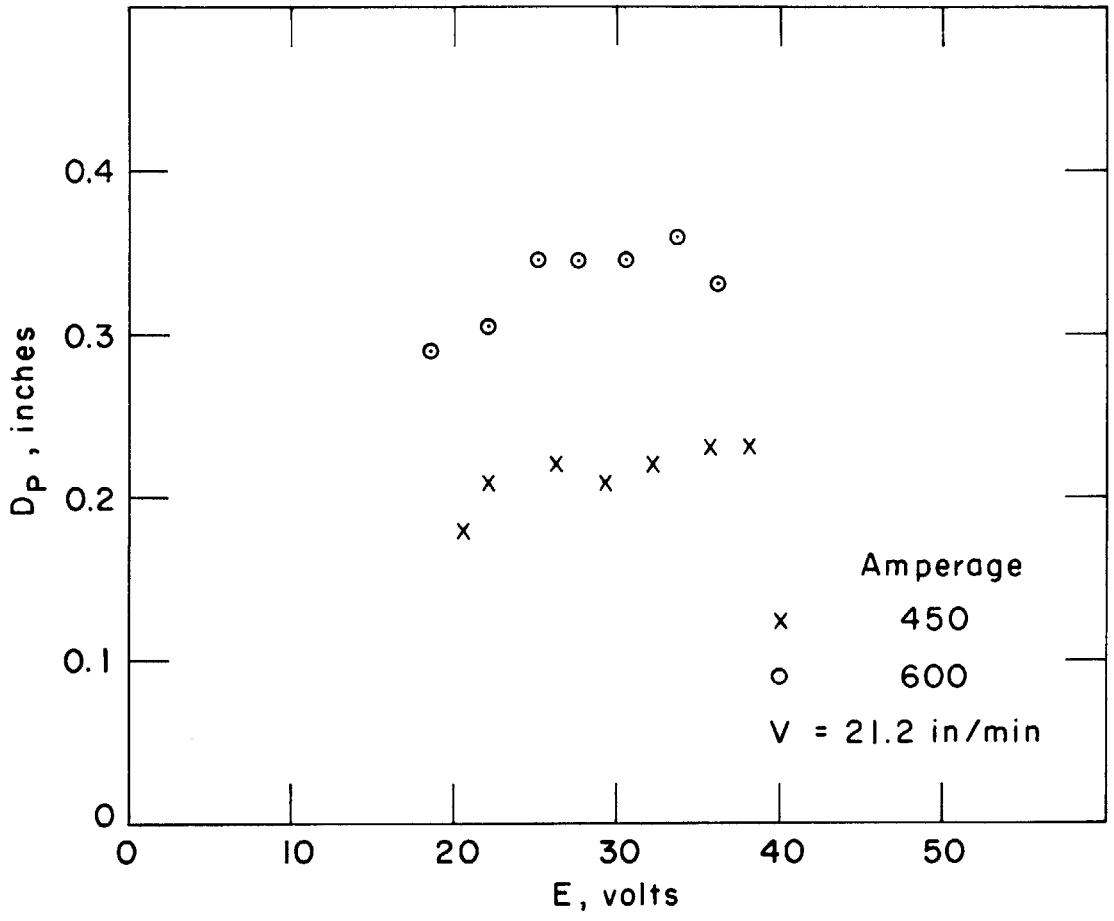

Figure 21 Penetration vs. voltage, penetration corrected to constant value of amperage, 3/32 inch wire

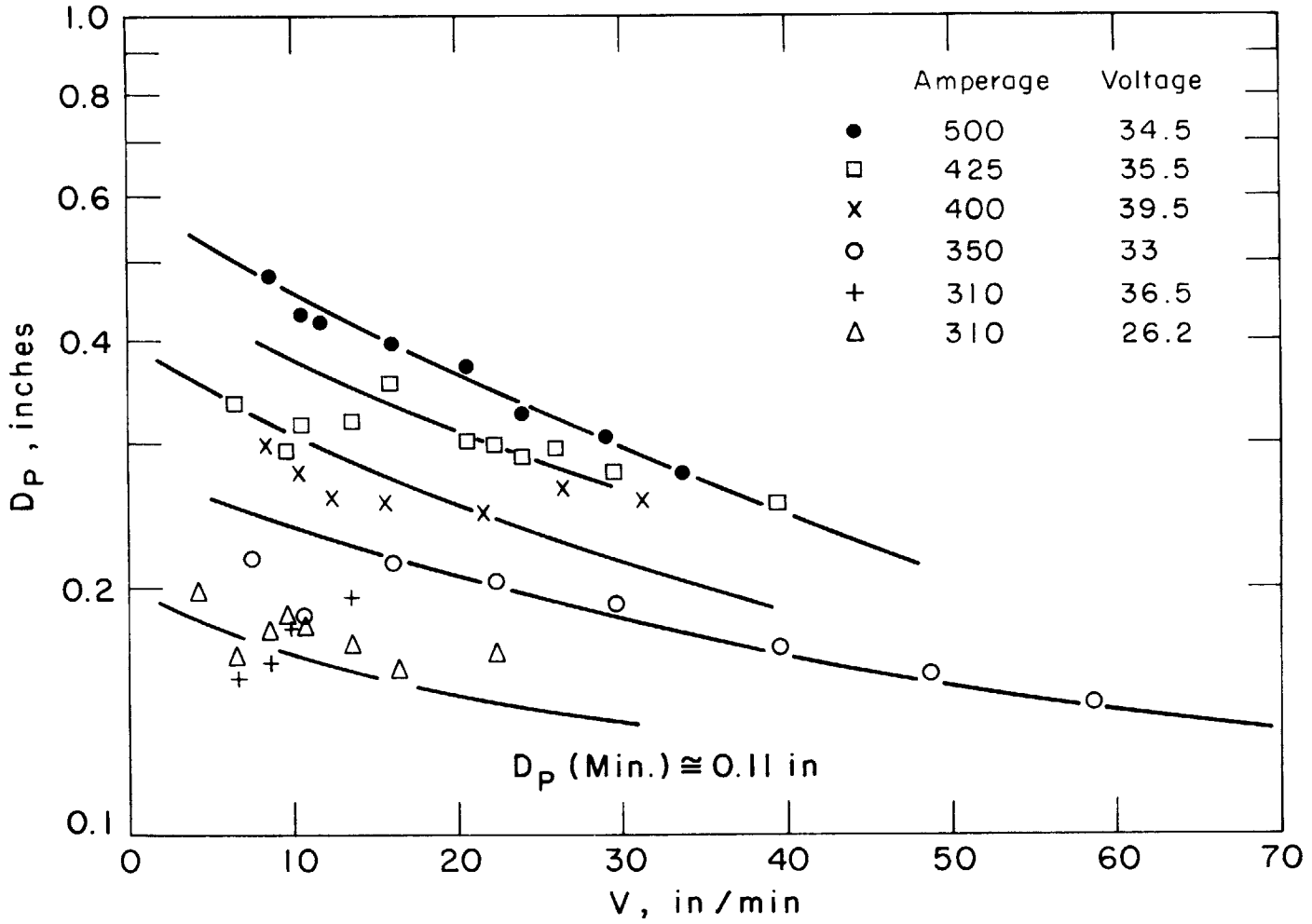

Figure 22. Penetration vs. travel speed, 1/16 inch wire.

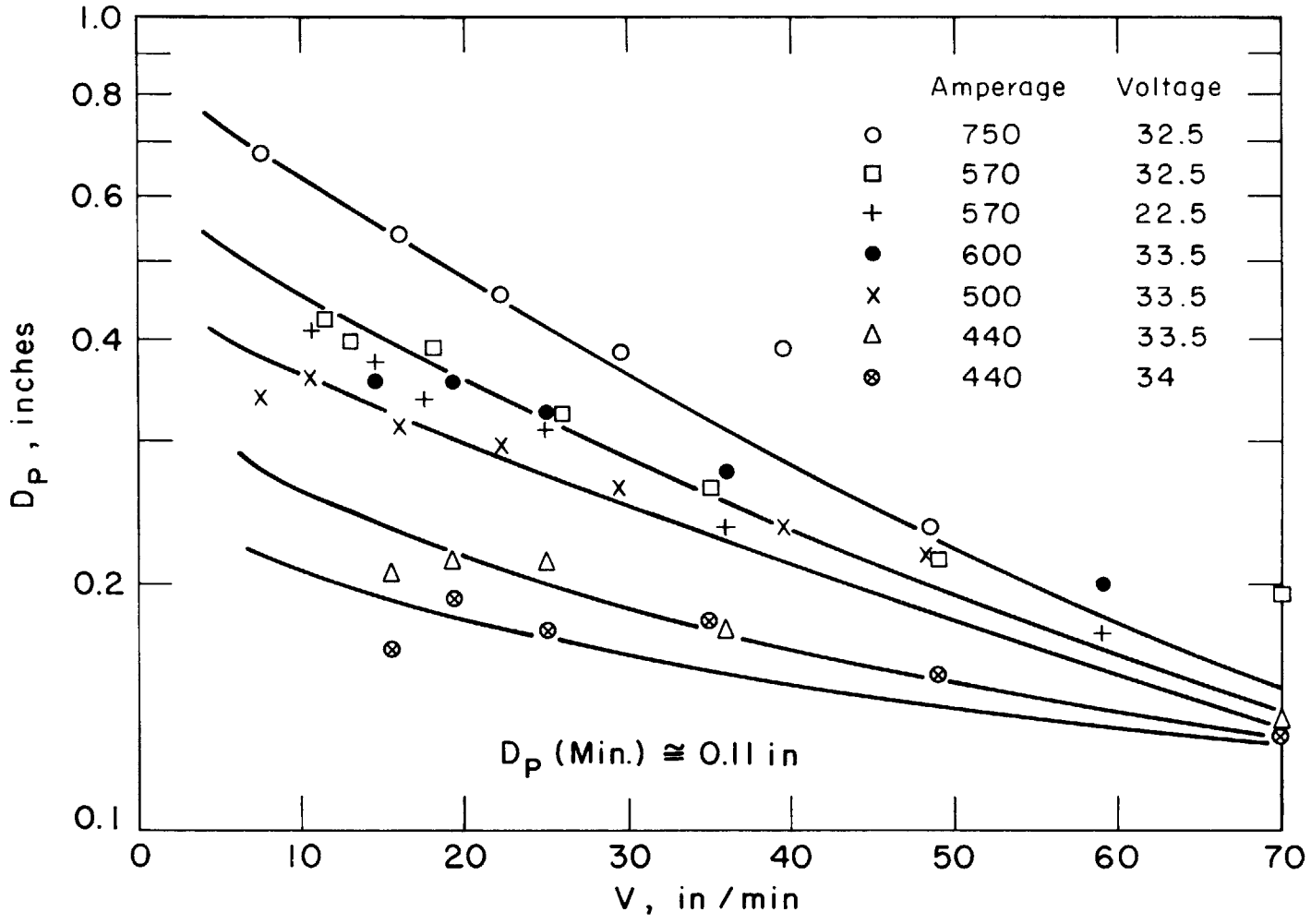

Figure 23. Penetration vs. travel speed, 3/32 inch wire.

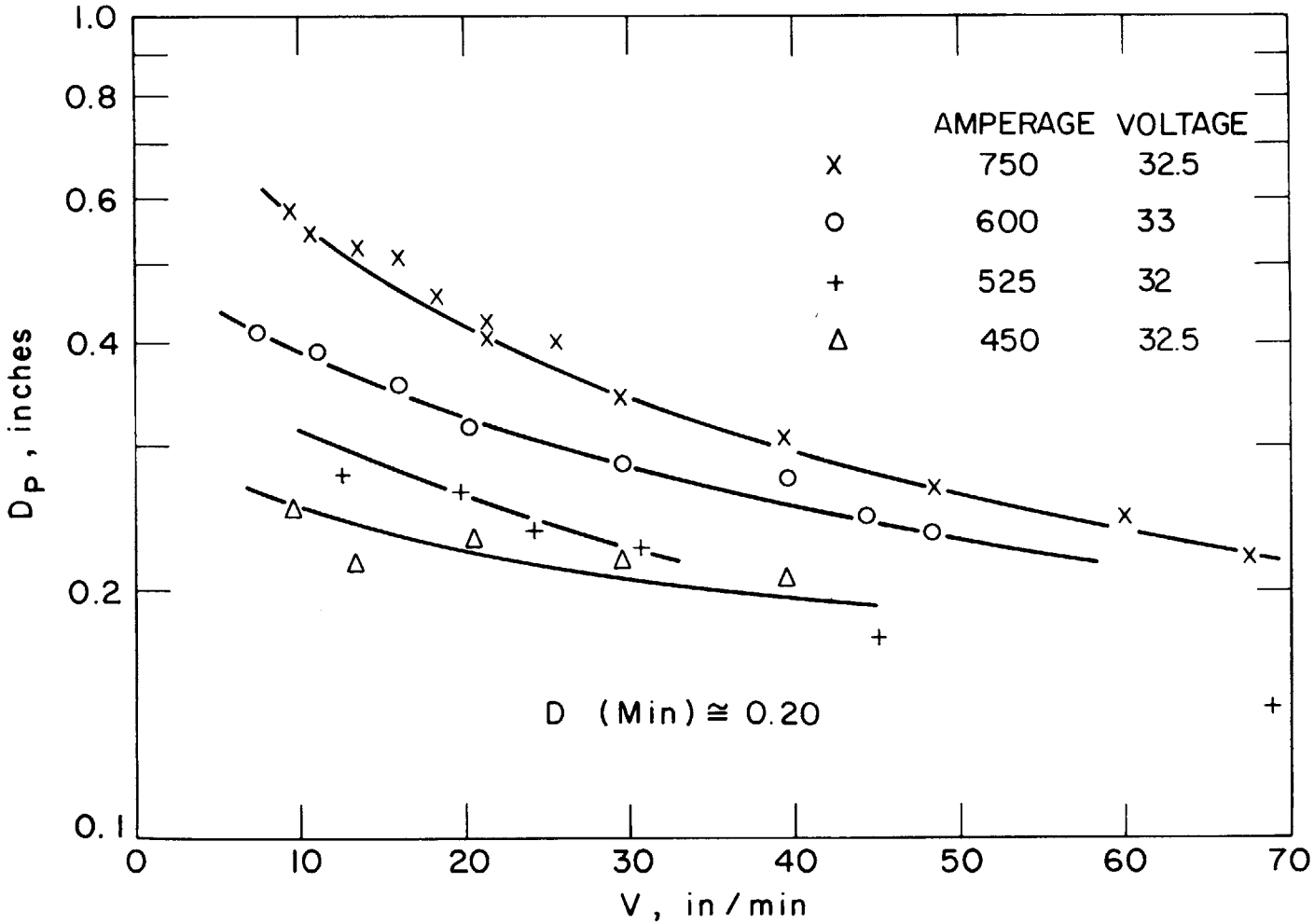

Figure 24. Penetration vs. travel speed, 1/8 inch wire.

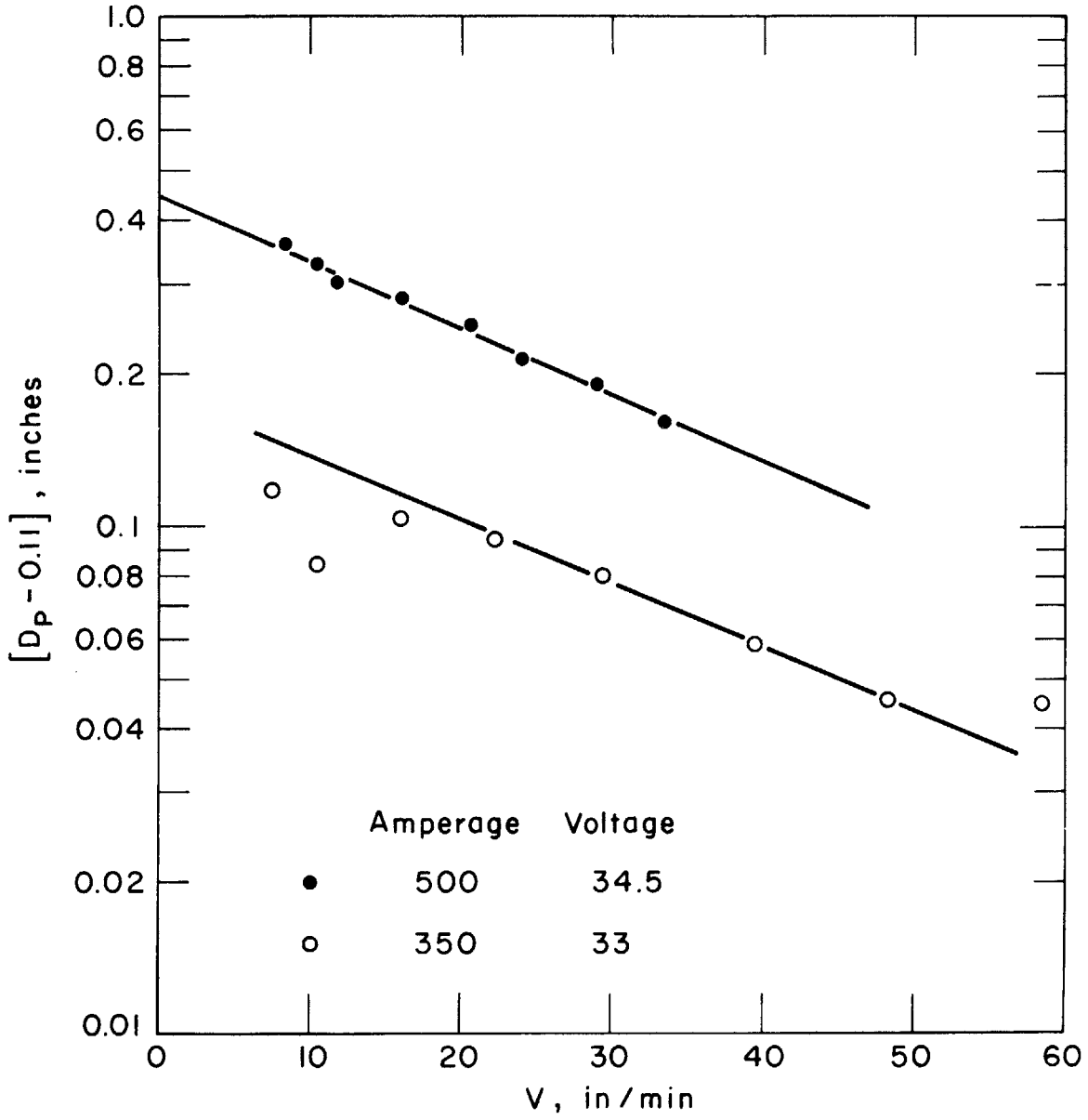

Figure 25. $[D_P - 0.11]$ vs. penetration, 1/16 inch wire

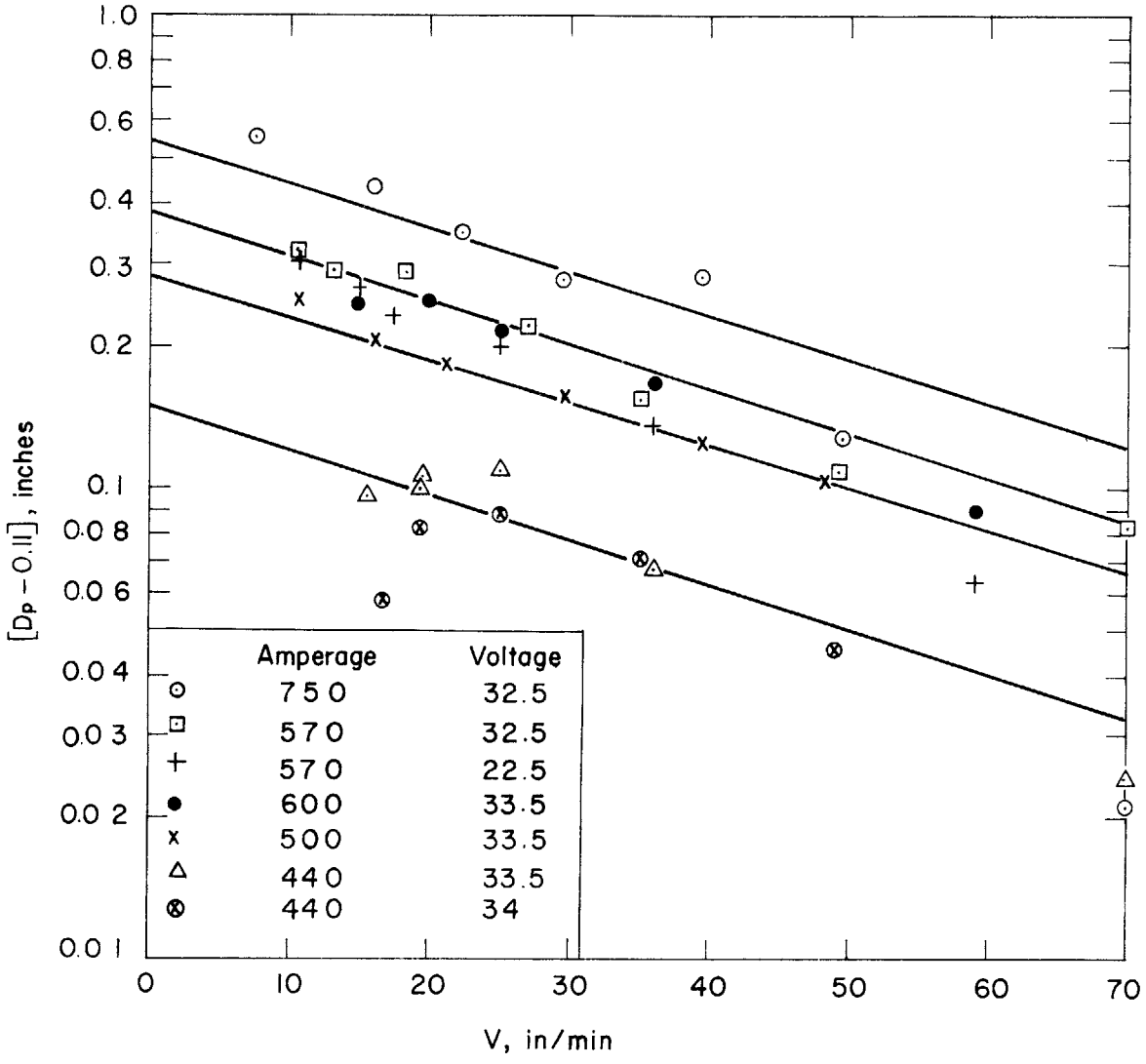

Figure 26, [Dp−0.11] vs. travel speed, 3/32 inch wire.

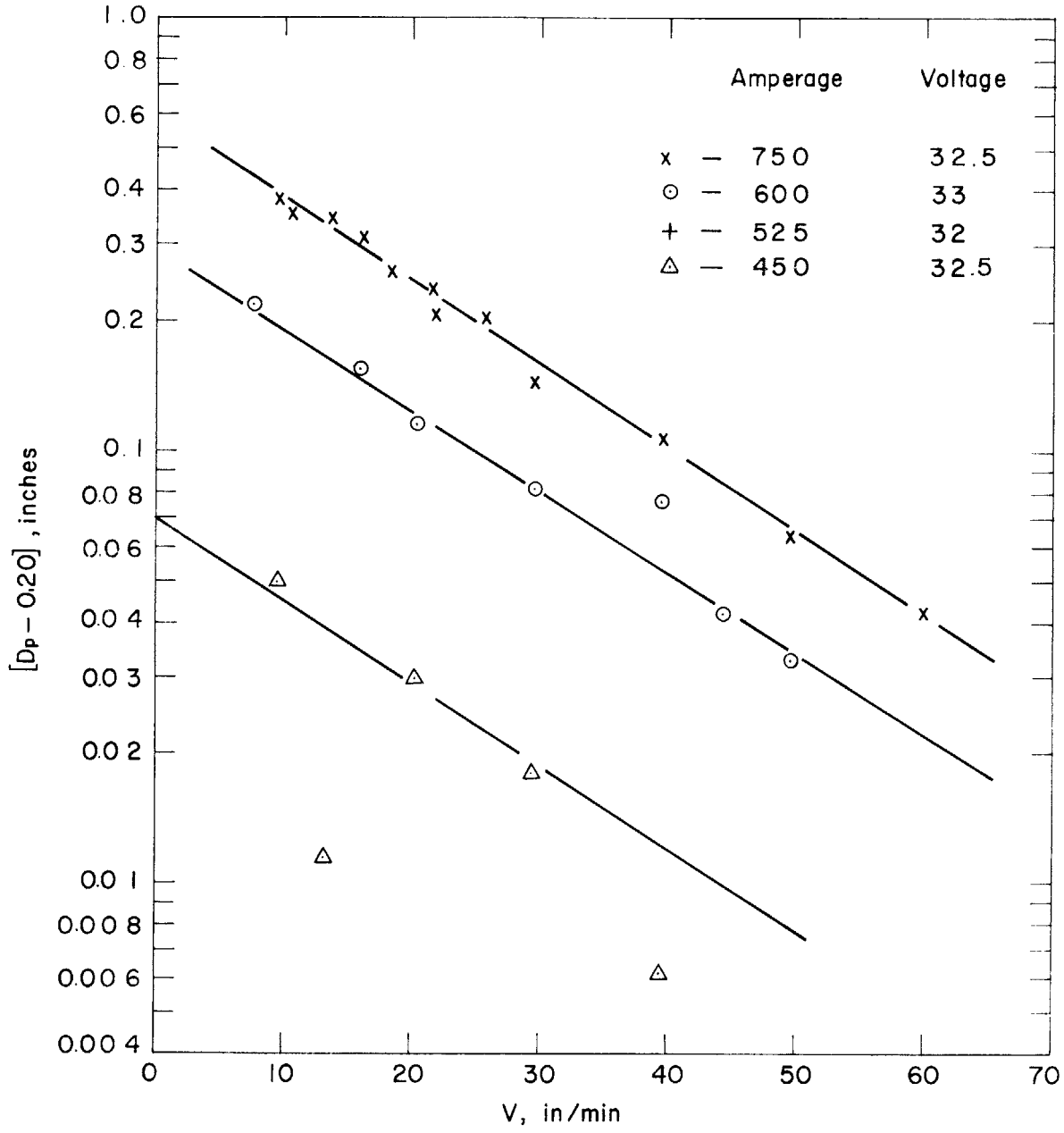

Figure 27. $[D_p - 0.20]$ vs. travel speed, 1/8 inch wire.

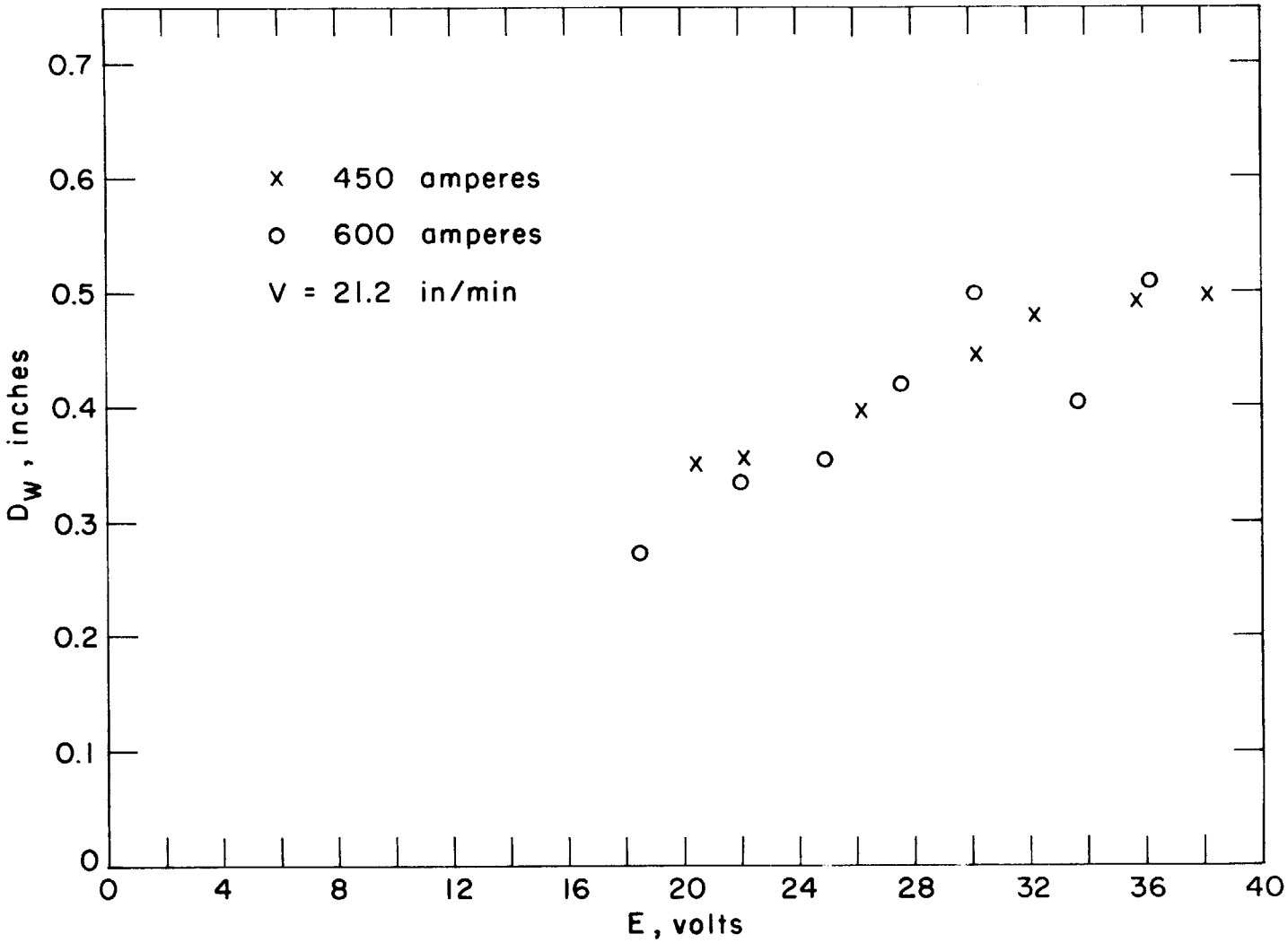

Figure 28. Bead width vs. voltage, 3/32 inch wire

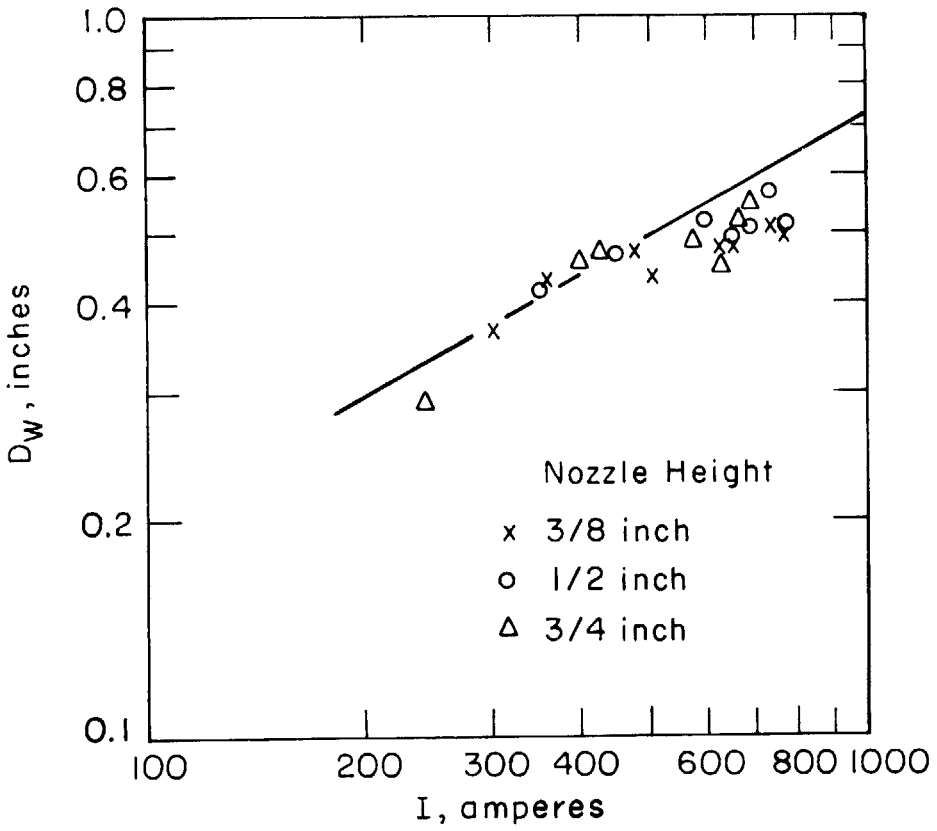

Figure 29. Bead width vs. amperage at different nozzle heights, 1/16 inch wire.

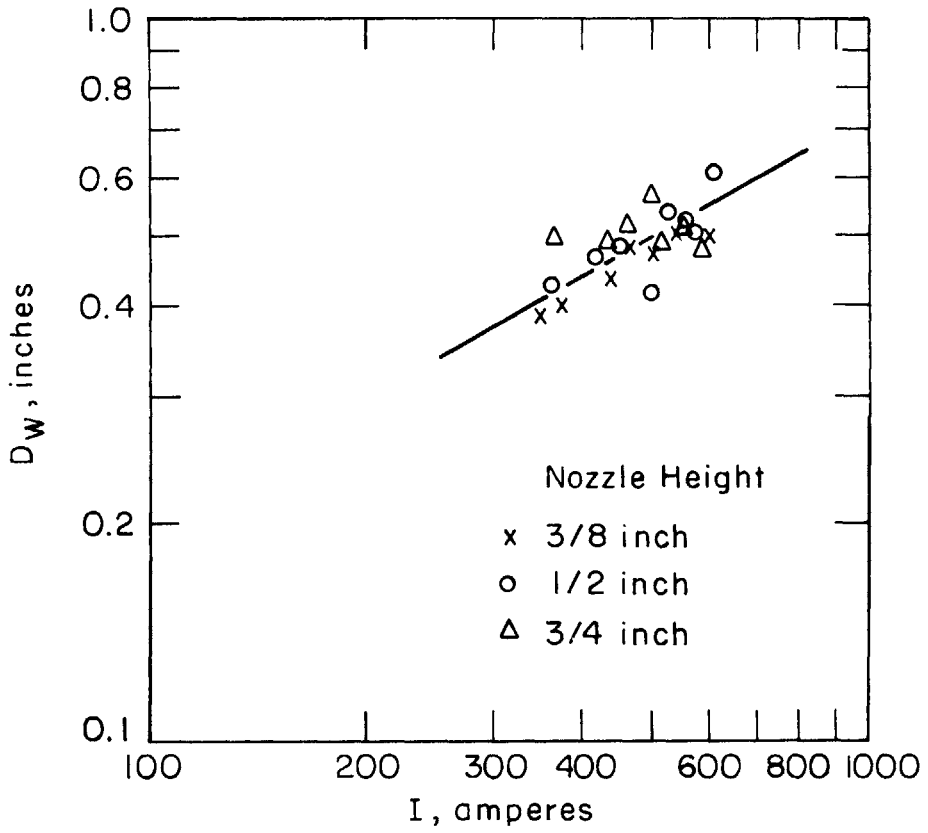

Figure 30. Bead width vs. amperage at different nozzle heights, 3/32 inch wire.

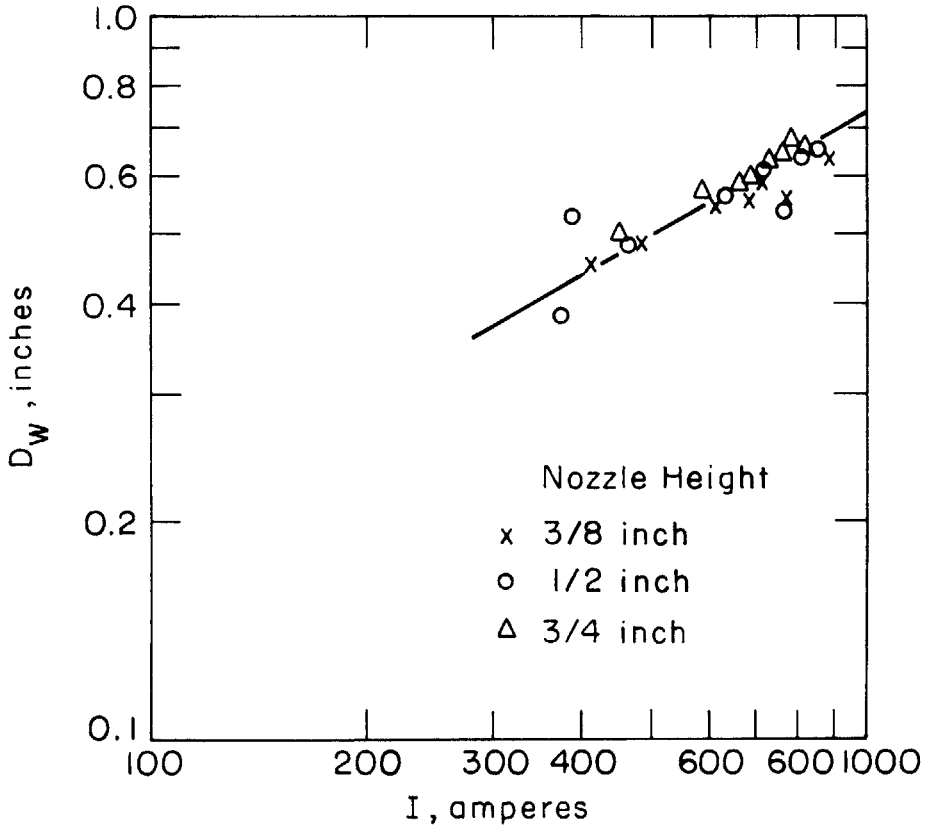

Figure 31. Bead width vs. amperage at different nozzle heights, 1/8 inch wire.

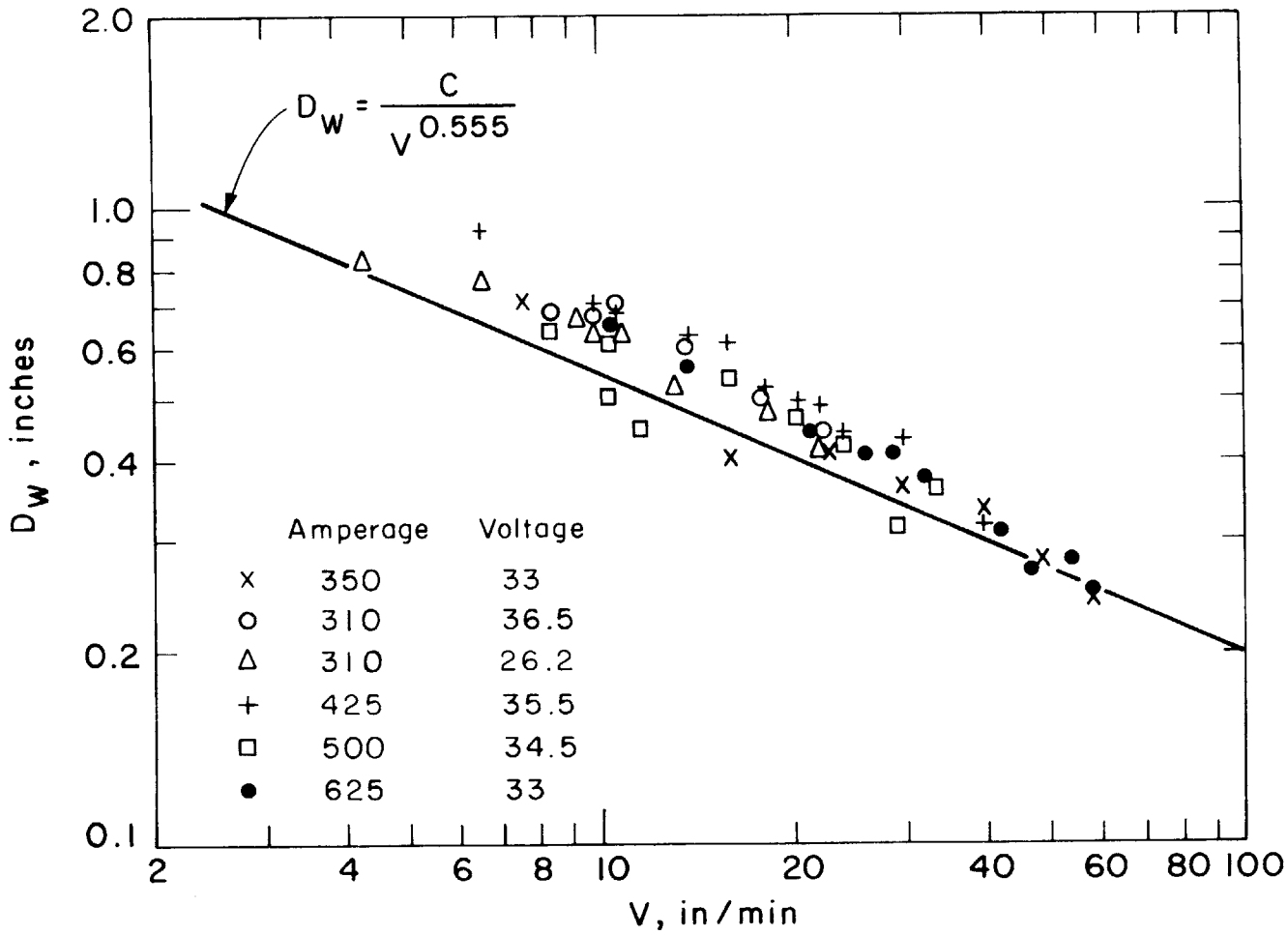

Figure 32. Bead width vs. travel speed, 1/16 inch wire.

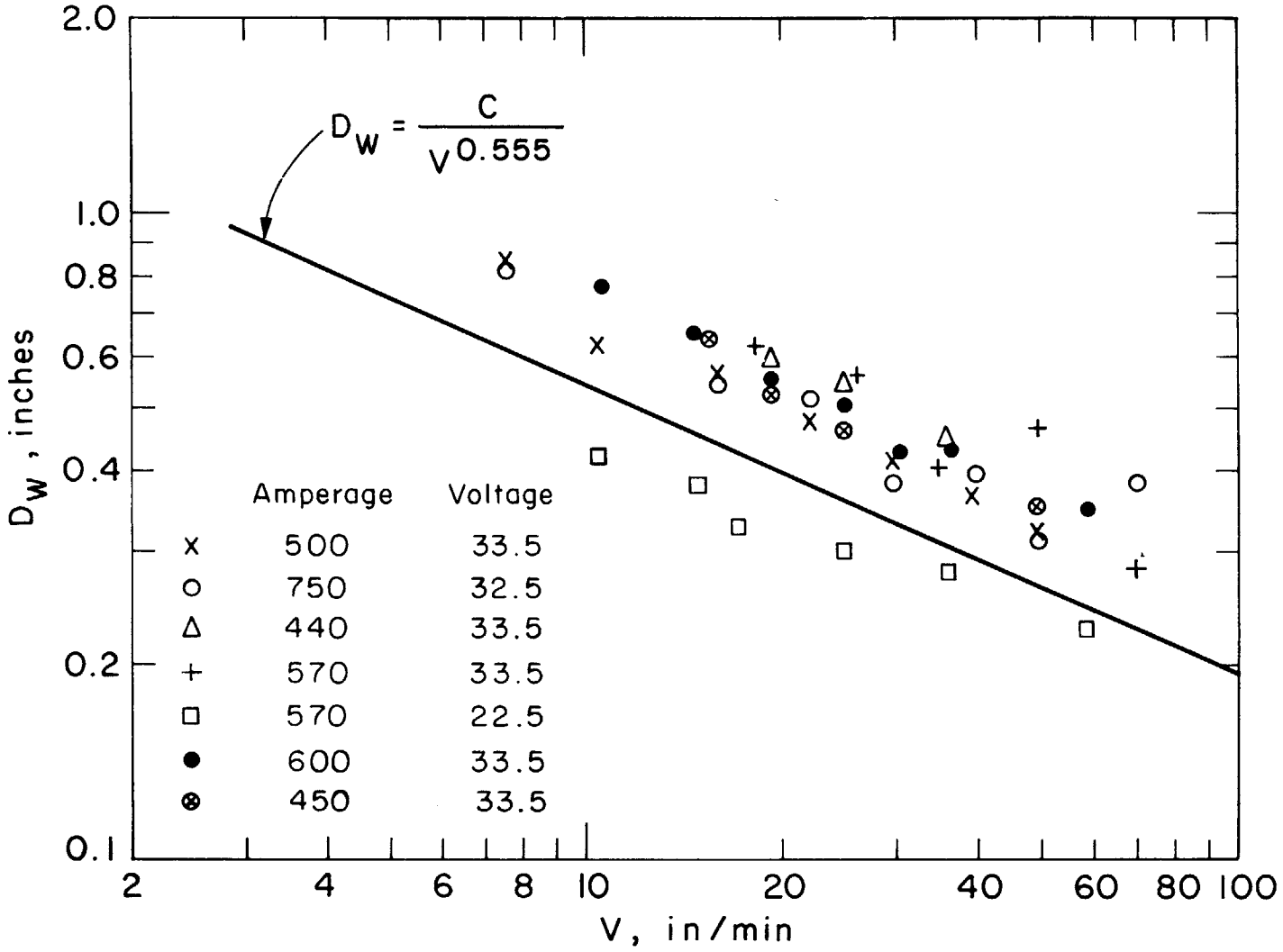

Figure 33. Bead width vs. travel speed, 3/32 inch wire.

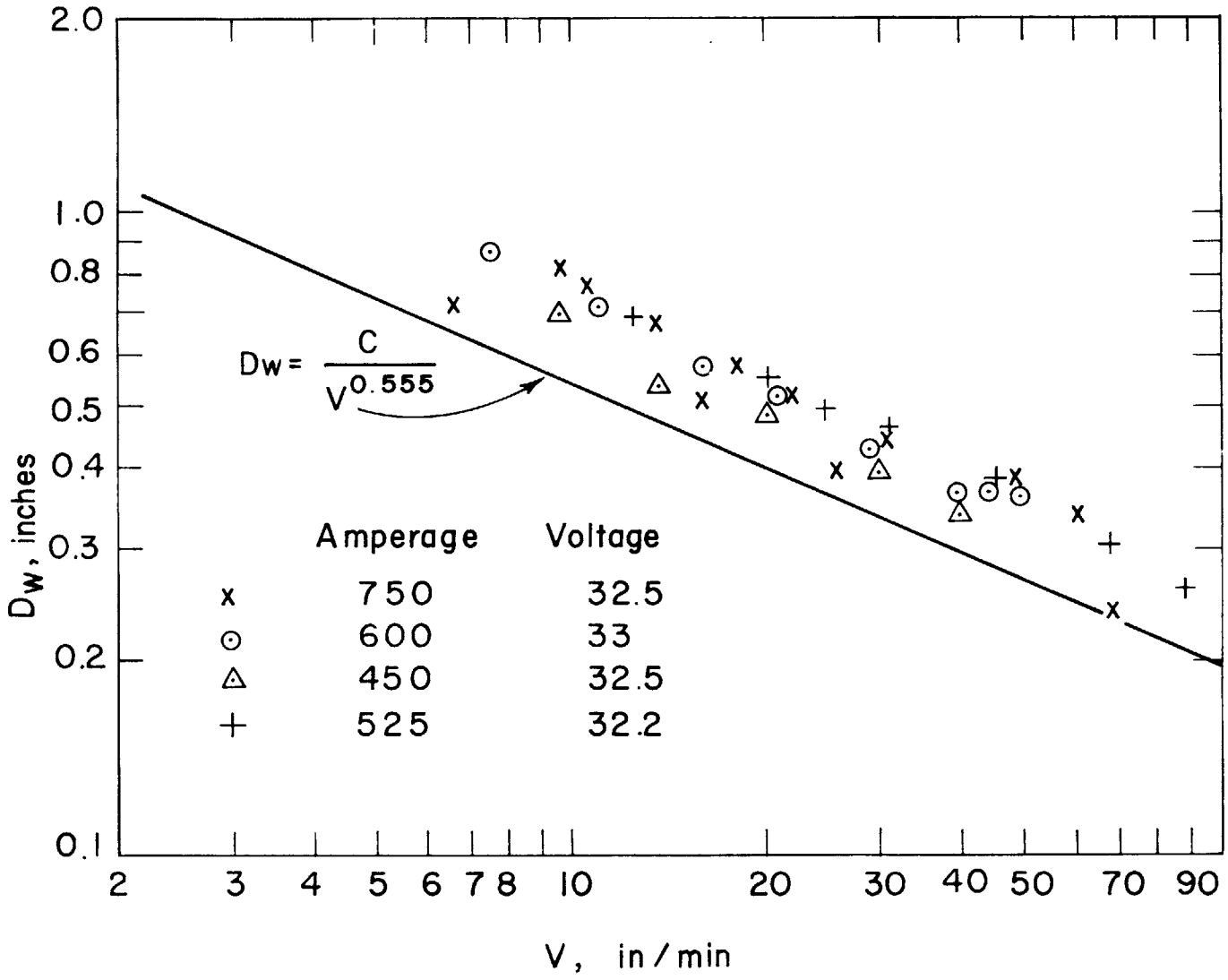

Figure 34. Bead width vs. travel speed, 1/8 inch wire

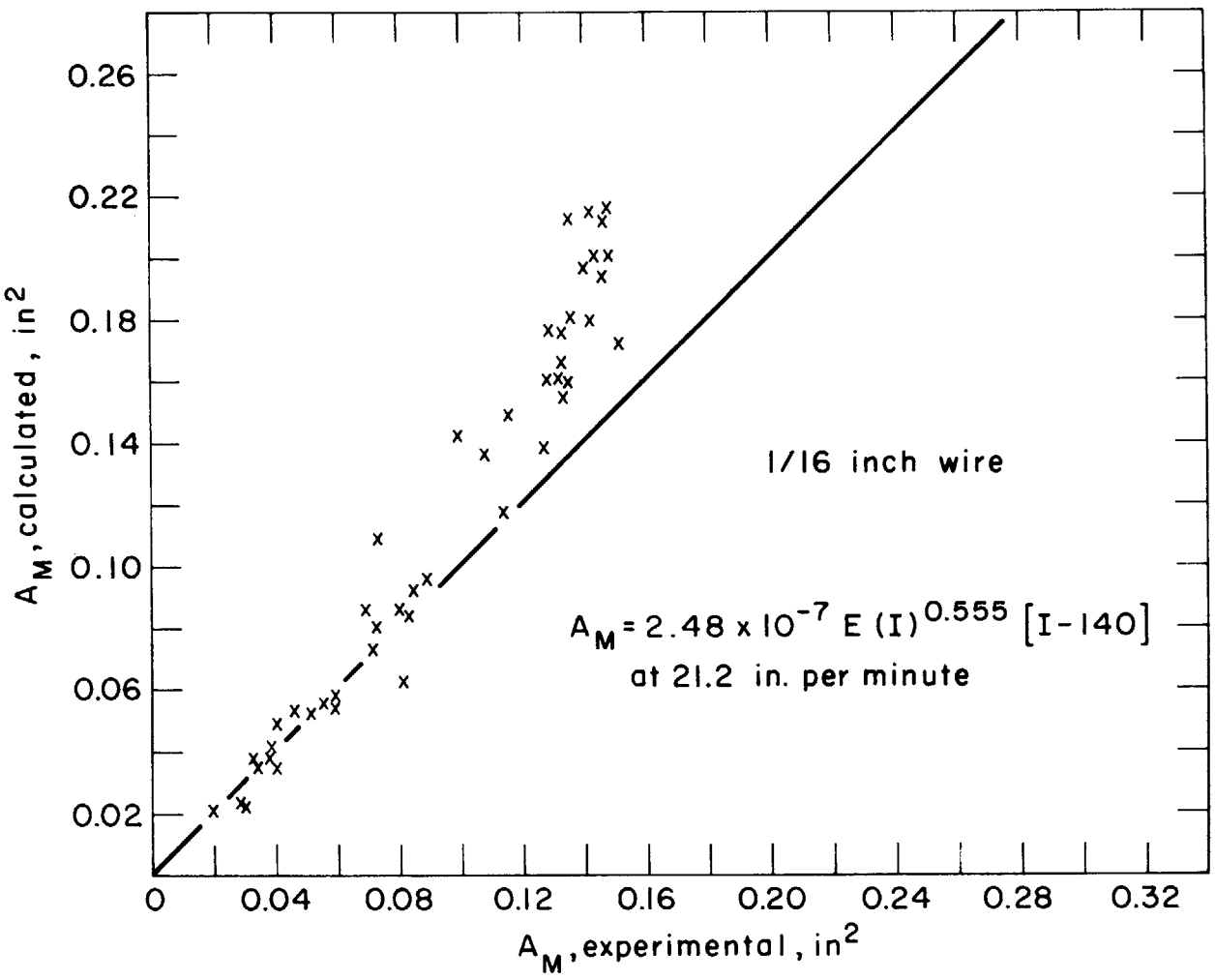

Figure 35. Independent check of the derived equations for the plate melted area, case in which amperage is varied.

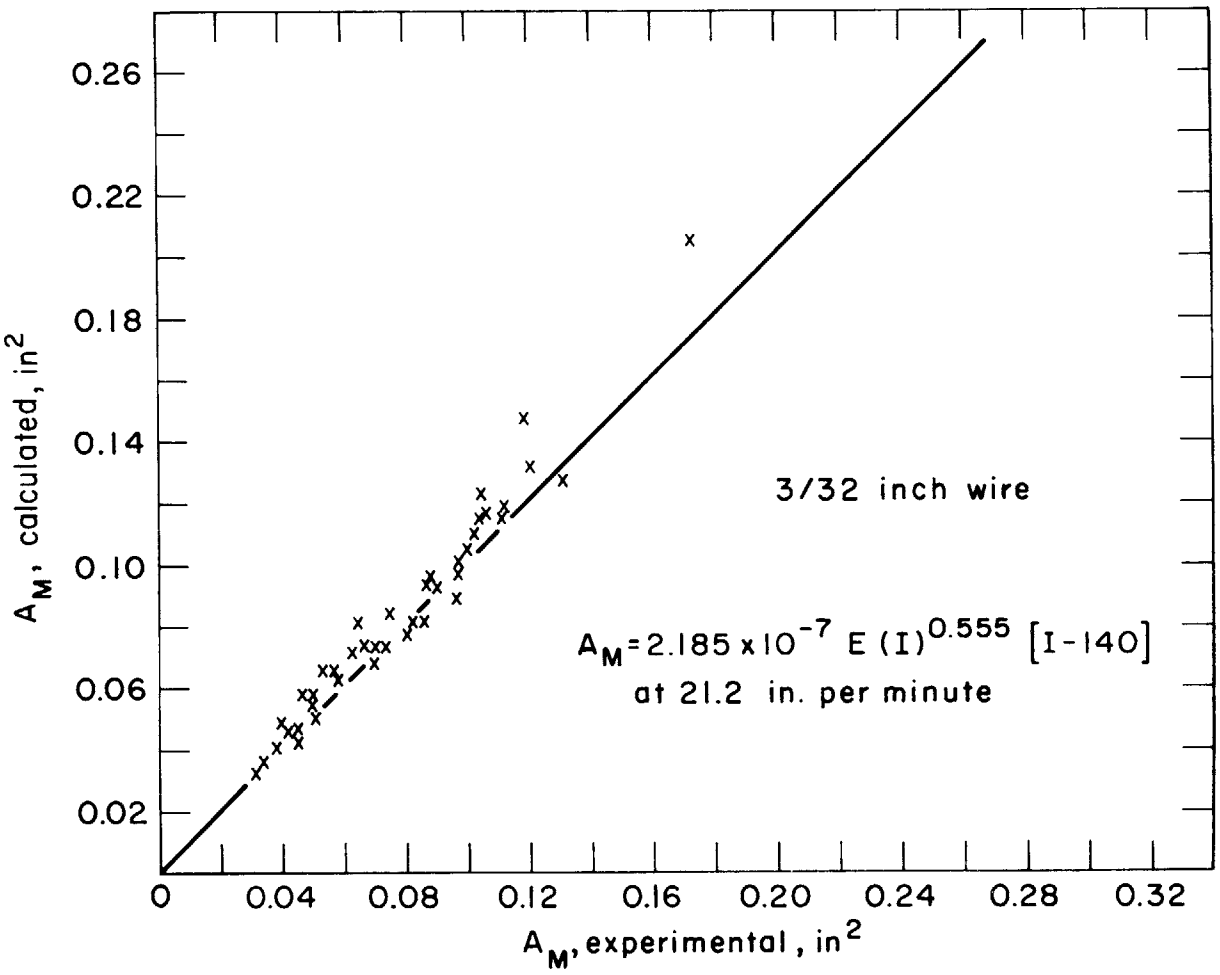

Figure 36. Independent check of the derived equation for the plate melted area, case in which amperage and voltage are varied.

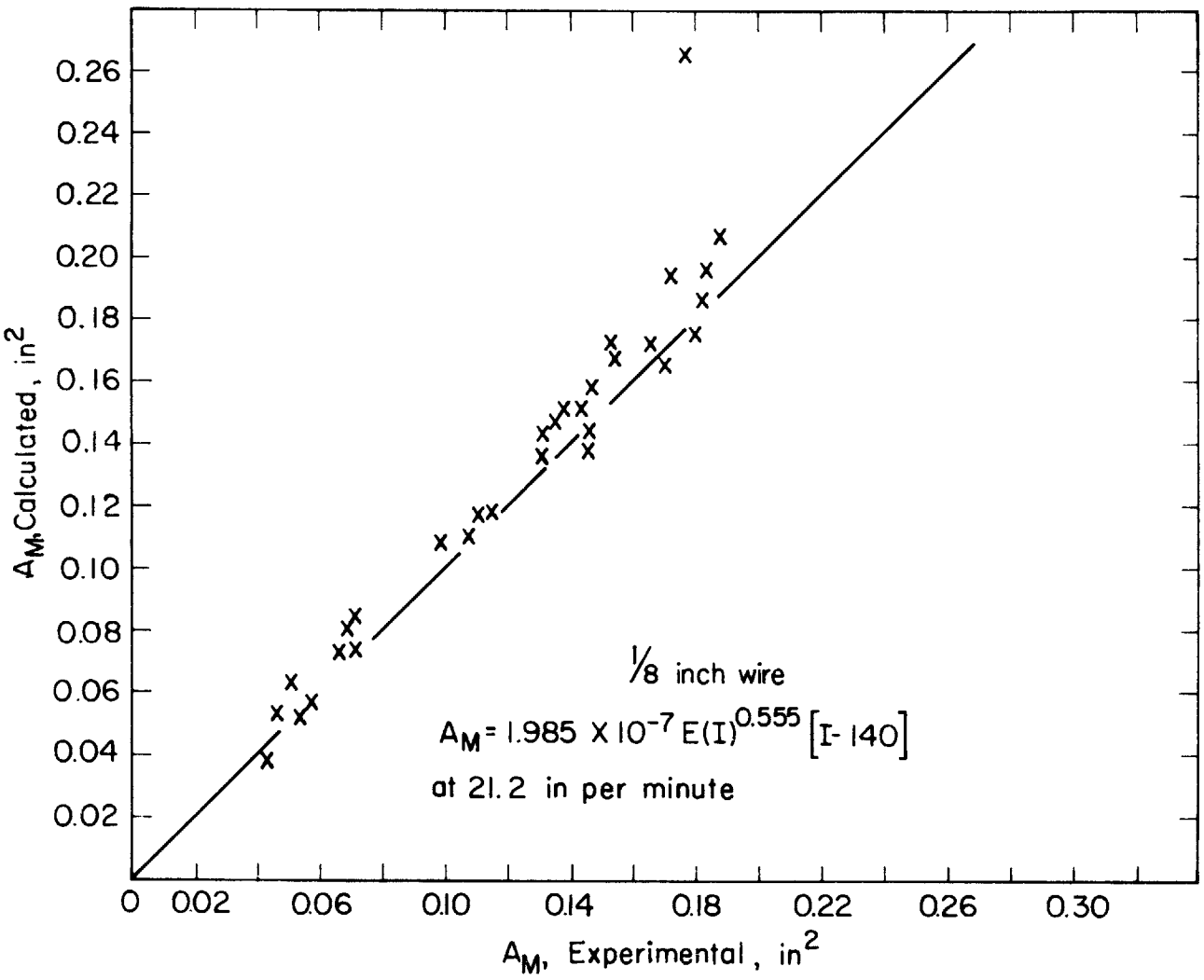

Fig. 37. Independent check of the derived equation for the plate melted area, case in which amperage is varied.

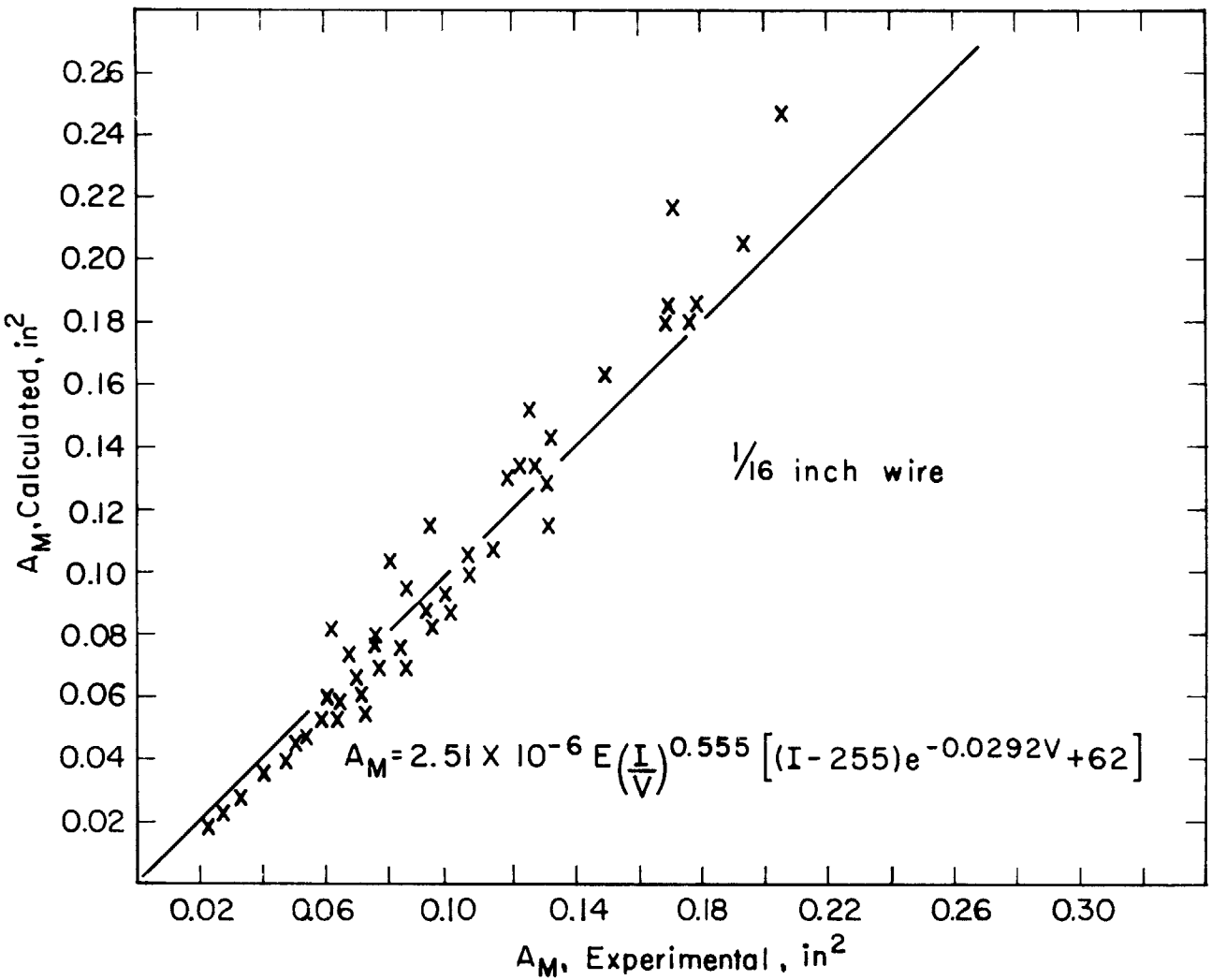

Fig. 38. Independent check of the derived equation for the plate melted area, case in which travel speed is varied.

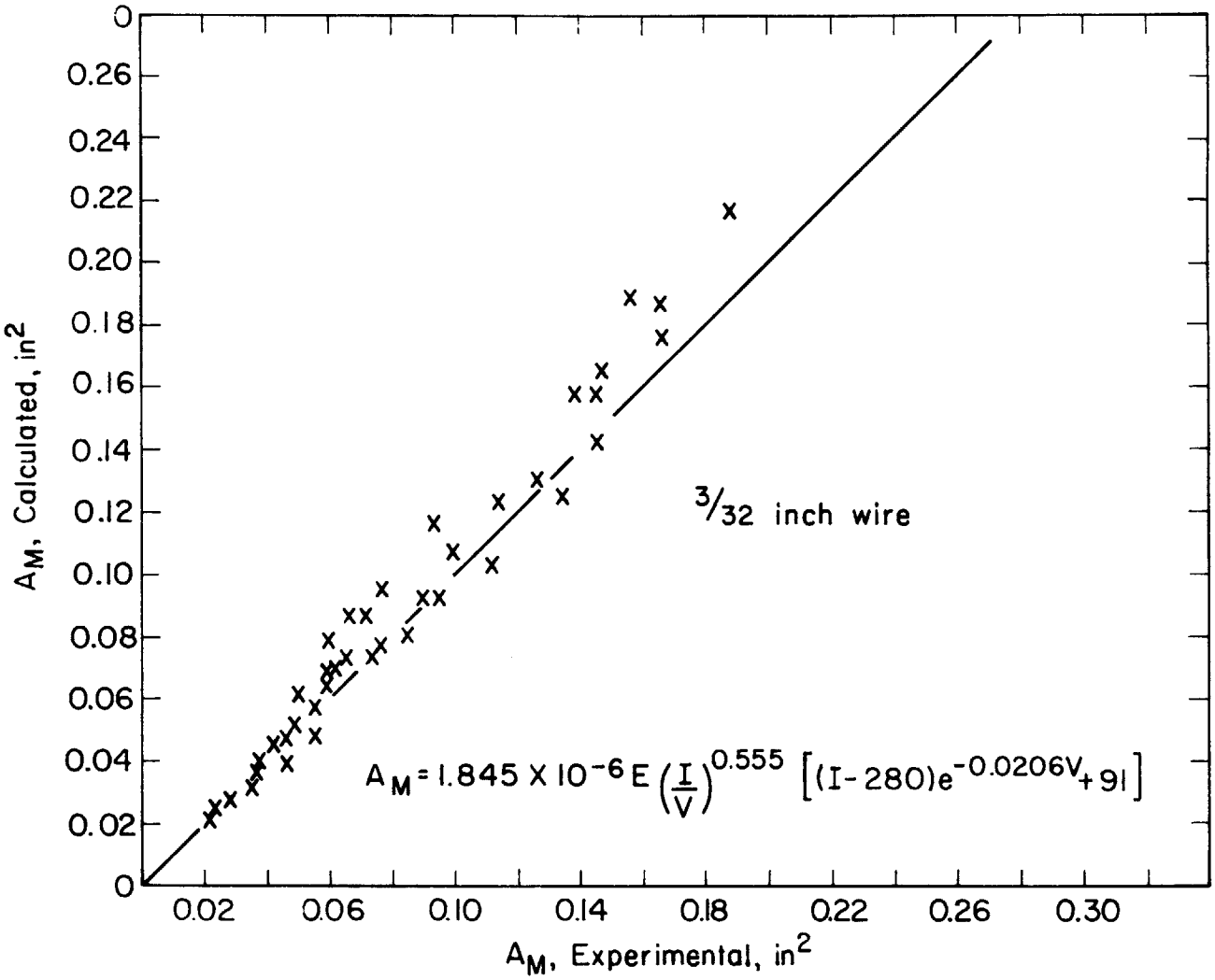

Fig. 39. Independent check of the derived equation for the plate melted area, case in which travel speed is varied

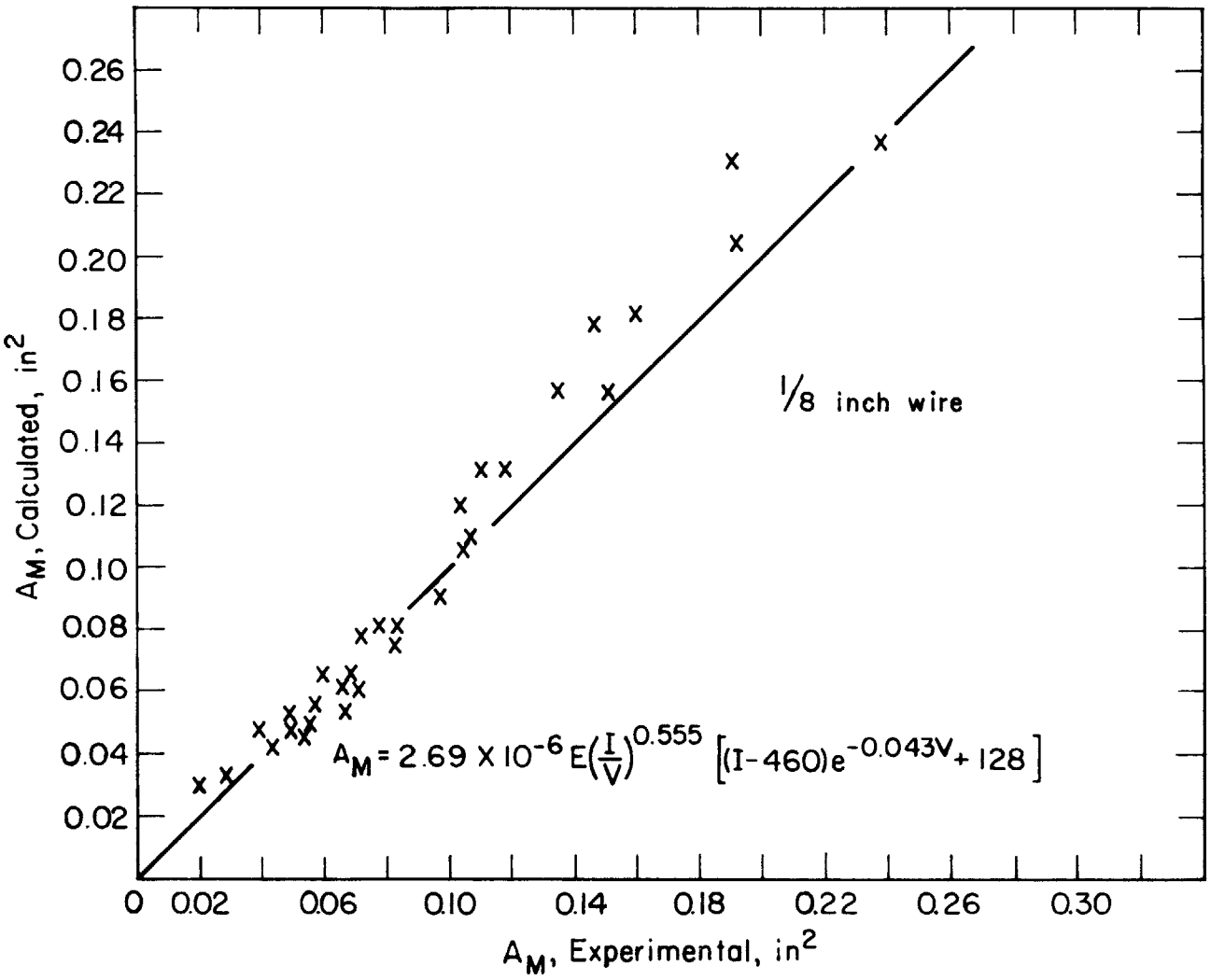

Fig. 40. Independent check of the derived equation for the plate melted area, case in which travel speed is varied

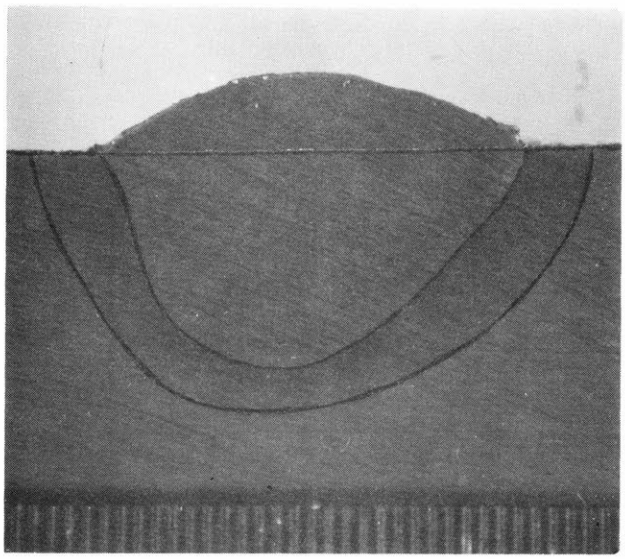

(a)

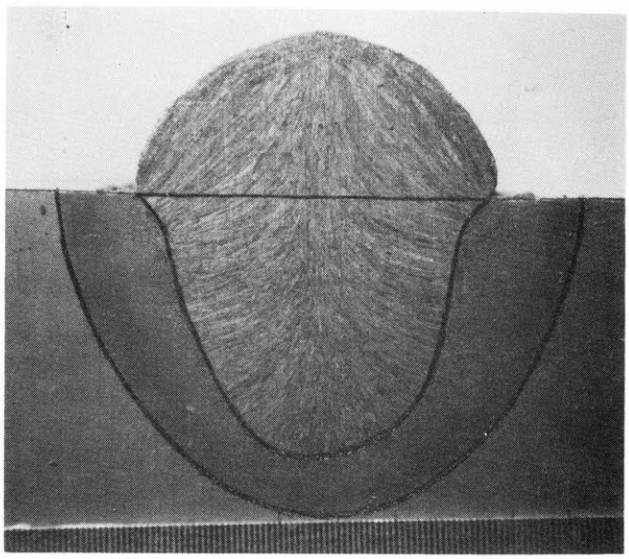

(c)

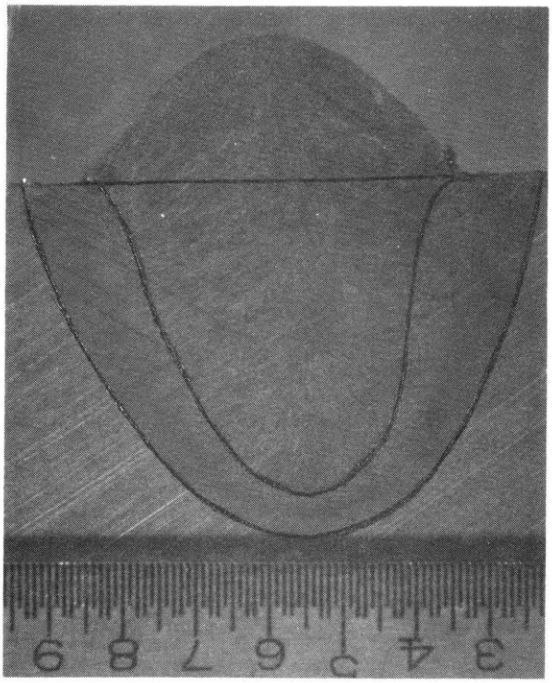

(b)

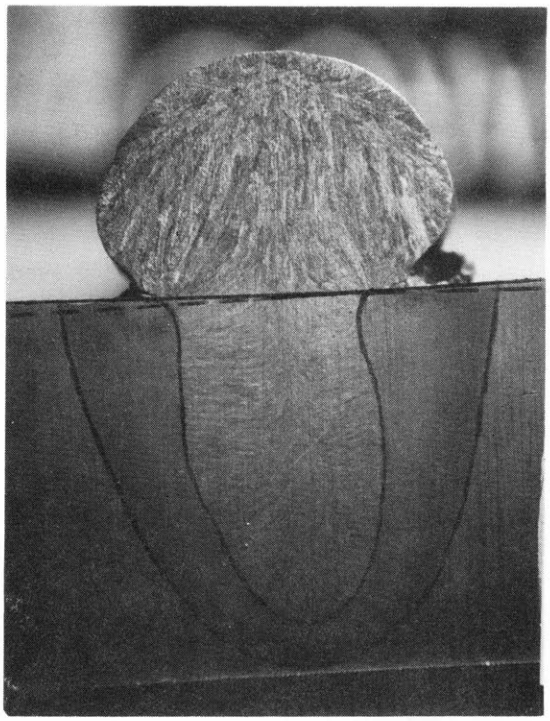

(d)

FIGURE 41 -- Welds showing transition from no overlap to overlap.

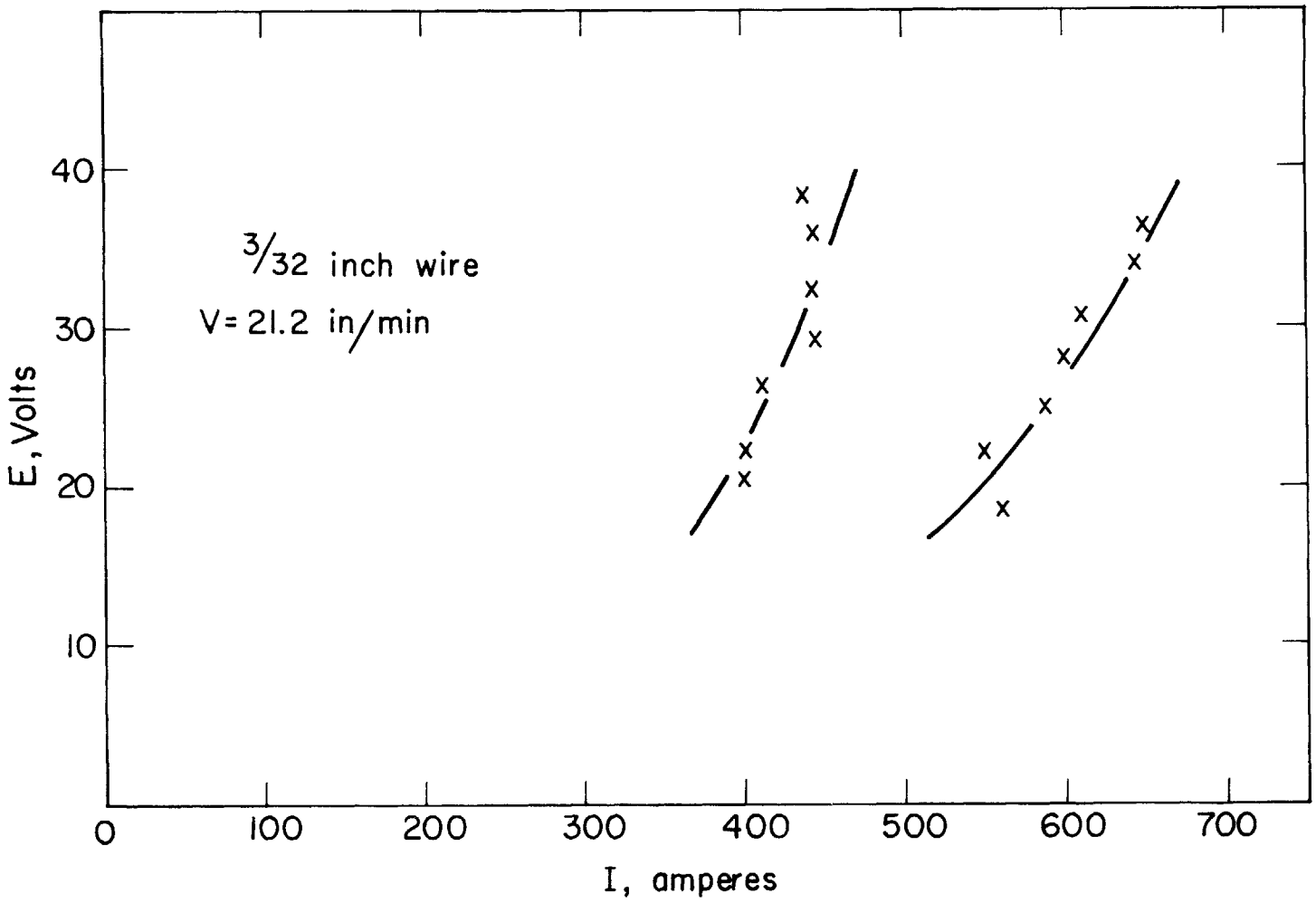

Fig. 42. Amperage — voltage relationship at constant travel speed and constant wire feed rate.

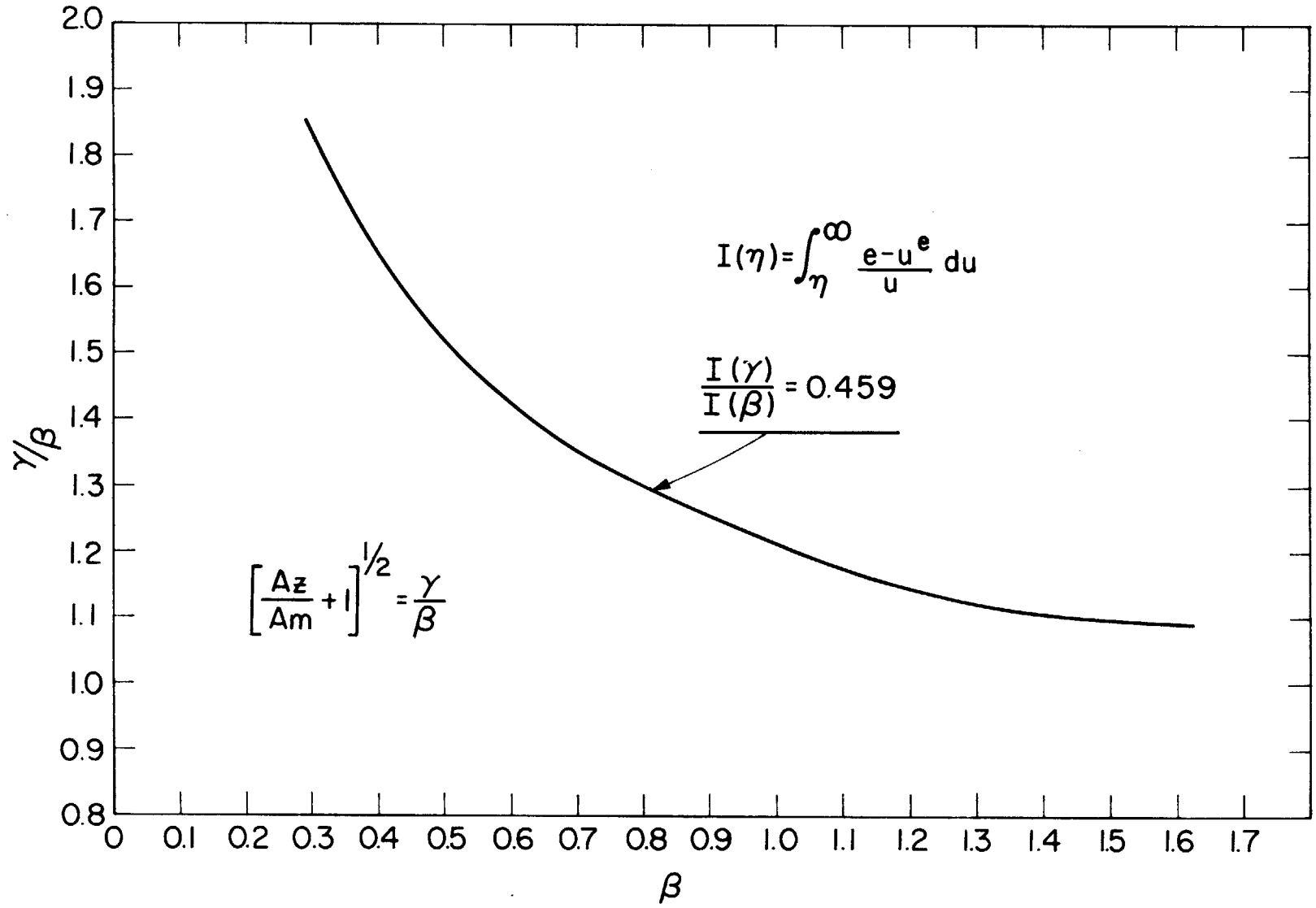

Fig. 43. Plot of γ/β vs. β such that the relationship $I(\gamma)/I(\beta) = 0.459$ is satisfied.

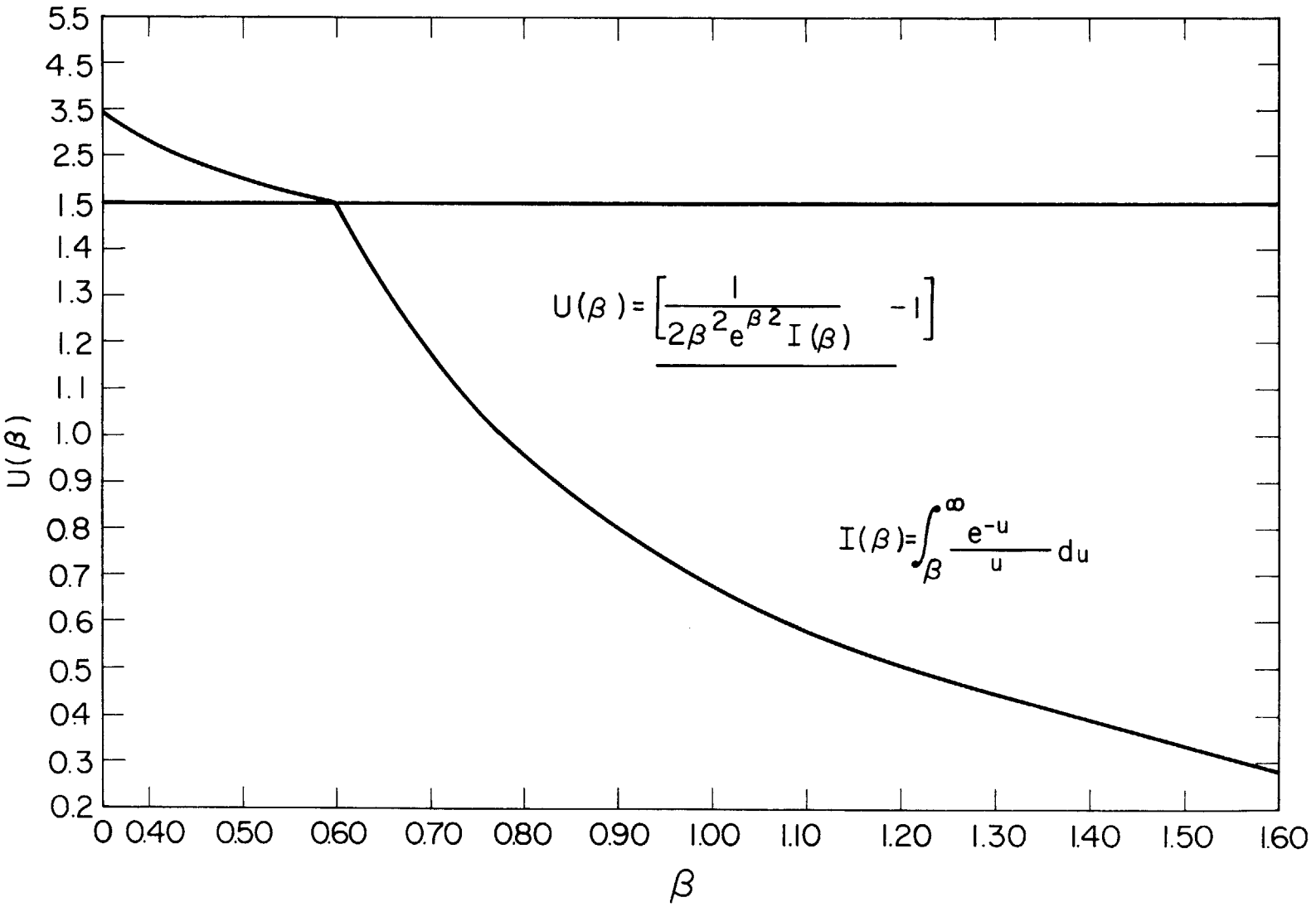

Fig. 44. Plot of the function $U(\beta)$ vs. β.

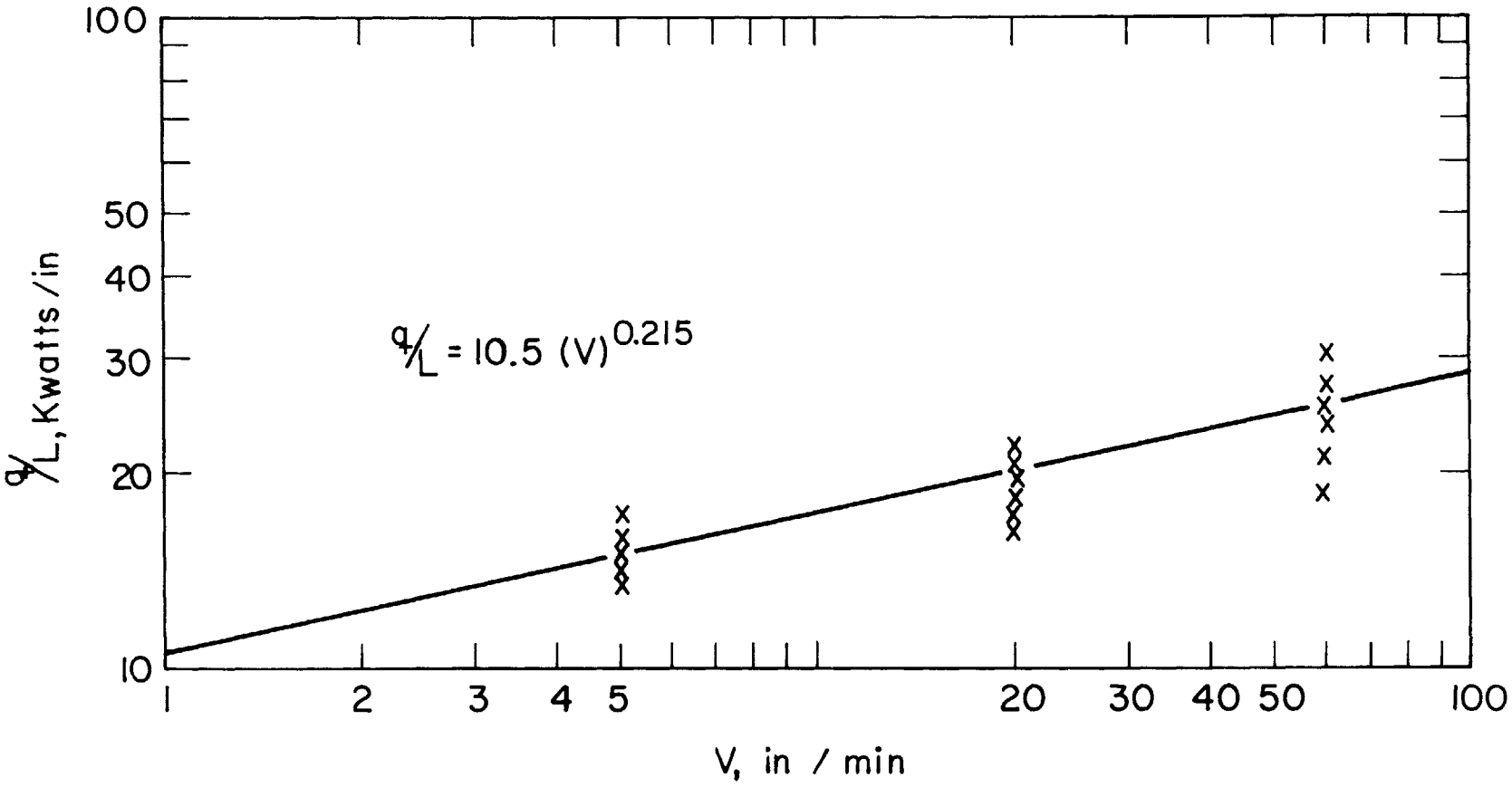

Fig. 45. Intensity vs. travel speed. Calculated data from tables VI, VII, and VIII.

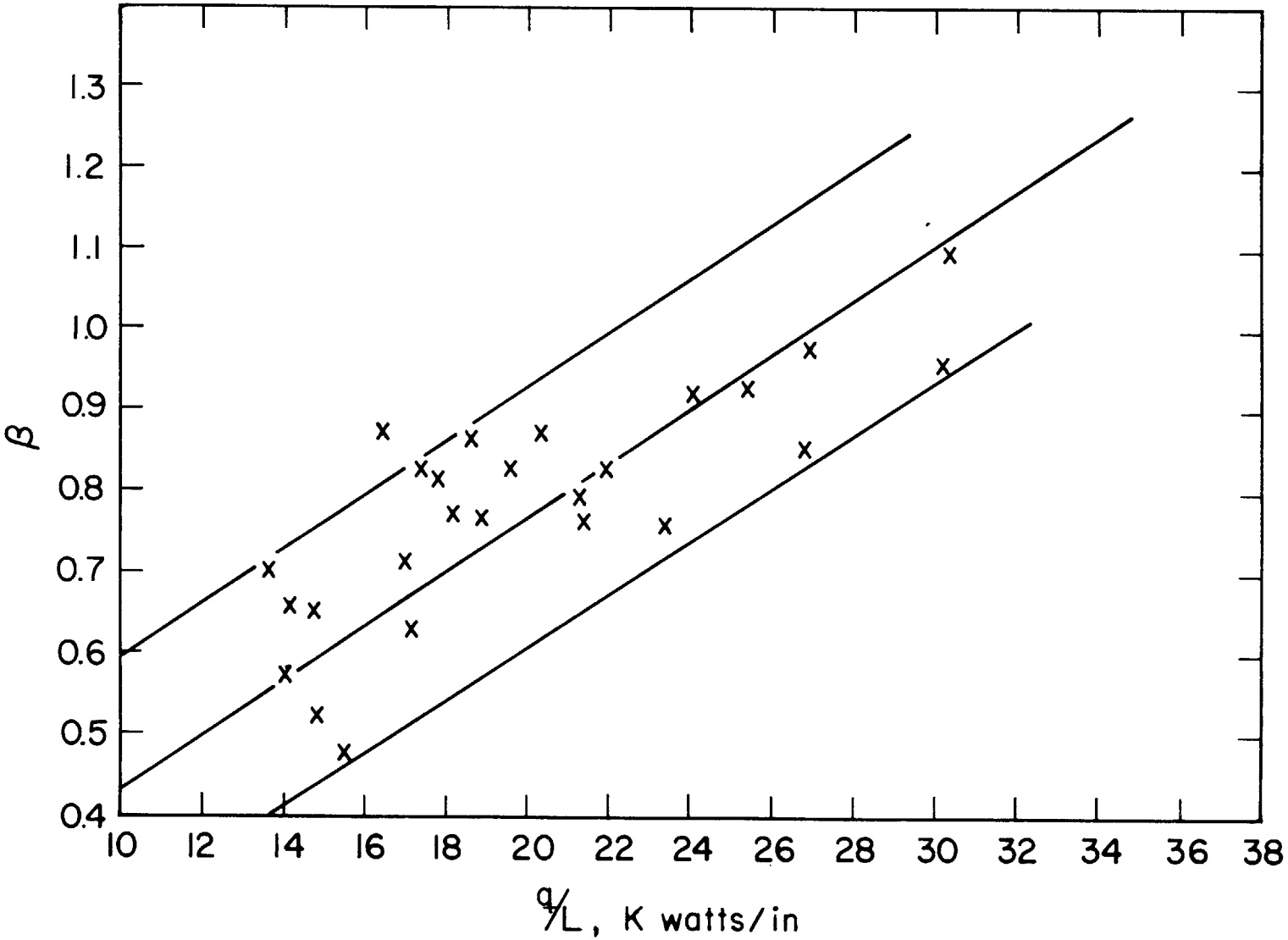

Fig. 46. β vs intensity. Calculated data from tables VI, VII, and VIII.

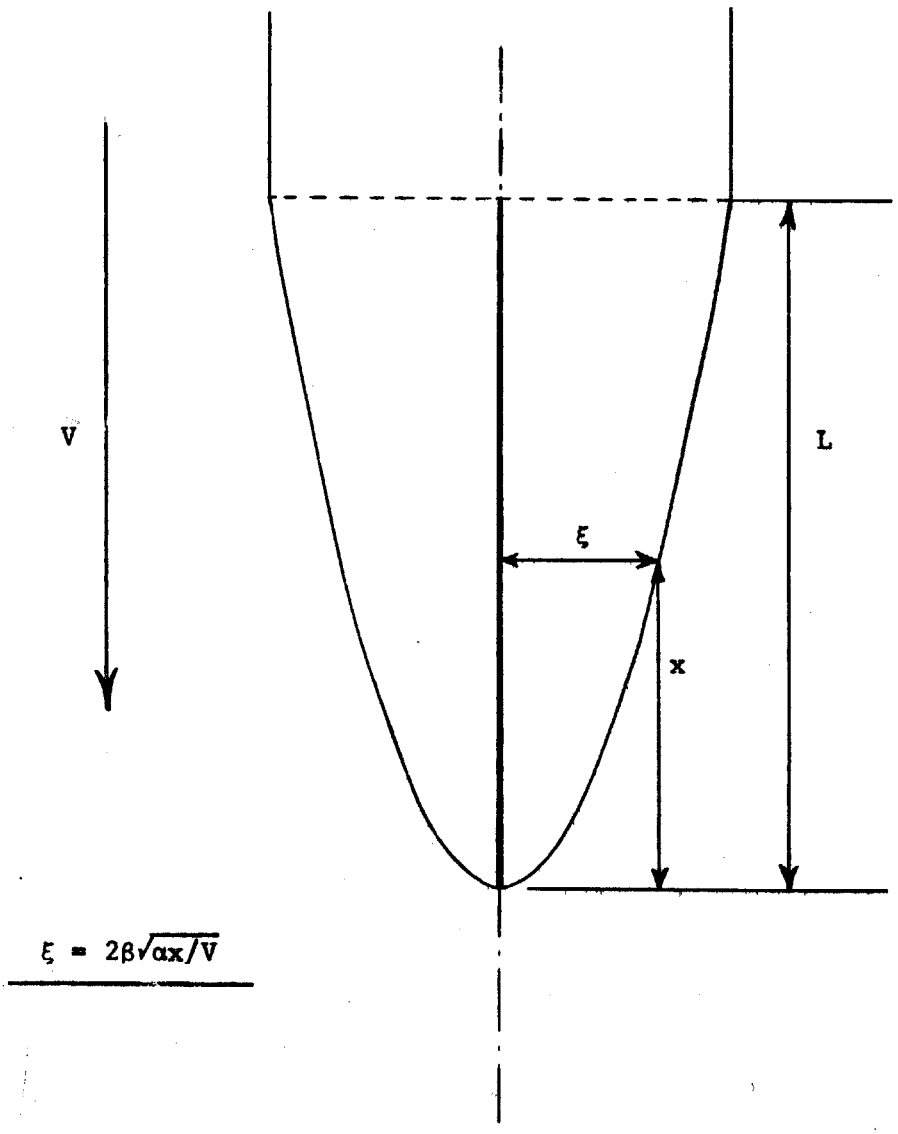

ξ - Location of melting point isotherm.
x - Distance from leading edge of heat source.
β - Shape factor.
L - Length of heat source.
V - Travel speed.
α - Thermal diffusivity

Figure 47. Schematic of parabolic isotherm and defining terms.